"In presenting the dissertation as a partial fulfillment of the requirements for an advanced degree from the Georgia Institute of Technology, I agree that the Library of the Institution shall make it available for inspection and circulation in accordance with its regulations governing materials of this type. I agree that permission to copy from, or to publish from, this dissertation may be granted by the professor under whose direction it was written, or, in his absence, by the dean of the Graduate Division when such copying or publication is solely for scholarly purposes and does not involve potential financial gain. It is understood that any copying from, or publication of, this dissertation which involves potential financial gain will not be allowed without written permission.

_____

_____

5 a
12 R

MASS TRANSFER IN THE ENTRANCE LENGTH

OF A PIPE -- LAMINAR FLOW

Approved:

Henderson C. Ward

W. M. Newton

Homer V. Grubb

Date Approved by Chairman: May 14, 1962

MASS TRANSFER IN THE ENTRANCE LENGTH OF A PIPE - LAMINAR FLOW

A THESIS

Presented to

the Faculty of the Graduate Division

by

Robert Thomas Bosworth

In Partial Fulfillment

of the Requirements for the Degree

Doctor of Philosophy in the School

of Chemical Engineering

Georgia Institute of Technology

June 1962

ACKNOWLEDGEMENTS

The author is indebted to many individuals who have contributed to the completion of this work. The encouragement and helpful criticisms of his advisor, Dr. Henderson C. Ward, are sincerely appreciated. The cooperation and advice of Dr. W. M. Newton and Dr. Homer V. Grubb, who served as members of the thesis committee, are gratefully acknowledged. The friendship, enthusiasm, and confidence of Dr. Grubb and Dr. Jack M. Spurlock provided a part of the stimulus needed to complete this work. The author is also indebted to Dr. W. F. Atchison and his staff at the Rich Electronic Computer Center.

Thanks are extended to the many undergraduate students who aided in the construction and operation of the experimental equipment, but in particular to Mr. Verne Lee Rhodes and Mr. Robert Larry Laurens.

The work reported in this thesis was made possible by the award to the author of a Humble Oil Company Fellowship for two years, teaching assistantships awarded by Dr. H. V. Grubb, Head of the School of Chemical Engineering, and the generous support of the author's mother, Mrs. Gertrude Bosworth, and mother-in-law, Mrs. Julia Averitt.

Finally, and most important, this work would not have been possible but for the loving devotion, understanding, and timely help given to the author by his wife. It is to her that this work is dedicated.

TABLE OF CONTENTS

LIST OF TABLES

LIST OF TABLES (Continued)

LIST OF TABLES (Continued)

LIST OF ILLUSTRATIONS

LIST OF ILLUSTRATIONS (Continued)

LIST OF ILLUSTRATIONS (Continued)

SUMMARY

Theoretical and experimental results are presented for the mass-transfer rates of a solid material A (naphthalene) subliming, at low mass-transfer rates, from the isothermal wall of a horizontal, cylindrical pipe into air flowing laminarly through the pipe with simultaneously developing velocity and concentration profiles.

Theoretical results were calculated, under certain restrictions, from the continuity equation of A using velocity profiles for the entrance length derived by Langhaar (14). A finite difference scheme was used to approximate the continuity equation of A.

Local mass-transfer rates were obtained experimentally at four angular positions along the length of a six foot, 2-inch Sch. 40 steel pipe coated with naphthalene, by measuring the local thickness decreases of the naphthalene coating. The experimental runs were made at 50°C, 55°C° 56°C, and 60°C (corresponding to Sc = 2.4) with air flow rates corresponding to Reynolds numbers of approximately 500 to 2000. The experimental local mass-transfer rates showed that: (a) free-convection due to density differences was not negligible, (b) there was a dependency of local mass-transfer rates on angular position, and (c) there was a rapid fall-off of mass-transfer rates at the exit end of the test pipe due to some factor that was not taken into account in the theoretical development. However, the effects mentioned in (b) and (c) were not observed for average mass-transfer rates calculated from local values by numerical integration. Overall mass balances obtained by weighing the coated test pipe before and

after the mass-transfer runs agreed, within an average deviation of ± 20 per cent, with results obtained from thickness decrease measurements.

A comparison of theoretical and experimental results showed that the mathematical model developed from the continuity equation of A satisfactorily predicts the mass-transfer rates. The average theoretical mass-transfer Nusselt numbers were expressed by the equation

$$(Nu_{AB})_m = \frac{k_{x,m} r_w}{C \mathcal{D}_{AB}} = 1.83 + \frac{0.0449 \left[\frac{ReSc}{z/D}\right]}{1 + 0.0139 \left[\frac{ReSc}{z/D}\right]^{0.8}}$$

for values of $ReScD/z < 1000$ to within ± 2 per cent. The average mass-transfer coefficients calculated from the above equations are used in the equation

$$w_A = \frac{k_{x,m} A_{ST} (X_{AbL_p} - X_{Abo})}{\ln \left[\frac{X_{Aw} - X_{Abo}}{X_{Aw} - X_{AbL_p}}\right]}$$

to determine the average mass-transfer rate w_A. Due to free-convection effects, the results will be approximately 20 per cent conservative.

NOMENCLATURE

Subscripts

m	Indicates mean or average value
loc	Indicates local value
w	Indicates quantity is at pipe wall
A	Component A
B	Component B
b	Bulk condition
ℓm	Log-mean
o	Refers to inlet condition
L_p	Refers to outlet condition
j,n	Quantity is evaluated at a mesh point (Equation (31))

Dimensionless Groups

Nu_{AB}	Nusselt number for mass transfer, $\frac{k_x, r_w}{C\mathcal{D}_{AB}}$
Re	Reynolds number, $\frac{Dv_m\rho}{\mu}$
Pr	Prandtl number, $\frac{c_p\mu}{k}$
Sc	Schmidt number, $\frac{\mu}{C\mathcal{D}_{AB}}$

Symbol

a_1, a_2, a_3	Coefficients of difference equation defined by equation (38)
a, b	Constants in equation (48)
A_{ST}	Total mass-transfer area, cm^2
A_{Si}	Incremental mass-transfer area, cm^2

C	Molar Concentration, gm-moles/cc
C^*	Dimensionless molar concentration defined by Equation (9)
C_p	Heat capacity, cal/gm-°C
C_n	Eigenvalue used in equations (51) - (55)
$\mathscr{D}_{AB}$	Diffusivity of mass, cm^2/sec
D	Pipe diameter, cm
E	Evaporation rate, gm/cm-sec
F	Height of duct, cm
h	Mesh width
I_o, I_2	Modified Bessel Function defined by equation (46)
k_x	Mass-transfer Coefficient, gm-moles/cm^2-sec
k	Thermal conductivity, cal/sec-cm-°C
k	Mesh length
L	Dimensionless length defined by equation (12)
L_p	Total length of pipe, cm
L_e	Hydrodynamic entrance length, cm
ℓ_e	Some length in hydrodynamic entrance length less than L_e, cm
M	Number of mesh points in pipe radius
MW	Molecular weight, gms/gm-mole
N	Molar flux gm-moles/cm^2-sec
P_T	Total pressure, mm Hg
p^o	Vapor pressure, mm Hg
r	Radius, cm
r, θ, z	Cylindrical coordinate system
R	Dimensionless radius, defined by equation (10)
S_p	Percentage saturation, defined by equation (2)

t_i	Thickness decrease, cm, in.
v	Velocity, cm/sec
V	Dimensionless velocity defined by equation (11)
V_i	Incremental volume , cm^3
$\mathcal{W}$	Average mass-transfer rate, gm-moles/sec
W_t	Weight loss, gm
X	Mole fraction
x, y, z	Cartesian coordinate system
Y_n	Eigenvalue used in equations (51) - (55)

Greek Symbols

ψ	Modified Graetz number, defined by equation (3)
ρ	Total density, gm/cc
ρ_N	Bulk density of naphthalene, gm/cc
μ	Viscosity, gm/cm-sec
γ	Dimensionless parameters for Langhaar velocity profiles
σ	Dimensionless parameter defined by equation (16)
λ	Mesh ratio, h/k^2
λ_n	Eigenvalue used in equation (51) - (55)
θ	$C_A - C_{Aw}$, gm-moles/cc
θ_T	Time, sec

CHAPTER I

INTRODUCTION

Mass transfer is the least understood of the three transport processes of mass, momentum, and energy. Recently, increased interest and usage of processes involving mass transfer have necessitated a better overall understanding of mass transport phenomena in almost all of the engineering disciplines. Examples of such processes are combustion of liquid and solid fuels, ion exchange and isotope separation methods, transpiration cooling, and rocket nose-cone ablation. In addition, mass-transfer rate control is important in the chemical industries where problems of catalysis, distillation, absorption, extraction, drying, and heterogeneous chemical reactions are involved.

An increasing amount of work in the field of mass transfer has been done in recent years (1), but most of this work treated already existing theory. A number of studies have been concerned with fundamental analyses of systems of well-defined physical geometry, including such areas as mass transfer from spheres at high Schmidt numbers (2) (3) (4) and from rotating disks (5). Boundary-layer theory for mass-transfer processes in flow systems has received considerable attention, but the studies have been concerned mainly with flow over flat plates. Relatively little work has been done for mass transfer in pipes and ducts.

In mass-transfer processes involving flow through pipes and ducts, the usual assumption made is that the velocity profile is fully developed at the entrance. However, considerable error may result by neglecting

the hydrodynamic entrance length. This error is greater for laminar flow than for turbulent flow since the velocity profiles develop slower in laminar flow than in turbulent flow.

It was the purpose of this study to investigate mass-transfer rates in a horizontal, cylindrical pipe with isothermal, laminar through-flow for the case where the velocity and concentration profiles are developed simultaneously. The physical system used was the sublimation of solid naphthalene from an isothermal pipe wall into air flowing in laminar flow. In the experimental portion of the study, the local mass-transfer rates were measured along the length of the pipe at four positions such that symmetry deviations could be analyzed. A mathematical model to describe the transfer system was developed from the basic equations of change, and, by the use of simplifying assumptions, a numerical solution was obtained. Several brief reviews of recent investigations that are either related to this study or to periphery considerations are presented below.

A number of theories have been proposed to predict the dependence of the transfer coefficients on the rate of mass transfer. The film theory uses a simplified unidirectional transport model to predict the variation of the momentum-, heat-, and mass-transfer coefficients with mass-transfer rates. The main limitation of this approach is the assumed one-dimensional dependence of pressure, velocity, temperature, and concentration. The penetration theory predicts the dependence of the heat- and mass-transfer coefficients on the rate of mass transfer assuming a flat velocity profile near the interface. Hence, it is mainly applicable to the liquid phase in gas-liquid systems. The boundary-layer theory

predicts the effect of mass transfer on the momentum-, heat-, and mass-transfer coefficients using a two-dimensional laminar flow model. An excellent summary of these theories is given by Bird, Stewart, and Lightfoot (6).

Sherwood and Träss (7) reported data on rates of sublimation mass transfer from an adiabatic, sharp-edged flat plate exposed to air streams at Mach numbers of 0.43, 2.0, and 3.5. To permit correlation and extrapolation of the data, they extended the theoretical analysis of heat transfer and friction by Deissler and Loeffler (8) to cover mass transfer. The data were obtained by measuring the thickness decrease of a naphthalene coating applied to the surface of the flat plate. Since the experimental work was concerned mainly with the turbulent flow region, the laminar flow data were not analyzed in detail but were compared to the Pohlhausen incompressible laminar heat-transfer solution modified to apply to mass transfer. From the meager results reported for laminar flow it appeared that the experimental values were higher than those predicted by the Pohlhausen equation.

Measurements of local mass-transfer rates by sublimation from the outer surfaces of hollow naphthalene cylinders to parallel laminar air streams were reported by Christian and Kezios (9). The experimental results were found to be in excellent agreement with the theoretical predictions of the laminar boundary-layer theory and were essentially identical with the corresponding values for flat surfaces. They concluded that the effect of surface curvature as a determining factor in mass transfer was minor.

Butler and Plewes (10) and Plewes, Butler, and Marshall (11) derived theoretical relations for the sublimation rate of a solid material which formed the bases of square and flat ducts through which air was flowing laminarly. The development assumed: (a) there was no diffusion along either the length or width of the duct, and (b) the variation in the partial pressure of the air in the air-vapor mixture could be neglected, that is, the mixture was dilute. No experimental work was conducted in flat ducts. The experimental investigations conducted in a square duct were at flow conditions that placed the results beyond the range of their theoretical development and, therefore, the results were compared to Leveque's asymptotic equation applied to mass transfer. Leveque's equation as applied to mass transfer is

$$S_p = 0.808 \left(\frac{H}{v_m} \frac{\partial v_z}{\partial x} \right)^{1/3} \psi^{2/3} \qquad (1)$$

where

$$S_p = \frac{EP_T}{P^o \rho H v_m} = \text{percentage saturation of the air leaving the solid bed} \qquad (2)$$

and

$$\psi = \frac{L_p \mathcal{D}_{AB}}{\rho H^2 v_m} = \text{a modified form of the Graetz number} \qquad (3)$$

The value of the velocity gradient used in equation (1) was found by solving the partial differential equation for the steady-state distribution of velocity in a straight tube of uniform cross-section,

$$\frac{\partial^2 v_z}{\partial x^2} + \frac{\partial^2 v_z}{\partial y^2} = \frac{1}{\mu}\left(\frac{\partial P_T}{\partial z}\right) \qquad (4)$$

by means of Southwell's (12) relaxation method. In equation (4), $\partial P_T / \partial z$ is the pressure gradient along the duct. The local velocities in the duct were then numerically integrated to give $\left[\frac{H}{v_m}\frac{\partial v_z}{\partial x}\right]_m^{1/3}$. This method resulted in a modified Leveque's equation of

$$S_p = 1.45\psi^{2/3} \qquad (5)$$

which is valid for $1/\psi > 20$.

The experimental system was a 2.77 inch square duct 15 feet in length. The subliming section was a 15 inch length of the bottom wall of the duct which could be removed and covered with a solid material. Sublimation rates were obtained by weighing this section before and after a run. The materials used in the experimental work were camphene, acetamide, camphor, phenol, p-dichlorobenzene, maleic anhydride, and naphthalene. The experimental results of this work are shown in Figures 1, 2, and 3. The authors attempt to explain the deviation from the theoretical by saying that since the data can be plotted with the theoretical slope but different intercepts, some factor other than viscosity is involved. They state that while the divergence could be explained by errors in the values of the diffusion coefficients and vapor pressure, the most plausible explanation is slip at the wall. They suggested that if the air in direct contact with the solid is moving, or slipping, there is an increased tendency for the solids to sublime. According to the authors, the difference

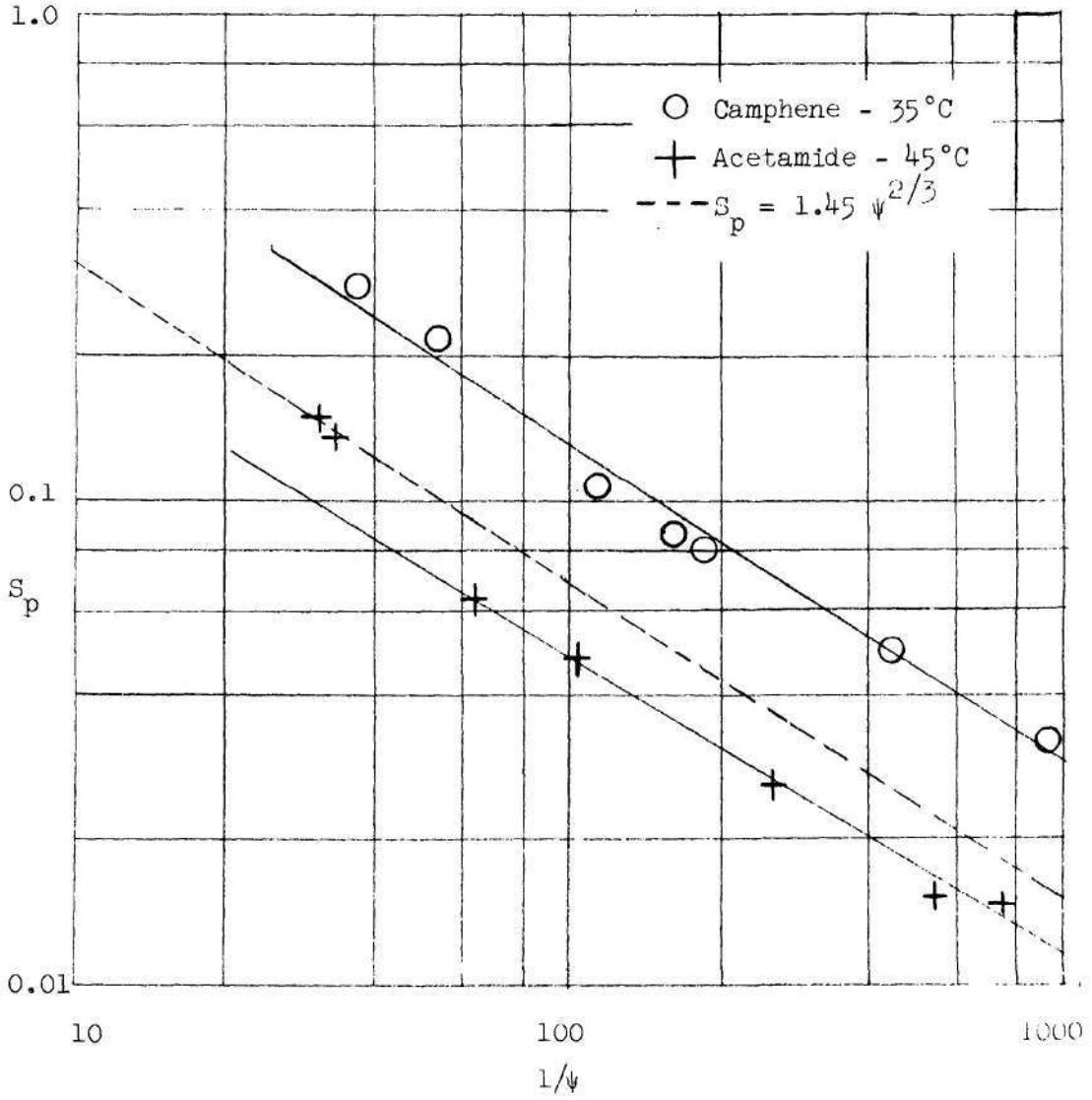

Figure 1. Percentage Saturation of Air Leaving Bed Versus Modified Graetz Number. References (10) and (11).

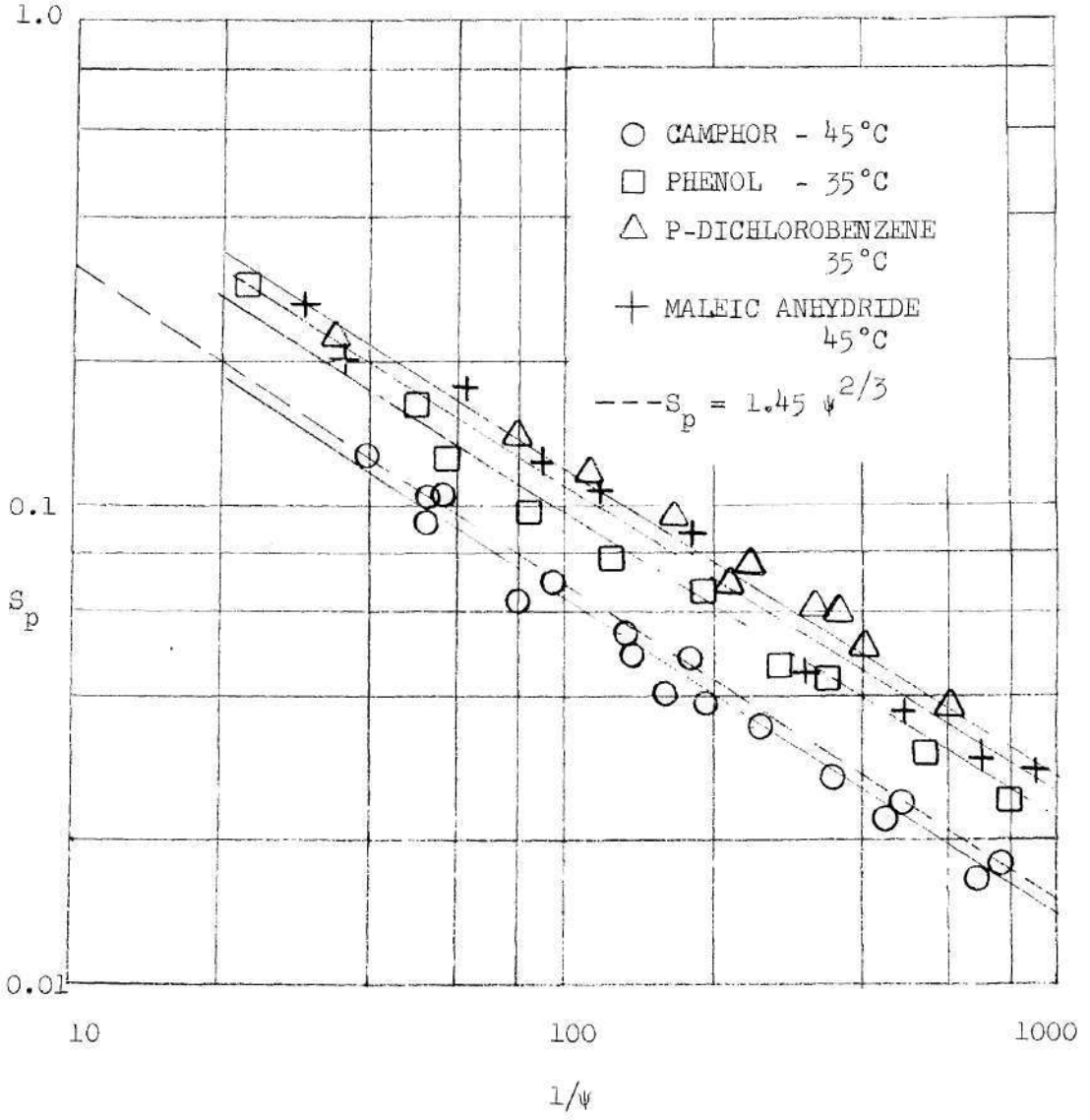

Figure 2. Percentage Saturation of Air Leaving Bed Versus Modified Graetz Number. References (10) and (11).

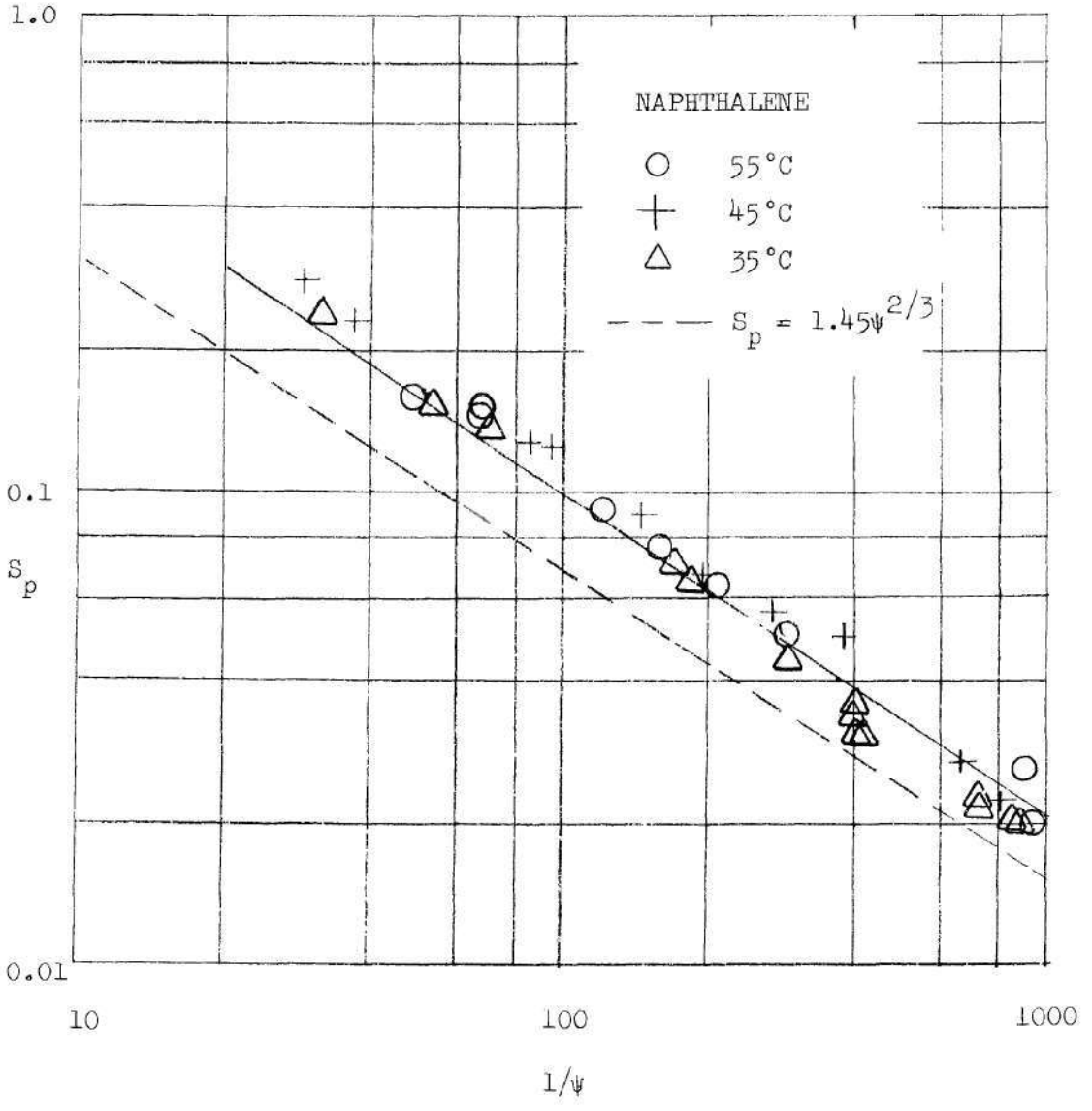

Figure 3. Percentage Saturation of Air Leaving Bed Versus Modified Graetz Number. References (10) and (11).

in the behavior of each solid could be explained by the variation in slippage among the compounds. Since the data could be plotted with the theoretical slope, they concluded that this fact lends support to the proposed theory and suggested that the percentage saturation of solids in viscous air streams in a given apparatus at a given flow is proportional to the diffusivity raised to the two-thirds power.

The two-thirds power relationship was duplicated by Linton and Sherwood (13) in experiments on the rates of solution of cast tubes. The test objects included cast tubes, cylinders, plates, and spheres of benzoic acid, cinnamic acid, and beta-naphthol. Rates of solution data were obtained by placing the test objects in water flowing both in laminar and turbulent flow. The results at low water velocities agreed well with Leveque's equation applied to mass transfer. In turbulent flow, good agreement was obtained with the Chilton-Colburn prediction involving the two-thirds exponent on the Schmidt group. The authors state that in view of the fact that the data represent a 1000-fold extension of the experimental range of the Schmidt number over previous investigations, the agreement can be considered quite remarkable.

CHAPTER II

DEVELOPMENT OF MATHEMATICAL MODEL

A mathematical model was developed to determine mass-transfer rates for a material subliming, at constant temperature and at low mass-transfer rates, from the wall of a horizontal, cylindrical pipe into a laminar air stream with simultaneously developing velocity and concentration profiles.

Consider an isothermal pipe, as shown in Figure 4, internally coated with a solid material which sublimes slowly into an air stream flowing laminarly through the pipe. The air stream and coated surface are maintained at a constant temperature such that the composition is constant along the air-solid interface. The air enters the coated pipe of radius r_w with uniform velocity v_m and uniform concentration C_{Ao}. The boundary for the system then is the inside surface of a cylindrical tube of radius r_w and length z. Any point within the domain prescribed by the boundary can be described in terms of the cylindrical coordinates r, θ, and z. Since this study is concerned with the entrance region, the analytical solution will terminate at a length down the pipe where the velocity profile can be considered nearly parabolic.

The general equations of change for steady, laminar flow which describe the velocity, temperature, and concentration profiles are simplified by imposing the following restrictions on the mathematical model.

1. The fluid enters the pipe with uniform velocity and concentration profiles.

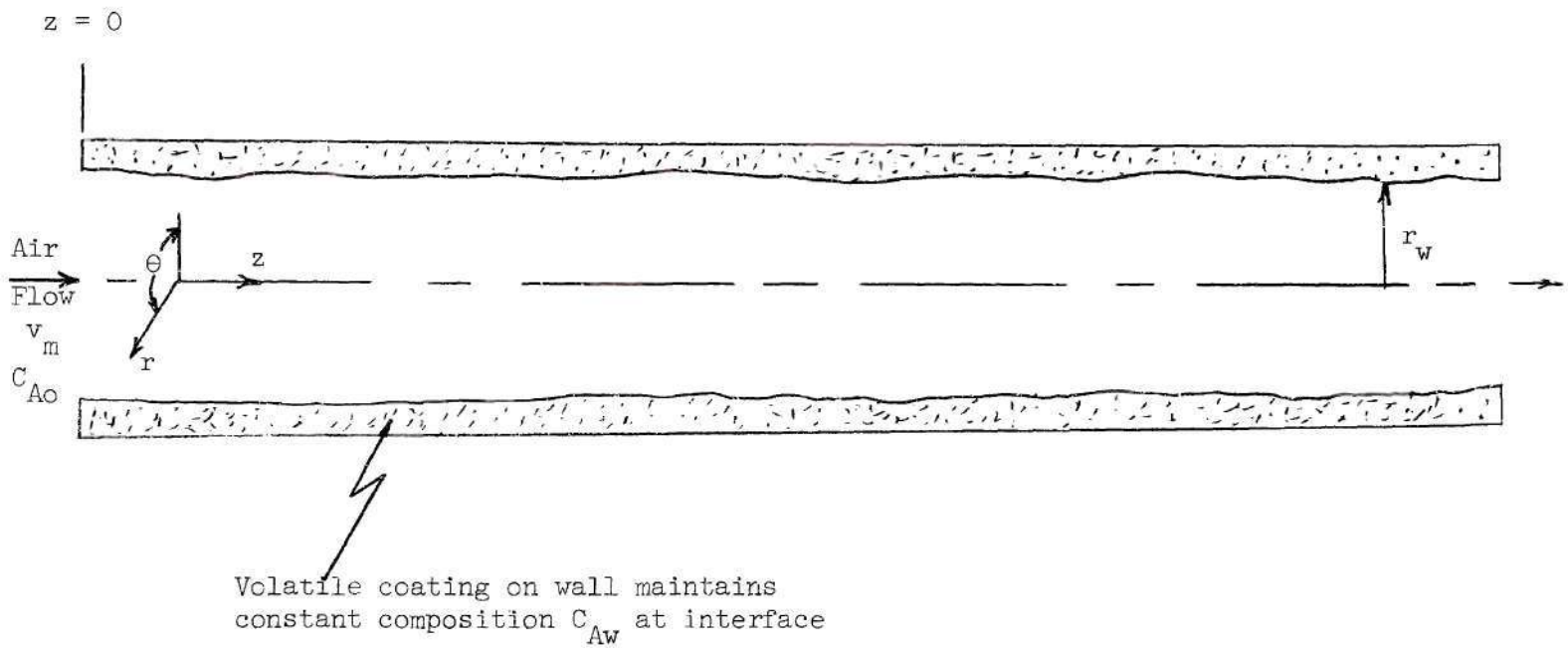

Figure 4. Schematic Diagram for Mathematical Model.

2. The system is isothermal and the concentration along the wall is constant.
3. The total density and the physical properties of each phase are constant.
4. Axial symmetry exists and $v_\theta = 0$.
5. Pressure is a function of z alone and the effects of gravity are negligible.
6. The diffusion of mass and momentum in the axial direction are negligible.
7. The mass transfer rate is small.
8. The velocity profile is unaffected by mass transfer.

The application of the above restrictions eliminates the energy equation and permits the continuity equation of A to be solved directly if the velocity profiles are known. The velocity profiles used in the continuity equation of A were those of Langhaar (14) developed from the equations of motion and continuity under restrictions consistent with those presented above. Attention can, therefore, be directed at a solution of the continuity equation of A. Under the above restrictions, the general continuity equation of A reduces to

$$v_r \frac{\partial C_A}{\partial r} + v_z \frac{\partial C_A}{\partial z} = \mathcal{D}_{AB} \left[\frac{\partial^2 C_A}{\partial r^2} + \frac{1}{r} \frac{\partial C_A}{\partial r} \right] \qquad (6)$$

Equation (6) defines the concentration field in a cylindrical pipe as a function of radius r and length z for steady state convective mass transfer. If the velocity profiles were fully developed, the radial velocity would be zero and the term involving v_r would be eliminated. But, in the

entrance region, the velocity profile is established simultaneously with the concentration profile and the radial velocity is finite. As pointed out by Kays (15) in his study on heat transfer, the analogous radial velocity term in heat transfer is of considerable importance near the pipe entrance but its magnitude is reduced to about ten per cent of the conduction terms at RePrD/z = 1000. The importance of v_r rapidly diminishes for RePrD/z < 1000 and becomes negligible for RePrD/z = 100. Therefore, for the analogous mass-transfer system studied here, the radial velocity term is ten per cent of the diffusion terms for ReScD/z = 3400 and becomes negligible for ReScD/z = 340. Since the velocity is nearly developed at ReScD/z = 40, the radial velocity term is important only for the first 1.2 per cent of the entrance length and can, therefore, be neglected. Neglecting v_r, equation (6) becomes

$$v_z \frac{\partial C_A}{\partial z} = \mathcal{D}_{AB}\left[\frac{\partial^2 C_A}{\partial r^2} + \frac{1}{r}\frac{\partial C_A}{\partial r}\right] \tag{7}$$

The boundary conditions are

$$C_A(r, 0) = C_{Ao}; \quad 0 \leq r \leq r_w \tag{8a}$$

$$C_A(r_w, z) = C_{Aw}; \quad z > 0 \tag{8b}$$

$$\frac{\partial C_A(0, z)}{\partial r} = 0; \quad z > 0 \tag{8c}$$

For ReScD/z values greater than 400, the last boundary condition is not unique only at the center line. However, it implies symmetry and is used thusly to obtain a solution to equation (7). Equation (7) can be put into

a more convenient form by introducing the non-dimensional variables

$$C^* = \frac{C_A - C_{Ao}}{C_{Aw} - C_{Ao}} \tag{9}$$

$$R = \frac{r}{r_w} \tag{10}$$

$$V = \frac{v_z}{v_m} \tag{11}$$

$$L = \frac{\mathcal{D}_{AB} z}{v_m r_w^2} = \frac{4(z/D)}{(ReSc)} \tag{12}$$

Equation (7) then becomes

$$\frac{\partial^2 C^*}{\partial R^2} + \frac{1}{R}\frac{\partial C^*}{\partial R} = \frac{V \partial C^*}{\partial L} \tag{13}$$

and the boundary conditions become

$$\begin{aligned} C^*(R,0) &= 0; \quad 0 \leq R \leq 1 \\ C^*(1,L) &= 1; \quad L > 0 \\ \frac{\partial C^*(0,L)}{\partial R} &= 0; \quad L > 0 \end{aligned} \tag{14}$$

The dimensionless velocity profiles used in equation (13) were those derived by Langhaar for laminar flow velocity development in the entrance length of a straight pipe. These profiles are given by

$$V = \frac{v_z}{v_m} = \frac{I_o(\gamma) - I_o(\gamma R)}{I_2(\gamma)} \tag{15}$$

where γ is a function of σ, and

$$\sigma = \frac{z}{r_w Re} = \frac{z\nu}{r_w^2 v_m} = (Sc)(L) \qquad (16)$$

Values of γ and σ are given in Table 1.

Table 1. Dimensionless Parameters for the Langhaar Velocity Profiles

γ	σ	γ	σ
16.00	0.00137	2.75	0.0625
14.50	0.00172	2.50	0.0715
13.00	0.00222	2.25	0.0821
12.00	0.00269	2.00	0.0947
11.00	0.00332	1.85	0.1034
10.00	0.00418	1.70	0.1132
9.00	0.00541	1.55	0.1241
8.00	0.00722	1.40	0.1365
7.00	0.00997	1.30	0.1459
6.50	0.01188	1.20	0.1560
6.00	0.0143	1.10	0.1671
5.50	0.0174	1.00	0.1795
5.00	0.0214	0.90	0.1934
4.50	0.0267	0.80	0.2091
4.00	0.0335	0.70	0.2270
3.50	0.0426	0.60	0.2479
3.25	0.0483	0.50	0.2730
3.00	0.0549	0.40	0.3040

Substituting equation (15) into equation (13), integrating, and applying the boundary conditions gives a solution for the concentration field in the entrance length as a function of R and L.

$$C^* = f(R, L) \qquad 0 \leq R \leq 1; \qquad 0 < L < Le \qquad (17)$$

The molar fluxes and Nusselt numbers for mass transfer can now be determined using the concentration profiles to obtain the concentration gradients at the wall. The molar flux $\vec{N}_A$ relative to stationary coordinates is given by Fick's first law of diffusion (6).

$$\vec{N}_A = X_A (\vec{N}_A + \vec{N}_B) - C\mathcal{D}_{AB} \vec{\nabla} X_A \tag{18}$$

Equation (18) can be solved for the local molar flux of A at the wall under restrictions 1 through 8, and the assumptions that the solubility of component B (air) in solid material A (naphthalene) is negligible, $X_A << 1$, and C is constant.

$$(N_{Aw})_{loc} = - \mathcal{D}_{AB} \left(\frac{\partial C_A}{\partial r} \right) \Bigg|_{r_w, z} \tag{19}$$

or, in dimensionless form,

$$(N_{Aw})_{loc} = - \frac{\mathcal{D}_{AB} (C_{Aw} - C_{Ao})}{r_w} \left(\frac{\partial C^*}{\partial R} \right) \Bigg|_{R=1, L} \tag{20}$$

The dimensionless concentration gradient at the wall is obtained by differentiating equation (17) and setting R = 1.

An average molar flux for a pipe of length ℓ_e ($\ell_e \leq L_e$) can be evaluated by integrating equation (20) over the length ℓ_e.

$$(N_{Aw})_m = \frac{\int_o^{\ell_e} (N_{Aw})_{loc} \, dL}{\int_o^{\ell_e} dL} = \frac{1}{\ell_e} \int_o^{\ell_e} (N_{Aw})_{loc} \, dL \tag{21}$$

The local, one-phase mass-transfer coefficient for the limiting condition of small mass-transfer rates is defined by (6)

$$k_{x,loc} = \frac{N_{Aw} - X_{Aw}(N_{Aw} + N_{Bw})}{X_{Aw} - X_{Ab}} \tag{22}$$

Using equation (19), equation (22) becomes

$$k_{x,loc}\,(X_{Aw} - X_{Ab}) = -\mathfrak{D}_{AB} \left.\frac{\partial C_A}{\partial r}\right|_{r_w,z} \tag{23}$$

Putting equation (23) into dimensionless form, the Nusselt number for mass transfer as a function of the dimensionless bulk concentration and concentration gradient is

$$(Nu_{AB})_{loc} = \frac{k_{x,loc}\, r_w}{C\mathfrak{D}_{AB}} = - \frac{\left.\frac{\partial C^*}{\partial R}\right|_{R=1,\ L}}{1 - C_b^*} \tag{24}$$

where

$$1 - C_b^* = \frac{C_{Aw} - C_{Ab}}{C_{Aw} - C_{Ao}} \tag{25}$$

and

$$C_{Ab} = \frac{\int_0^{2\pi}\int_0^{r_w} v_z(r,z)C_A(r,z)\,r\,dr\,d\theta}{\int_0^{2\pi}\int_0^{r_w} v_z(r,z)\,r\,dr\,d\theta} \tag{26}$$

Or, in dimensionless form

$$C_{Ab} = (C_{Aw} - C_{Ao}) \frac{\int_0^{2\pi} \int_0^1 V(R,L) C^* (R,L) R dR d\theta}{\int_0^{2\pi} \int_0^1 V(R,L) R dR d\theta} \tag{27}$$

The average Nusselt number for mass transfer for a tube of length ℓ_e is found by integration of equation (24)

$$(Nu_{AB})_m = \frac{1}{\ell_e} \int_0^{\ell_e} (Nu_{AB})_{loc} \, dL \tag{28}$$

The average mass-transfer coefficients defined by equation (28) are used in equation (29) to determine the average molar mass-transfer rate for a cylindrical pipe of length L_p

$$w_A = k_{x,m} (\pi D L_p)(\Delta X_{Ab})_{\ell m} \tag{29}$$

where

$$(\Delta X_{Ab})_{\ell m} = \frac{X_{AbL_p} - X_{Abo}}{\ln \frac{(X_{Aw} - X_{Abo})}{(X_{Aw} - X_{AbL_p})}} \tag{30}$$

Proof that $(\Delta X_{Ab})_{\ell m}$ is the appropriate concentration difference for the mass-transfer coefficient defined by equation (28) is given in Appendix C.

CHAPTER III

SOLUTION OF THE MATHEMATICAL MODEL

An exact, closed form, general solution of equation (13) could not be obtained due to the complexity of the velocity term V. Hence, an explicit numerical scheme was used. An excellent summary of this method is given by Keller (16). The interested reader is also referred to other works (17-20) for more detailed and formal presentations.

The continuity equation of A is a linear, second-order, parabolic differential equation.

$$\frac{\partial^2 C^*}{\partial R^2} + \frac{1}{R} \frac{\partial C^*}{\partial R} = V \frac{\partial C^*}{\partial L} \qquad (13)$$

A solution of equation (13) is uniquely determined in the region G

$$G: \left[0 \leq R \leq 1; \quad L > 0\right]$$

by specifying the boundary conditions.

$$\begin{aligned} &\text{B.C. 1:} \quad C^*(R,0) = 0; \quad 0 \leq R \leq 1 \\ &\text{B.C. 2:} \quad C^*(1,L) = 1; \quad L > 0 \\ &\text{B.C. 3:} \quad \frac{\partial C^*}{\partial R}(0,L) = 0; \quad L > 0 \end{aligned} \qquad (14)$$

The following analysis assumes that the solution determined has as many continuous derivatives as required (16).

A net, or grid, is superimposed on the strip G

$$G_{h,k}: \left[R_j = jh,\ j = 0,1,2,.....M;\ L_n = nk,\ k = 1,2..\right] \quad (31)$$

where $h = 1/M$. At each point (R_j, L_n) a quantity $U(R_j, L_n)$ is sought which approximates the solution $C^*(R_j, L_n)$ of equations (13) and (14). The approximating quantities U are determined as the solution of a system of linear algebraic equations, the difference equations. There is no one unique procedure by which the difference equations are determined, since each problem requires special attention. However, any system of difference equations must be required to have a solution which can be effectively computed and that this computed numerical solution, at least for sufficiently small h, k,and round-off error, be close to the exact solution.

The reduction of equation (13) to a suitable finite difference approximation is most easily effected by means of Taylor's series. Consider a mesh of width h and length k to be superimposed over the mathematical model as shown in Figure 5 below.

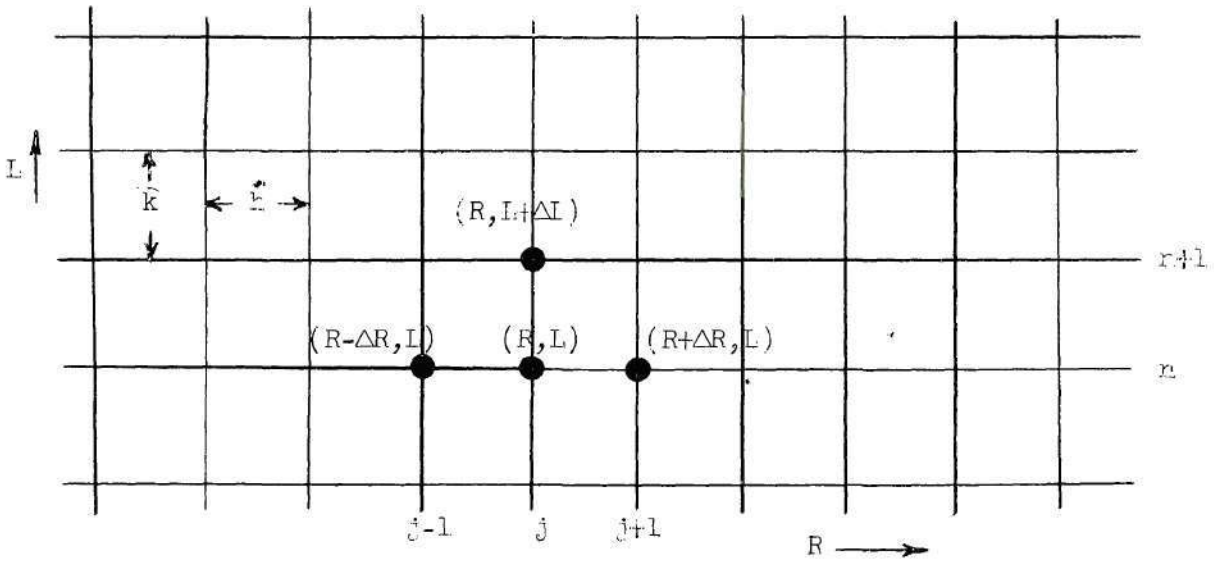

Figure 5. Grid Used to Approximate Mathematical Model

Since $C^* = f(R,L)$, $f(R,L)$ may be expanded in a Taylor's series about L for a fixed value of R:

$$C^*(R,L + \Delta L) = C^*(R,L) + \Delta L \frac{\partial C^*}{\partial L} + \frac{\Delta L^2}{2} \frac{\partial^2 C^*}{\partial L^2} + \frac{\Delta L^3}{6} \frac{\partial^3 C^*}{\partial L^3} + \ldots . \qquad (32)$$

As long as ΔL is sufficiently small, terms of the order of ΔL^2 and higher may be neglected, and a first approximation of $(\partial C^*/\partial L)$ is

$$\frac{\partial C^*}{\partial L} = \frac{C^*(R,L + \Delta L) - C^*(R,L)}{\Delta L} = \frac{C^*_{j,n+1} - C^*_{j,n}}{k} \qquad (33)$$

Two Taylor series expansions are needed to obtain the first approximation to $\partial^2 C^*/\partial R^2$.

$$C^*(R + \Delta R,L) = C^*(R,L) + \Delta R \frac{\partial C^*}{\partial R} + \frac{\Delta R^2}{2} \frac{\partial^2 C^*}{\partial R^2} + \frac{\Delta R^3}{6} \frac{\partial^3 C^*}{\partial R^3}$$

$$+ \frac{\Delta R^4}{24} \frac{\partial^4 C^*}{\partial R^4} + \ldots\ldots \qquad (34a)$$

and

$$C^*(R-\Delta R,L) = C^*(R,L) - \frac{\Delta R \partial C^*}{\partial R} + \frac{\Delta R^2}{2} \frac{\partial^2 C^*}{\partial R^2} - \frac{\Delta R^3}{6} \frac{\partial^3 C^*}{\partial R^3}$$

$$+ \frac{\Delta R^4}{24} \frac{\partial^4 C^*}{\partial R^4} - \ldots\ldots \qquad (34b)$$

If equations (34a) and (34b) are added and terms of the order of ΔR^4 neglected, the first approximation to $\partial^2 C^*/\partial R^2$ is

$$\frac{\partial^2 C^*}{\partial R^2} = \frac{C^*(R + \Delta R, L) - 2C^*(R, L) + C^*(R - \Delta R, L)}{\Delta R^2}$$

$$= \frac{C^*_{j+1,n} - 2C^*_{j,n} + C^*_{j-1,n}}{h^2} \tag{35}$$

Similarly, the first approximation to $\partial C^*/\partial R$ is determined to be

$$\frac{\partial C^*}{\partial R} = \frac{C^*(R + \Delta R, L) - C^*(R - \Delta R, L)}{2\Delta R} = \frac{C^*_{j+1,n} - C^*_{j-1,n}}{2h} \tag{36}$$

Substitution of equations (33), (35), and (36) into equation (13) yields, after rearranging, the difference equation

$$C^*_{j,n+1} = a_1 C^*_{j+1,n} + a_2 C^*_{j,n} + a_3 C^*_{j-1,n} \tag{37}$$

where the mesh ratio λ is defined as k/h^2 and

$$\begin{aligned} a_1 &= \frac{\lambda}{V}\left(1 + \frac{h}{2R}\right) \\ a_2 &= 1 - \frac{2\lambda}{V} \\ a_3 &= \frac{\lambda}{V}\left(1 - \frac{h}{2R}\right) \end{aligned} \tag{38}$$

The boundary conditions of equation (14) are replaced by

$$C^*_{j,0} = 0 \tag{39a}$$

$$C^*_{M,n} = 1.0 \tag{39b}$$

$$C^*_{0,n+1} = \frac{4C^*_{1,n+1} - C^*_{2,n+1}}{3} \tag{39c}$$

For the difference equation to be valid, three criteria must be met. These are consistency, convergence, and stability. The difference scheme is consistent with the differential equation provided that the difference equation actually does approximate the differential equation; it is convergent if its solution, at least for a sufficiently fine mesh, is a close approximation to the exact solution of the differential equation; and it is stable if any cumulative errors introduced at the boundary or initially remain bounded as the computation progresses. Also, the problem of round-off errors must be considered. The difference scheme used to approximate equation (13) satisfies the properties of consistency, convergence, and stability (16) provided that

$$1 - \frac{h}{R} \geq 0 \tag{40}$$

and

$$1 - \frac{2\lambda}{V} \geq 0 \tag{41}$$

Equations (40) and (41) are actually restrictions on the mesh size. Equation (40) states that, since R = 1.0, h must be equal to or less than 1.0. However, once the mesh width is set, equation (41) dictates the length of "march step" which is allowed. The error-bound for this scheme is of the order of h^2 (16).

In the numerical calculations used for the solution of the difference equation, a mesh ratio of $\lambda = 0.10$ with $h = 0.10$ was used. The numerical accuracy of this mesh size was checked by employing a smaller mesh size, $h = 0.05$. The difference in computed results between using ten

segments in the radius R and 20 segments was negligible and ten segments were deemed sufficient.

At the initial boundary, n = 1, the concentrations and velocities are given for each mesh point. The initial dimensionless velocity is 1.0, and C^* is zero at all points except j = 10. Trouble at n = 1 and j = 10 arises from the fact that the concentration is zero at an infinitesimal distance "upstream" and is 1.0 at an infinitisimal distance "downstream" of this point. The procedure used was to assign an average value of 0.5 to $C^*_{10,1}$ and $V_{10,1}$ in order to start the computation.

Langhaar velocities for n = 2 and j = 0,1,2....., 10 were first calculated. The values of σ given in Table 1 can be expressed as

$$\sigma = LSc \tag{42}$$

where L = nk.

From a knowledge of σ, a value of γ can be obtained for use in equation (15). However, to utilize the computer it was convenient to reduce Table 1 into the three equations

$$\gamma = \exp(1.4448 - 7.937\sigma);\ \sigma > 0.0947 \tag{43}$$

$$\gamma = (0.1148 + 3.98\sigma)^{-1};\ 0.0947 \geq \sigma > 0.0143 \tag{44}$$

$$\gamma = \exp(2.895 - 0.415 \ln(1000\sigma));\ \sigma \leq 0.0143 \tag{45}$$

The bessel functions of equation (15) were expressed in series notation for use in the computer. The modified Bessel function is defined as

$$I_n(\gamma) = i^{-n} J_n(i\gamma) \tag{46}$$

Using the known velocities at n = 1, j = 0,1,2...,10, the coefficients of equation (37) were calculated. At L = 0.200, a_2 becomes equal to zero, but since the profiles are nearly fully established at L = 0.100, numerical calculations are not required for L > 0.100.

The concentrations at all n = 2 (except j = 0 and j = 10) could then be calculated from equation (37). $C^*_{10,2}$ was specified as 1.0 and $C^*_{0,2}$ was calculated from equation (39c). The procedure was repeated for the next march step and so on to L = 0.100. This procedure established the concentration field in the entrance length.

Equation (20) was used to determine the molar flux at the wall for each length point. The diffusivity, the pipe radius, and the concentration at the wall were constant for a given temperature and run. The pipe radius used was that obtained from the experimental data. The concentration at the wall was calculated from the vapor pressure (7) assuming that the ideal gas law applied.

$$C_{Aw} = \frac{P^o}{P_T} = \frac{\exp\,(-8670.795/T + 26.59965)}{(82.06)T\,(P_T)} ; \qquad (47)$$

$$[T] = {}^\circ K$$

$$[P_T] = \text{mm Hg}$$

The local mass-transfer Nusselt number was calculated from equation (24) with the bulk concentration calculated from equation (27) using Simpson's rule for the integration. In order to calculate the concentration gradient at the wall, it was assumed the concentration profile was parabolic near the wall.

$$C_A^* = C_{Aw}^* + a(1-R) + b(1-R)^2 \qquad (48)$$

The concentrations at R = 0.8 and 0.9 were used to evaluate the constants a and b. After differentiating, the slope at the wall was expressed in the following convenient computing equation

$$\left(\frac{\partial C^*}{\partial R}\right)_{R=1} = -5\left[4C^*_{M-1,n} - C^*_{M-2,n} - 3C^*_{M,n}\right] \qquad (49)$$

The numerical scheme was used to calculate the concentration field for $L \leq 0.100$. The Graetz equation applied to mass transfer was used to extend the results for $L > 0.100$. The mathematical derivation of the Graetz equation will not be dealt with here since it appears elsewhere in the literature (21), and only a brief outline will be presented.

Assuming that the velocity is fully developed at z = 0, the dimensionless velocity term can be expressed as

$$V = 2(1 - R^2) \qquad (50)$$

Substituting this into equation (7), and solving with the appropriate boundary conditions, gives the concentration field as

$$\frac{\theta_A}{\theta_o} = \sum_{n=1}^{\infty} C_n Y_n \exp\left(-\lambda_n^2 2 \frac{\mathfrak{D}_{AB} z}{D^2 v_m}\right) = \sum_{n=1}^{\infty} C_n Y_n \exp(-\lambda_n^2 L/2) \qquad (51)$$

The bulk concentration is

$$\frac{\theta_b}{\theta_o} = \sum_{n=1}^{\infty} \frac{8\left(\frac{\partial Y_n}{\partial y}\right)_{y=1}}{\lambda_n^3 \left(\frac{\partial Y_n}{\partial \lambda_n}\right)_{y=1}} \exp\left(-\lambda_n^2 L/2\right) \tag{52}$$

and the slope of the concentration profile at a particular L is

$$\frac{\partial \theta_A}{\partial r} = \theta_o \left[\sum_{n=1}^{\infty} C_n \left(\frac{\partial Y_n}{\partial y}\right)_{y=1} \exp(-\lambda_n^2 L/2) \right] \tag{53}$$

The local molar flux, local mass-transfer Nusselt number, and mean mass-transfer Nusselt number, defined by equations (20), (24) and (28), respectively, are

$$(N_{Aw})_{loc} = \frac{\mathcal{D}_{AB}\,\theta_o}{r_w} \left[\sum_{n=1}^{\infty} C_n \left(\frac{\partial Y_n}{\partial y}\right)_{y=1} \exp\left(-\lambda_n^2 L/2\right) \right] \tag{54}$$

$$(Nu_{AB})_{loc} = \frac{\sum_{n=1}^{\infty} C_n \left(\frac{\partial Y_n}{\partial y}\right)_{y=1} \exp\left(-\lambda_n^2 L/2\right)}{\sum_{n=1}^{\infty} \frac{8\left(\frac{\partial Y_n}{\partial y}\right)_{y=1}}{\lambda_n^3 \left(\frac{\partial Y_n}{\partial y}\right)_{y=1}} \exp\left(-\lambda_n^2 L/2\right)} \tag{55}$$

and

$$(Nu_{AB})_m = -\frac{1}{4L} \ln \sum_{n=1}^{\infty} \frac{8\left(\frac{\partial Y_n}{\partial y}\right)_{y=1}}{\lambda_n^3 \left(\frac{\partial Y_n}{\partial \lambda_n}\right)_{y=1}} \exp\left(-\lambda_n^2 L/2\right) \tag{56}$$

At present, only the first ten eigenvalues (C_n, λ_n, $(\partial Y_n/\partial_y)$, and $(\partial Y_n/\partial\lambda_n)$) of equations (54), (55), and (56) are available. These were determined by Brown (22).

Theoretical results were obtained by programming the numerical difference method and equations (54), (55), and (56) using Brown's eigenvalues on a Digital computer located at the Rich Electronic Computer Center at the Georgia Institute of Technology, Atlanta, Georgia. The programs used for computation appear in Appendix B. They are written in the Burroughs version of Algol. The computer employed for the calculations was a Burroughs 220 machine with a 5,000-word memory and auxiliary magnetic tape storage units.

CHAPTER IV

EQUIPMENT AND INSTRUMENTATION

Mass-Transfer System.--The experimental test system is shown schematically and pictorially in Figures 6 through 10. The test pipe was a 72.0 inch length of two inch schedule 40 seamless steel pipe with 5.125 inch diameter slip-on type flanges welded to each end. The test pipe was bolted to the inlet plenum chamber and the exit sections with six 3/8-inch bolts. Teflon gaskets were used to insure against leakage. The inlet plenum chamber was constructed of 1/2-inch plywood. A bell-shaped entrance to the test pipe, made from laminated mahogany, was included as an integral part of the inlet plenum chamber. The test air entering the chamber was diffused by a wire screen. The exit plenum chamber was constructed similar to the inlet chamber. However, when preliminary runs indicated that naphthalene was depositing inside the exit chamber it was replaced by a straight length of two-inch pipe with a flange at one end designed to mate with the test pipe flange. Pressure taps were located in the inlet and exit chambers such that chamber air pressure and pressure drop measurements could be measured with an inclined manometer. An insulated air bath chamber, 17 by 18 by 97 inches, was constructed from 1/2-inch plywood to house the inlet and exit plenum chambers and test pipe. The front panel was removable to provide easy access to the plenum chambers. Rubber gasket material was used to seat the front panel when it was bolted into position. All inside surfaces were insulated with one-inch, aluminum backed fiberglass insulation.

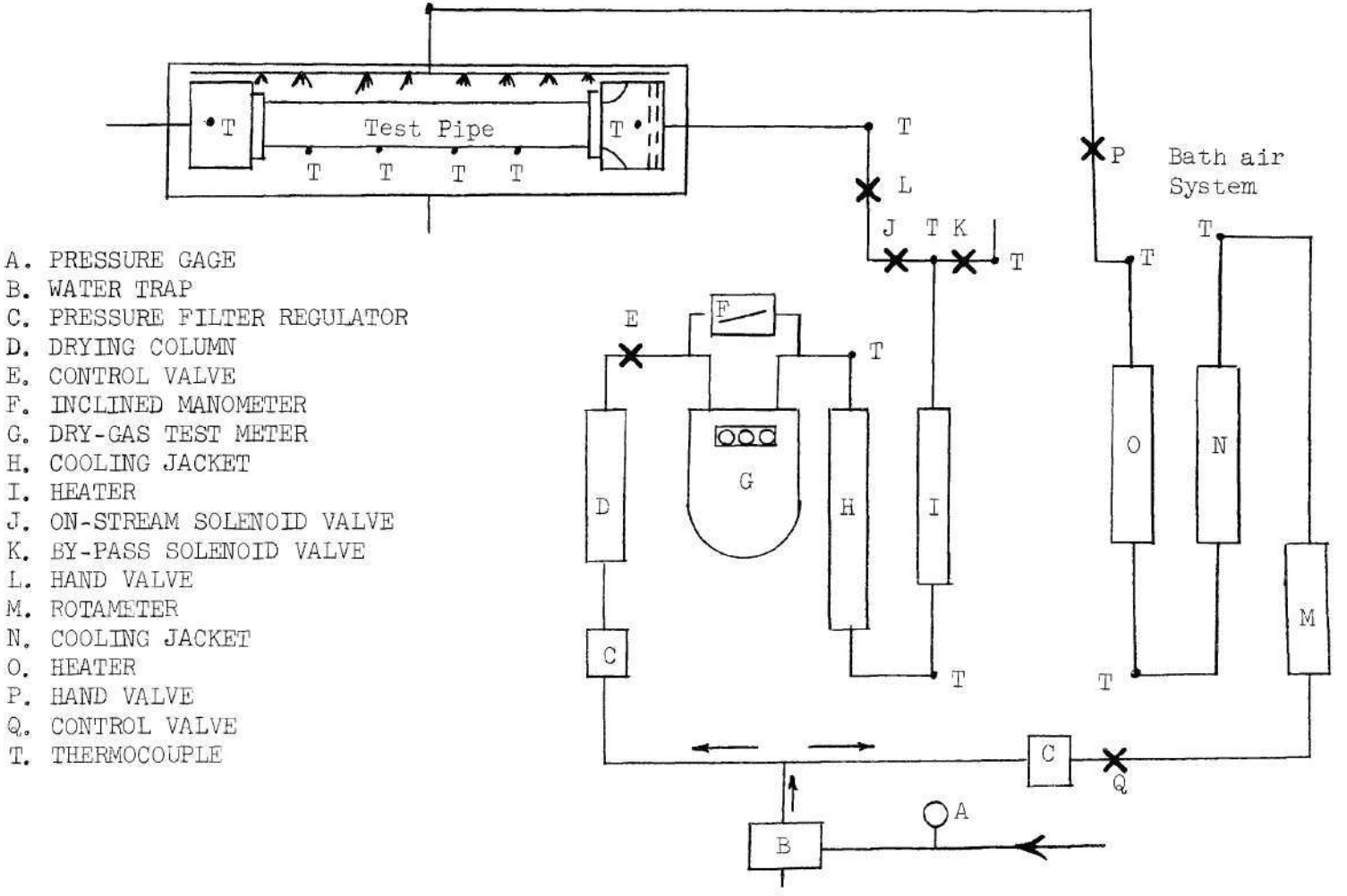

Figure 6. Schematic Diagram of Mass-transfer Equipment.

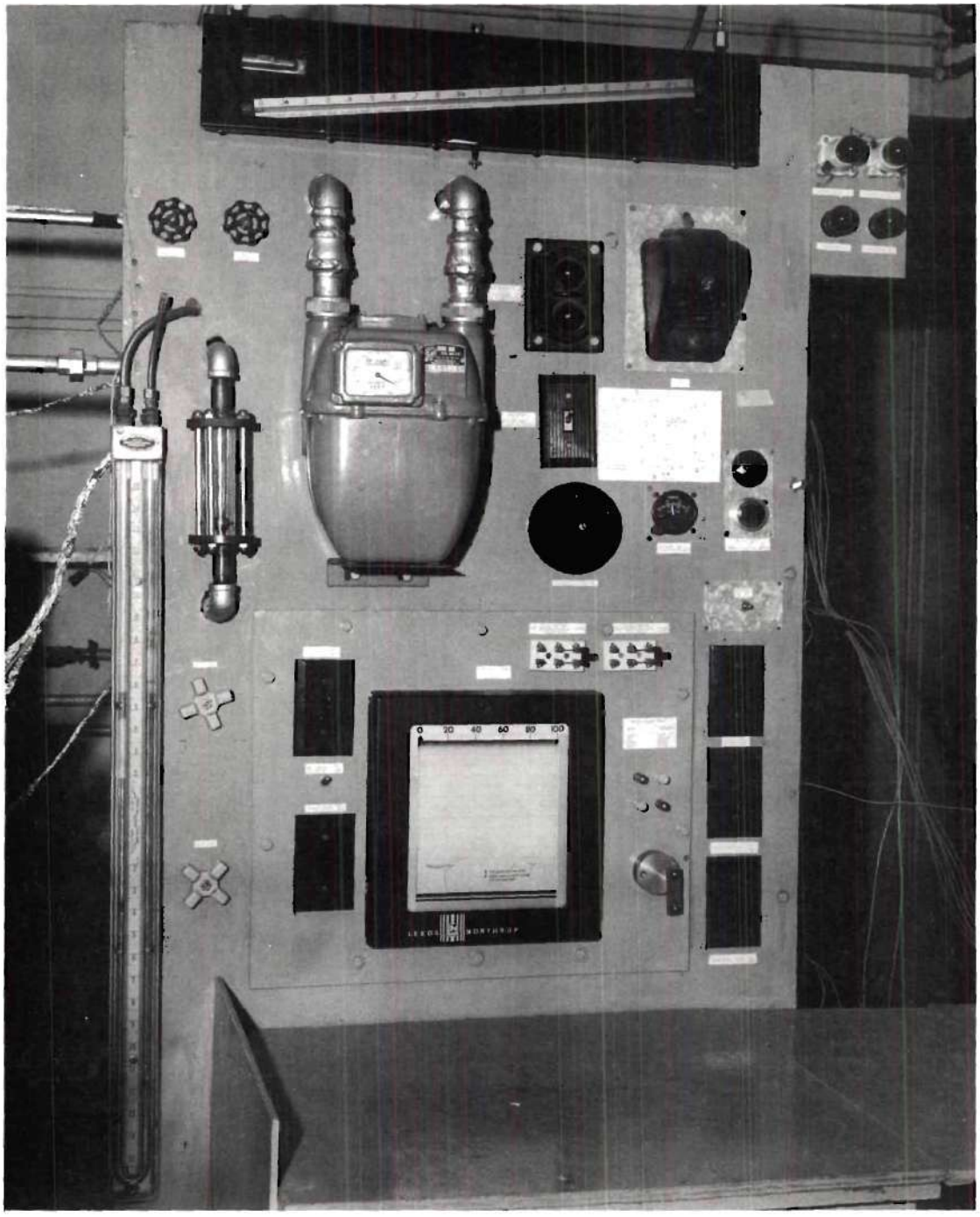

Figure 7. Panel Board.

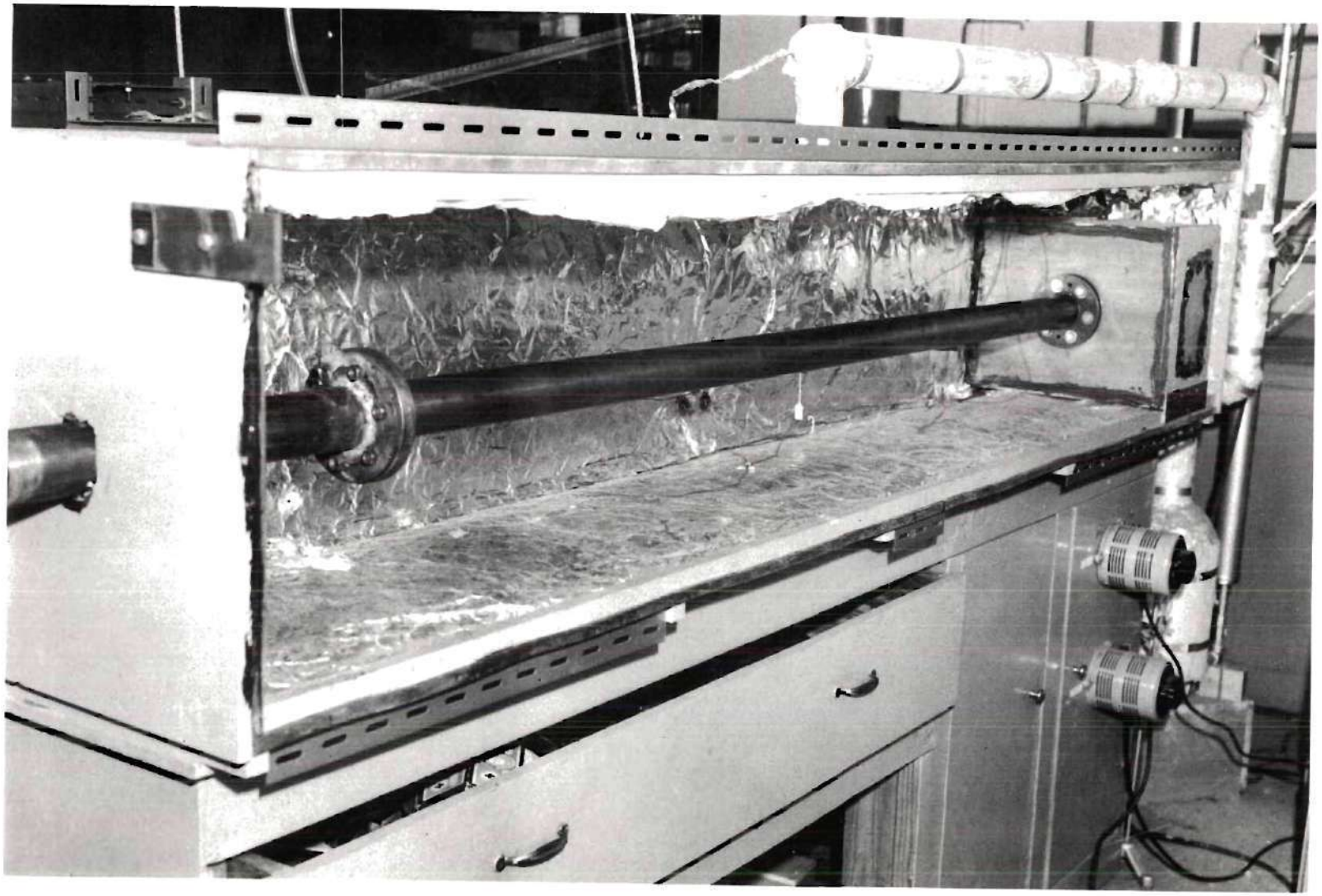

Figure 8. Air Bath Chamber, Test Pipe, Entrance Plenum Chamber, and Exit Pipe. Bath Chamber Lid is Not Shown.

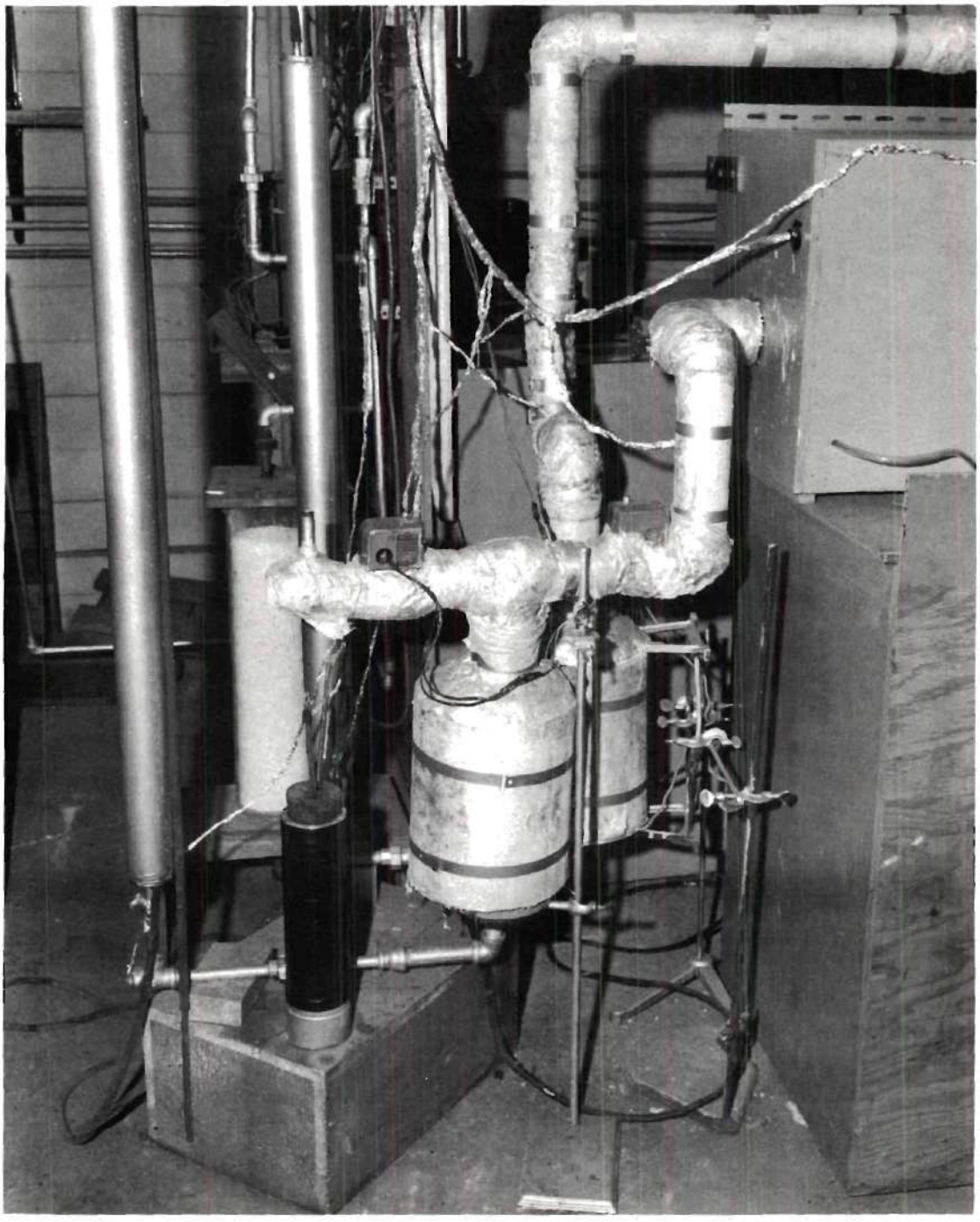

Figure 9. Cooling Jackets, Drying Column, Heaters, and Auxillary Piping.

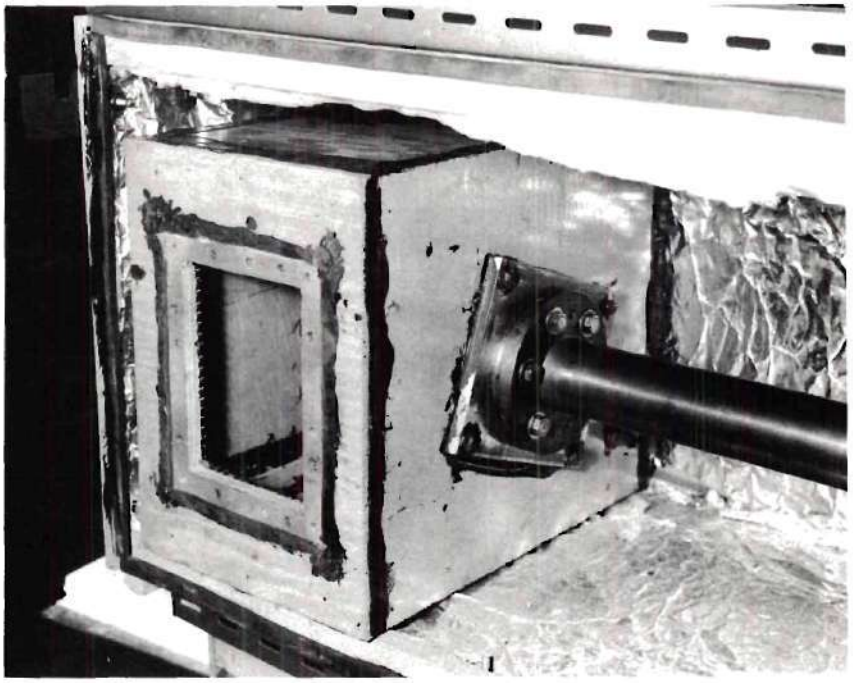

Figure 10a. Exit Plenum Chamber.

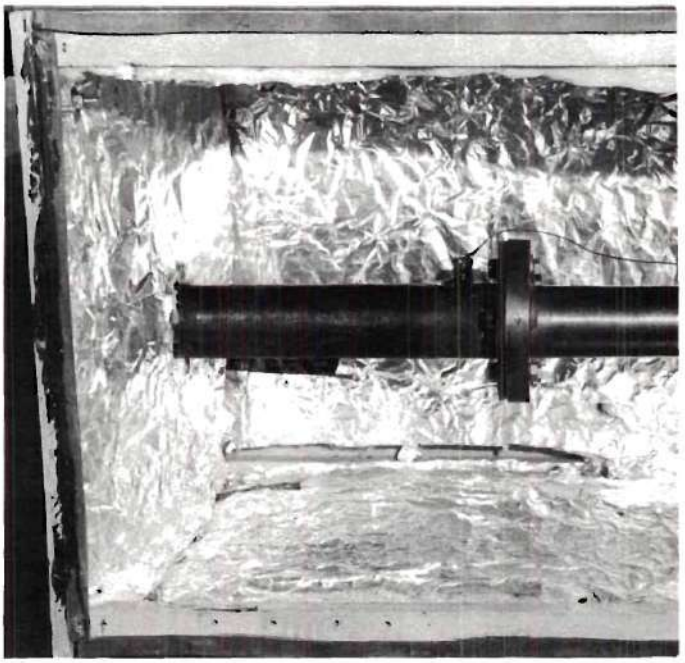

Figure 10b. Exit Pipe.

The bath air, which maintained a constant temperature environment for the test pipe, flowed in series through a filter regulator, rotameter, cooling jacket, and heater. A manifold distributed the bath air throughout the bath chamber. The air was vented to the atmosphere from a one-inch pipe located in the back wall of the bath chamber.

The test air supplied to the inlet plenum chamber flowed, in series, through a filter regulator, Drierite drying column, dry-gas test meter, cooling jacket, and heater. A by-pass line was located downstream of the heater such that the test air could be vented to the atmosphere during warm-up. Normally closed solenoid valves, operated by a common switch, were used to direct the air to either the test pipe or the atmosphere. An electric timer was made operative when the on-stream solenoid was energized. An override switch was included to allow both solenoid valves to be operated in parallel. The 300 cfh capacity dry-gas test meter was capable of measuring to the nearest 0.01 cubic foot. An inclined manometer measured pressure drop across the meter.

The cooling jackets were installed during construction to aid in temperature control if necessary. However, they were not used in this study. The air used in both the bath chamber and test pipe was supplied from a compressor located in the building. Power to the electric heaters was regulated by a powerstat and off-on control supplied by Brown Potentiometer Pyrometers. All heated air lines were lagged with asbestos insulation. Test air and bath air line pressure taps for a manometer were located up-stream from the respective flow-rate meters.

Copper-constantan thermocouples were used to measure the temperature of the air entering and leaving the test pipe, the outside test pipe

wall, and various air temperatures throughout the system. The locations of the thermocouples are shown in Figure 6. The electromotive force produced by the thermocouples was measured with a Leeds and Northrup portable precision potentiometer.

Air leaks were sealed with Resiweld Black Sealant, No. 400.

Coating Equipment.--The purpose of the coating equipment was to apply a thin, smooth coat of naphthalene to the inside pipe wall. The test pipe, containing crystalline naphthalene, was spun on its longitudinal axis in a horizontal plane. Heat was applied externally with a gas burner until the naphthalene melted. After the molten naphthalene had spread along the length of the test pipe it was solidified by pouring ice water over the test pipe.

The equipment used is shown schematically and pictorially in Figures 11 through 15. The test pipe was rotated on flanged axles which mated to the test pipe flanges. A flanged axle was made by welding a six inch piece of one-inch diameter steel bar to a blank flange having the same dimensions as the pipe flange. Six 3/8-inch bolts were used to join each pair of flanges and dowel pins assured proper positioning. Teflon gaskets were used to prevent leakage of coating material. The test pipe, when in position for coating, was supported at each axle with a Seal Master SF flange-unit bearing mounted on a face plate which moved vertically in a support stand. Lateral alignment of the test pipe was fixed by bolting the bearing support stands to the table top. However, horizontal alignment could be effected by vertical adjustment of the face plates with the two adjusting bolts on which each face plate rested. The face plates were locked in position with an Allen-head screw

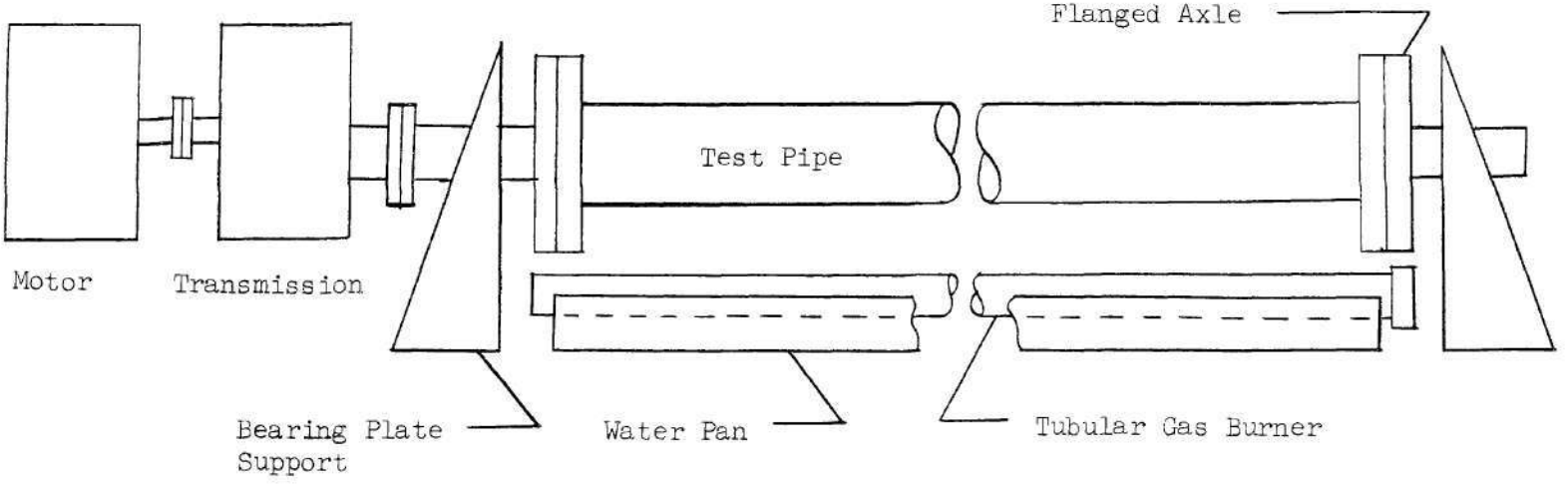

Figure 11. Schematic Diagram of Coating Equipment.

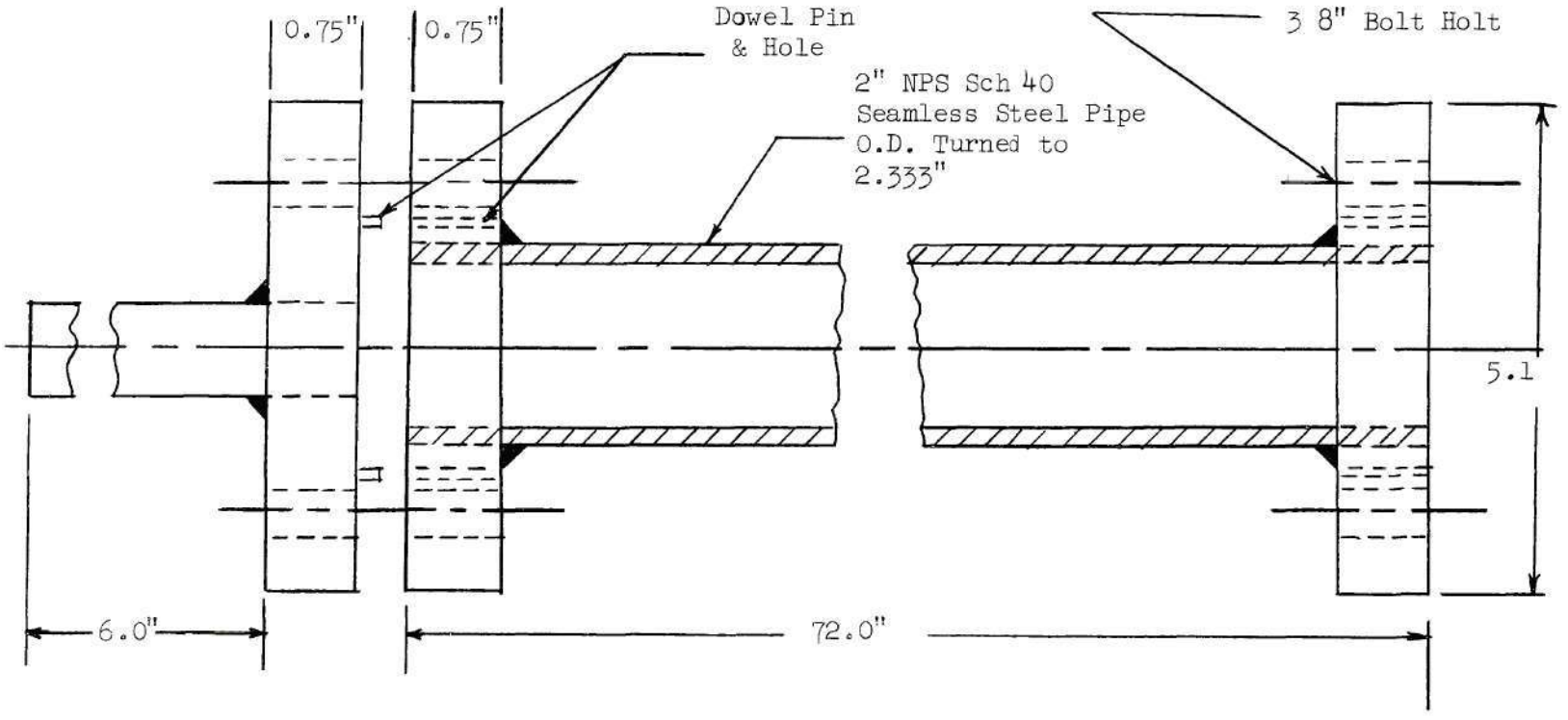

Figure 12. Test Pipe and Flanged Axle.

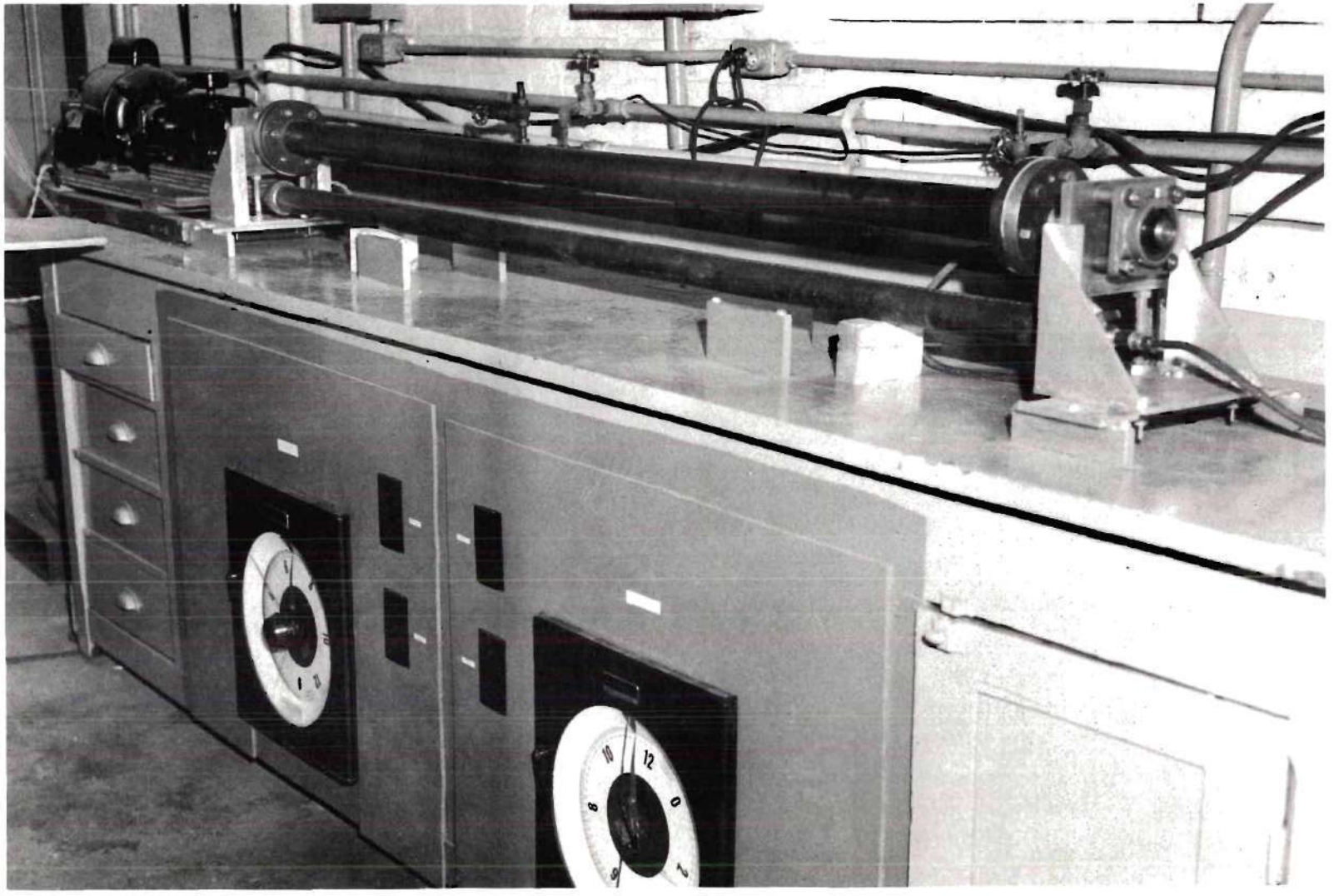

Figure 13. Test Pipe in Position for Coating Procedure. Water Pan is Not Shown.

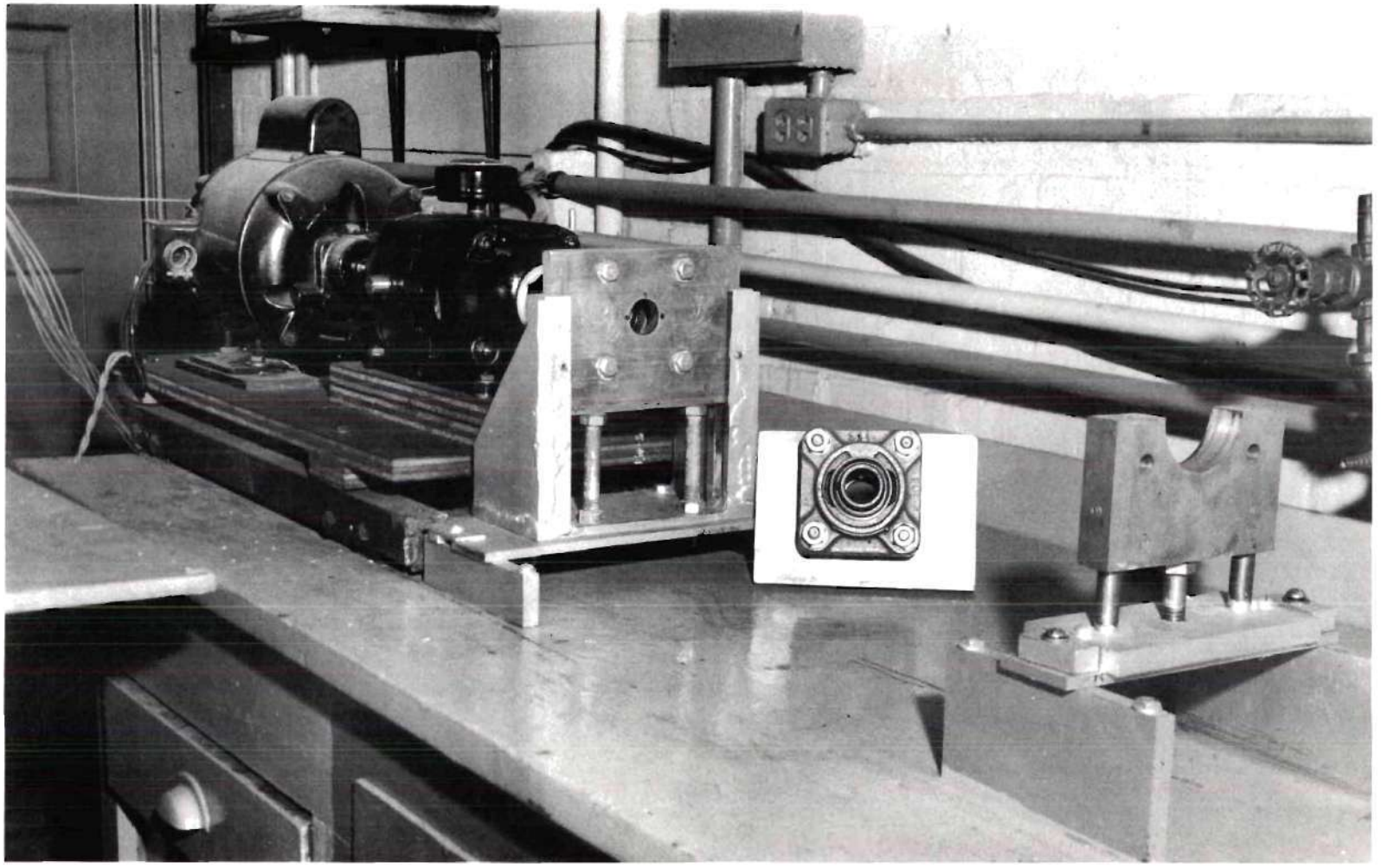

Figure 14. Drive and Support Components for Coating and Tracing Procedures. l to r., Motor, Transmission, Bearing Plate Support with Bearing Plate, Bearing Plate (back view), Pipe Support.

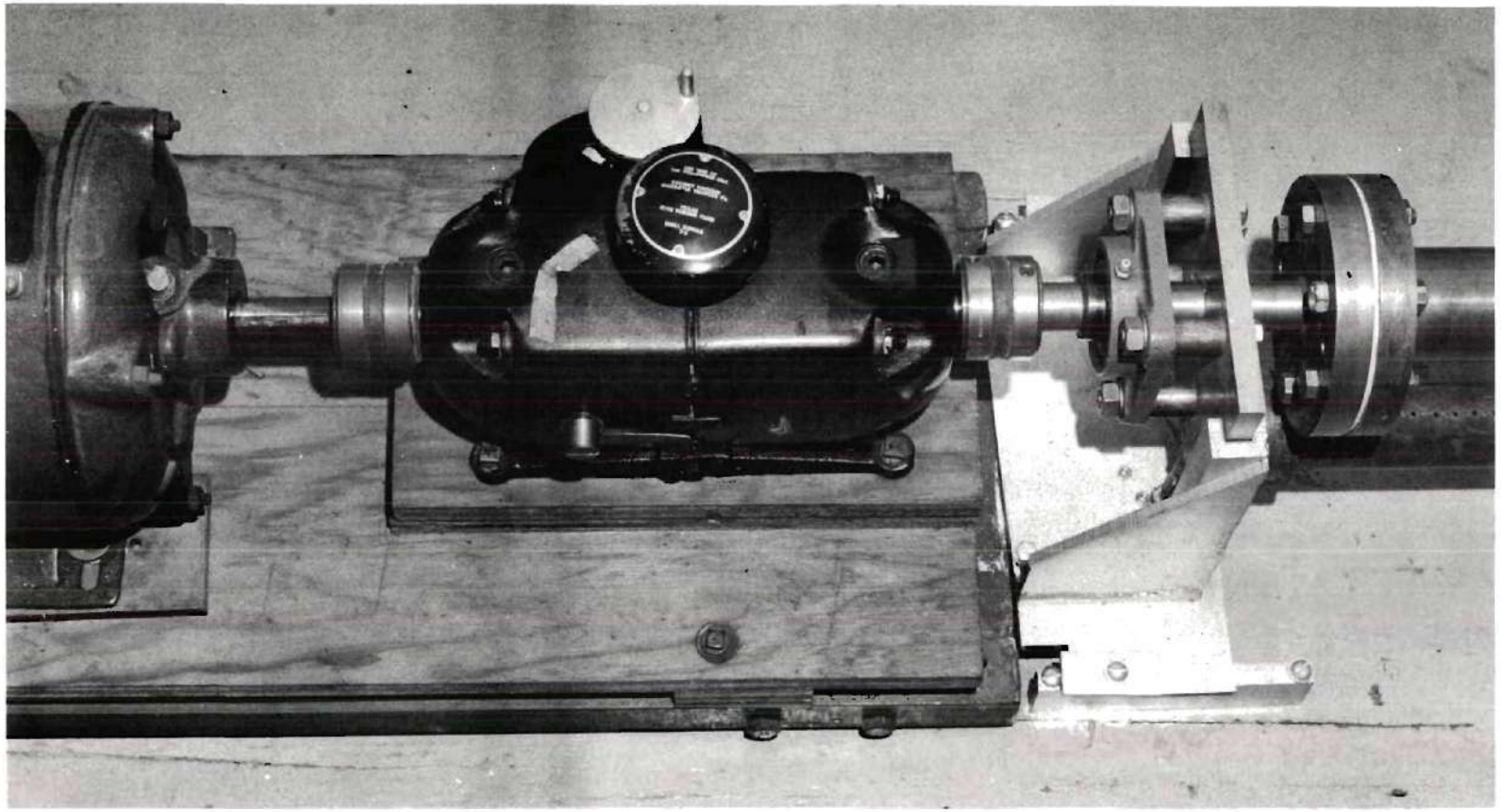

Figure 15. Transmission and Bearing Support Set Up for Coating Procedure.

located in each leg of the face-plate support stands. One axle was coupled to a Vickers 3/4-Hp hydraulic, variable-speed transmission with a flexible coupling. A 1/2-Hp, 115-volt A.C. electric motor was used to drive the transmission. Horizontal alignment of the test pipe was ascertained with a Dumpy Engineer's Level.

The tubular gas burner used to heat the test pipe was a six foot length of 2-inch Sch. 40 steel pipe sealed at one end with a pipe cap. Holes, 1/8-inch in diameter, were drilled along the length of the pipe at 1/2-inch intervals. A standard air-gas mixer introduced city gas into the other end.

A water pan was used to collect the water during the quenching operation.

Surface Trace Equipment and Instrumentation.--The purpose of this equipment and instrumentation was to measure the amount of naphthalene sublimed during a mass-transfer run. This was accomplished by measuring the before and after surface profiles of the naphthalene coating, both relative to the same stationary coordinate. Records of the surface profiles were obtained by use of sensitive strain gages attached to a cantilevered beam equipped with a foot touching the surface. The beam (or tracer arm) was mounted on a nut which travelled through the test pipe on a screw. The output from the strain gages was amplified and fed to a L & N strip-chart recorder. The output of the strain gages was proportional to the position of the tracer foot.

The surface trace equipment and related instrumentation are shown schematically and pictorially in Figures 16 through 22. The tracer arm was made from a two-inch piece of annealed 75S aluminum metal. Preliminary

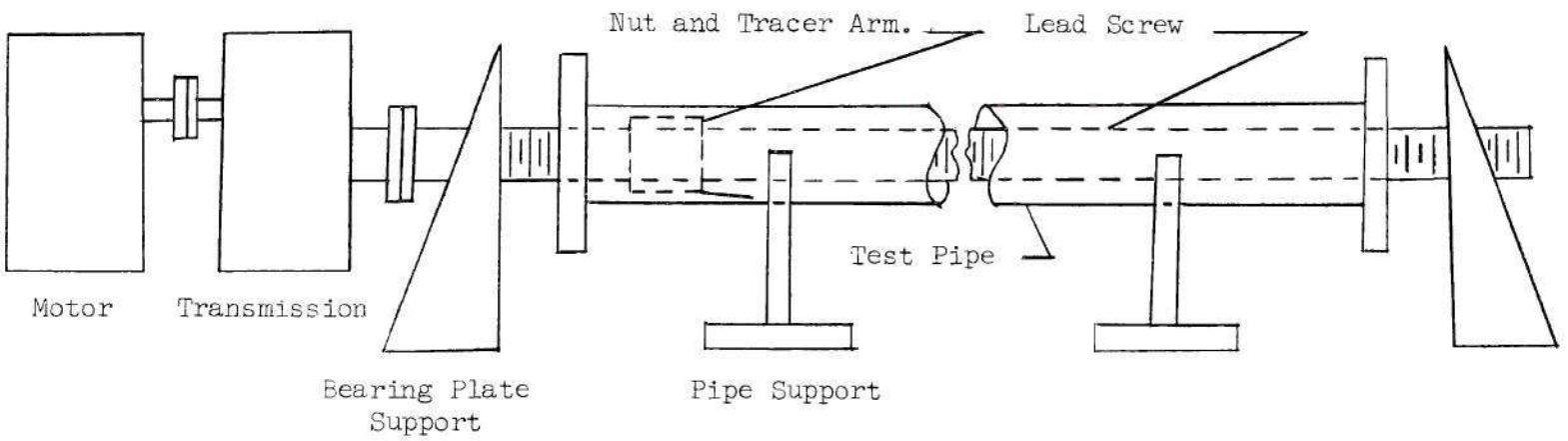

Figure 16. Schematic Diagram of Surface Trace Equipment.

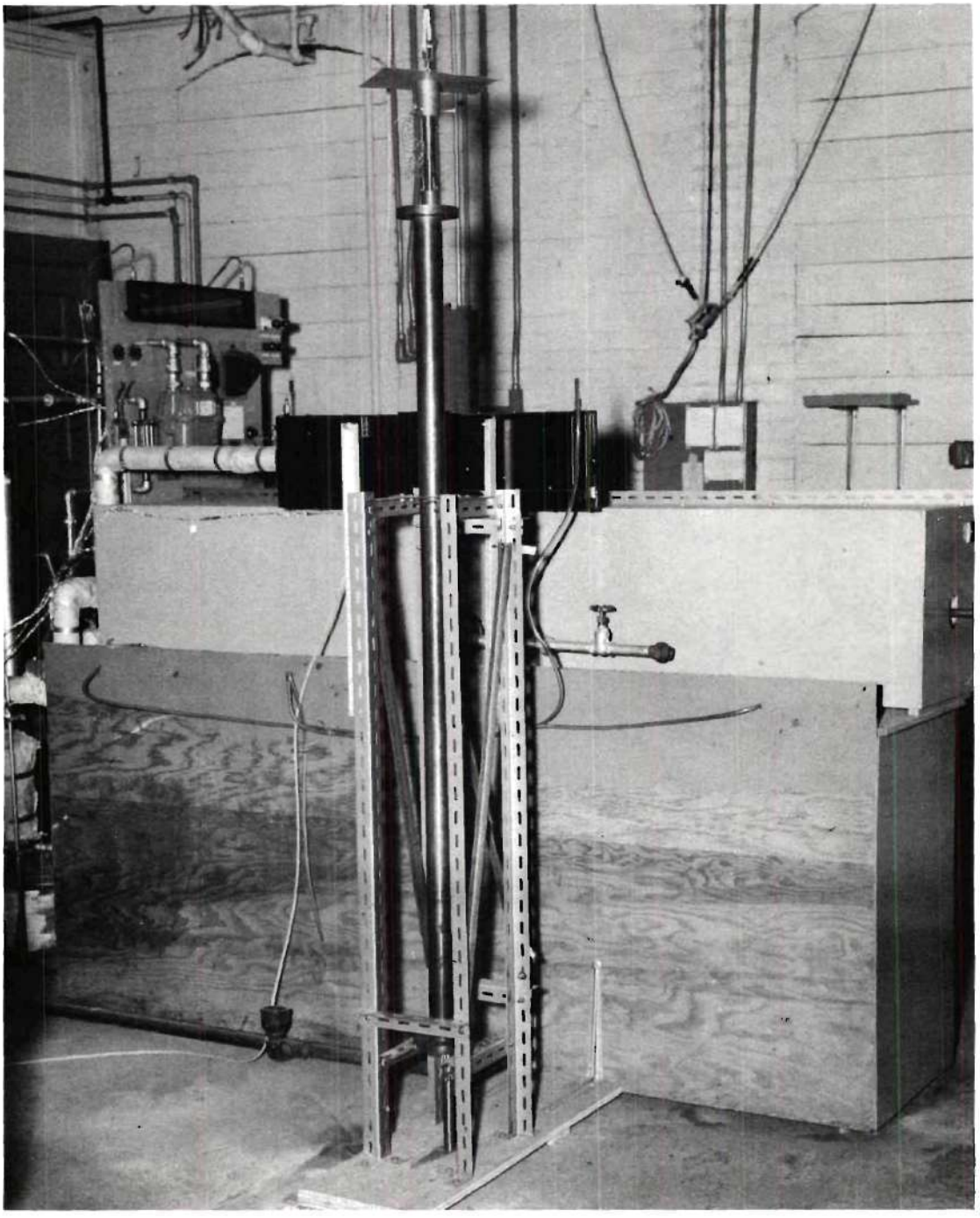

Figure 17. Pipe Stand and Screw Insertion Equipment.

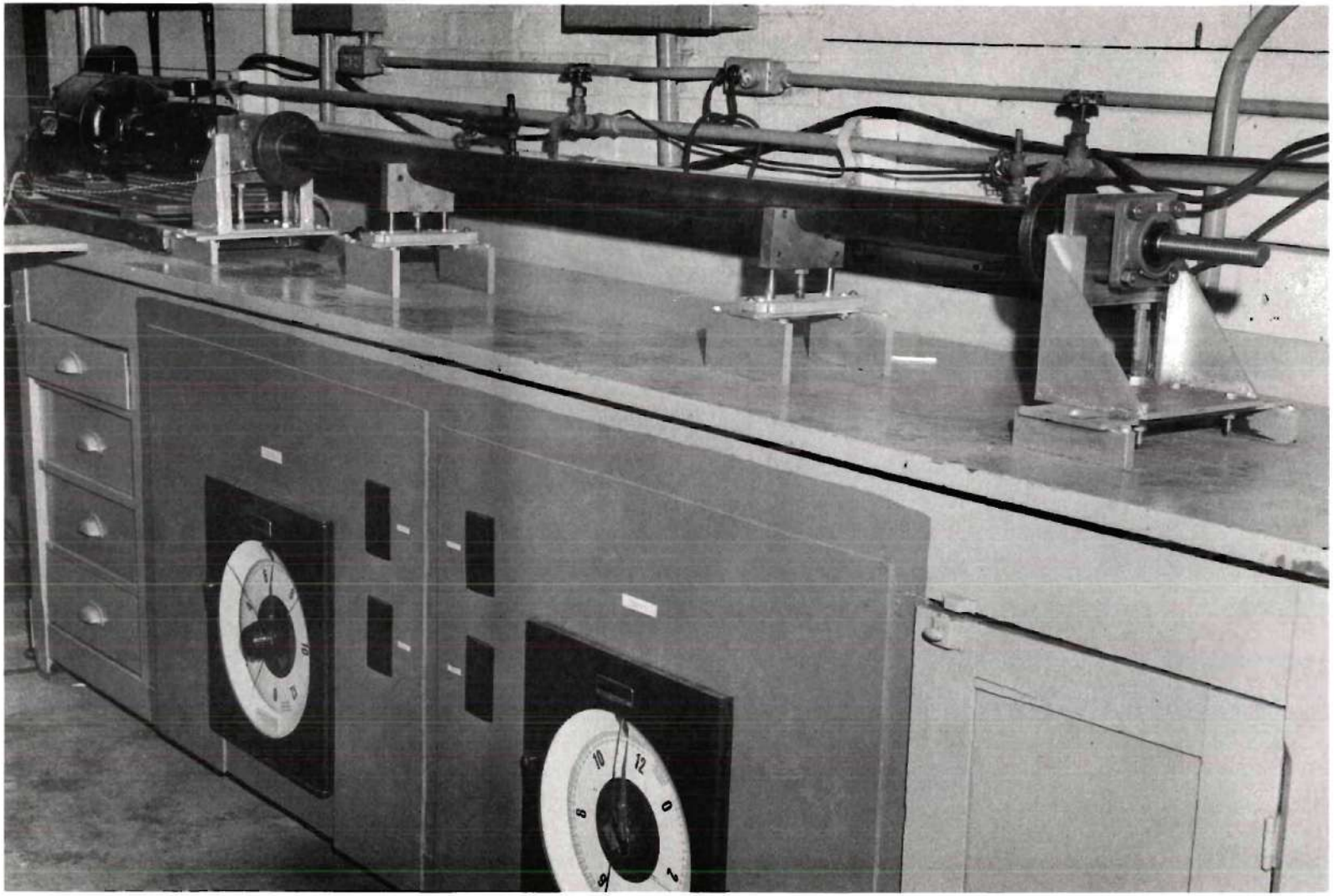

Figure 18. Surface Trace Equipment. (Note Temperature Controllers Below.)

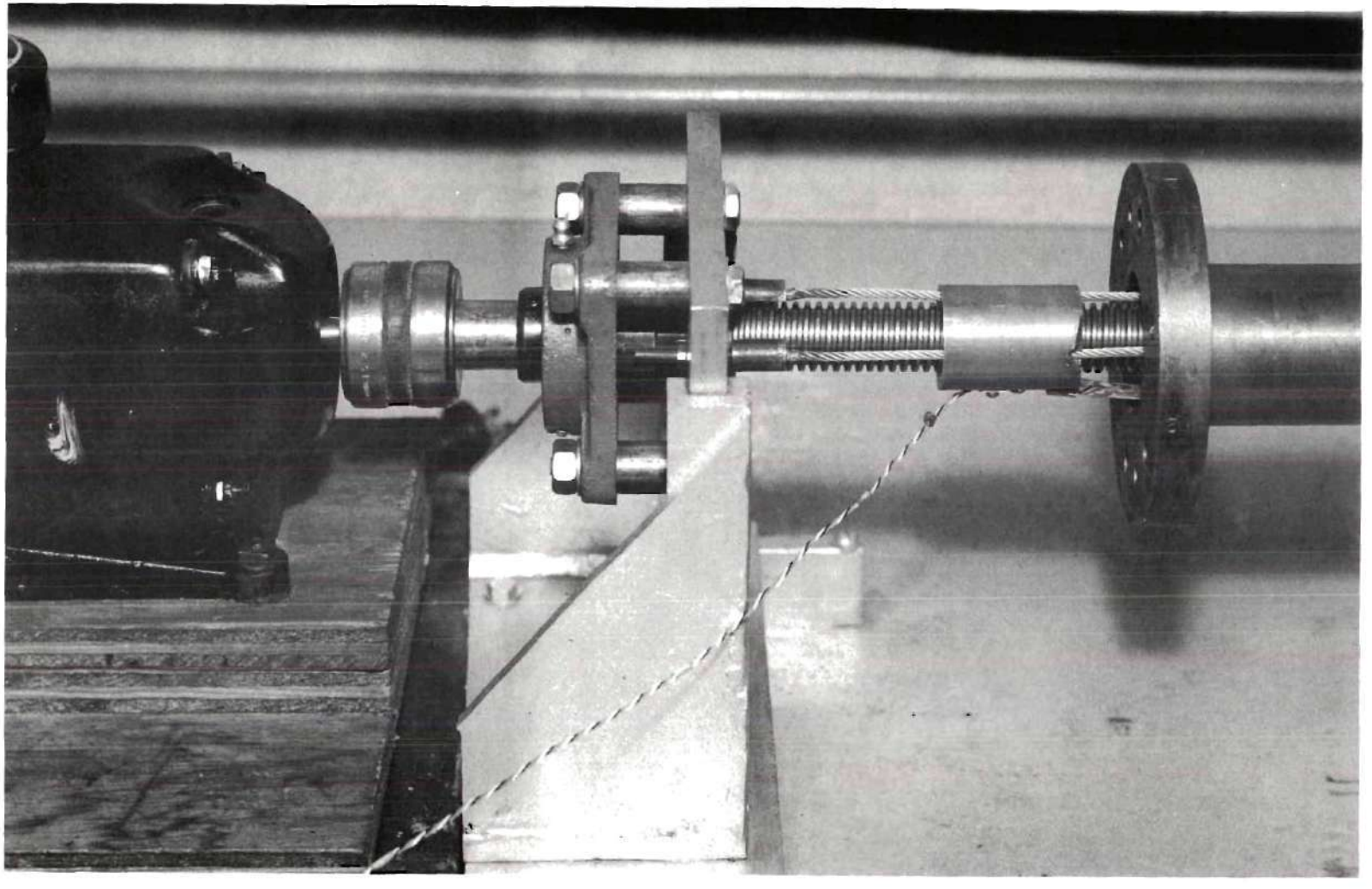

Figure 19. Drive Transmission and Bearing Plate Supports for Tracing Procedure. (Note Guide Wires and Guide Wire Nuts.)

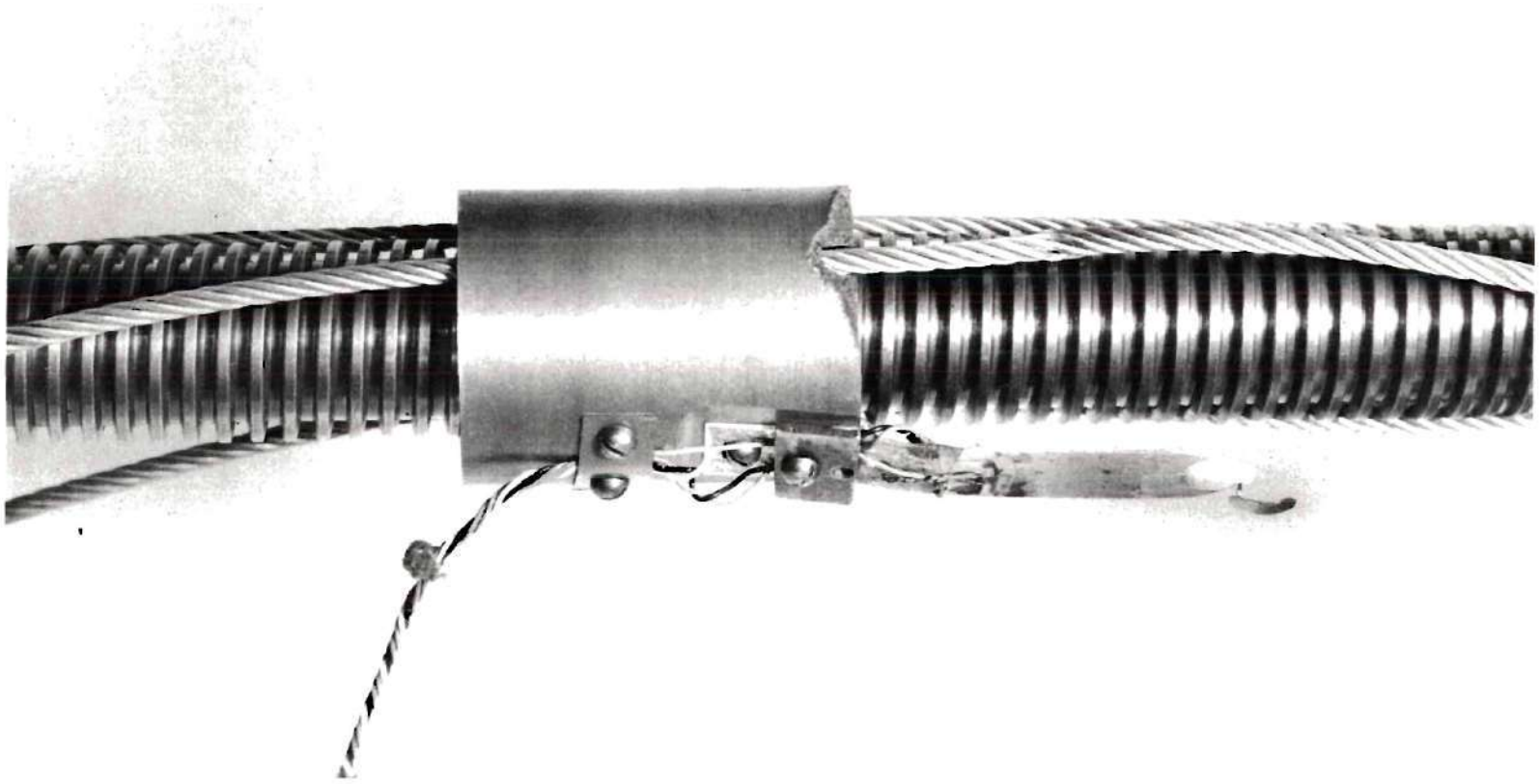

Figure 20. Tracer Nut, Arm, and Foot. (Nut was Damaged During Disassembly.)

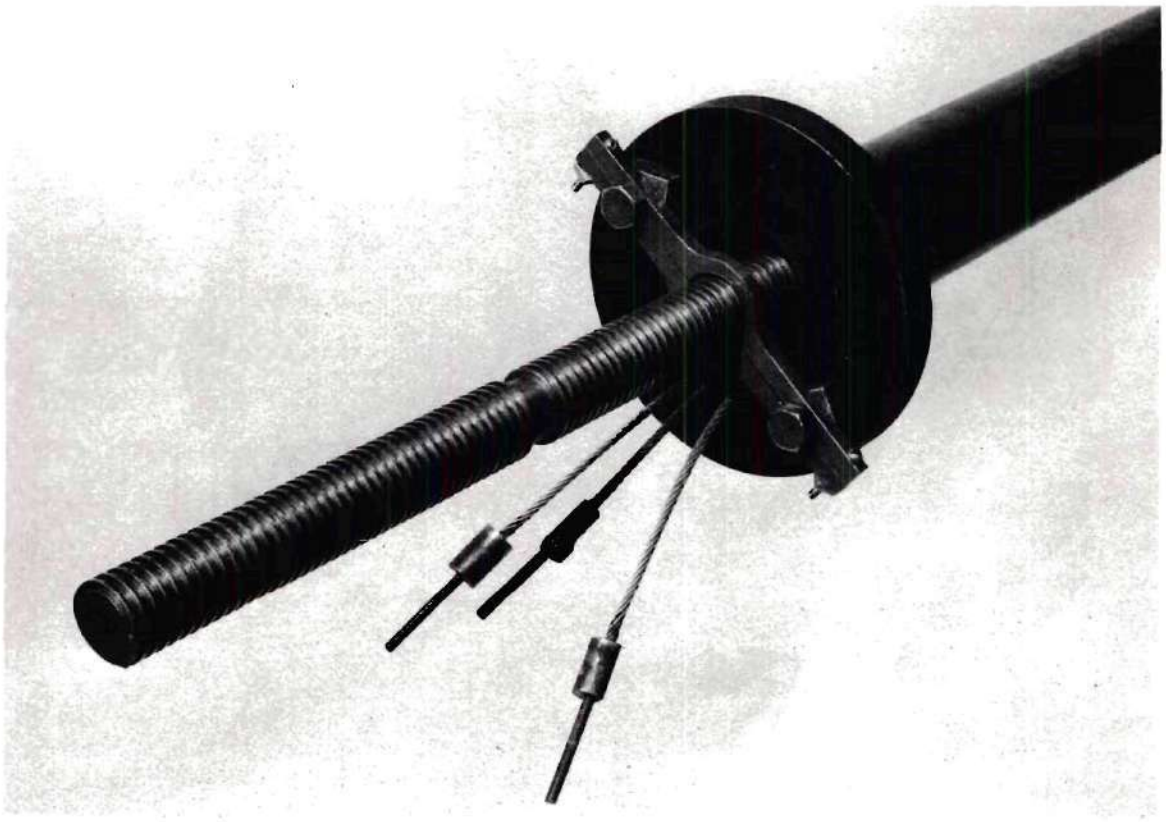

(a)

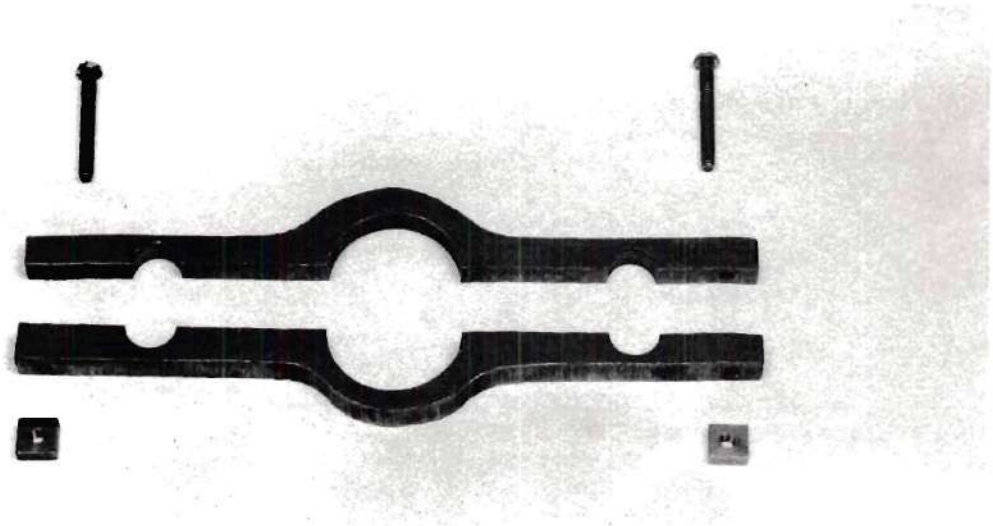

(b)

Figure 21. Centering Clamps.

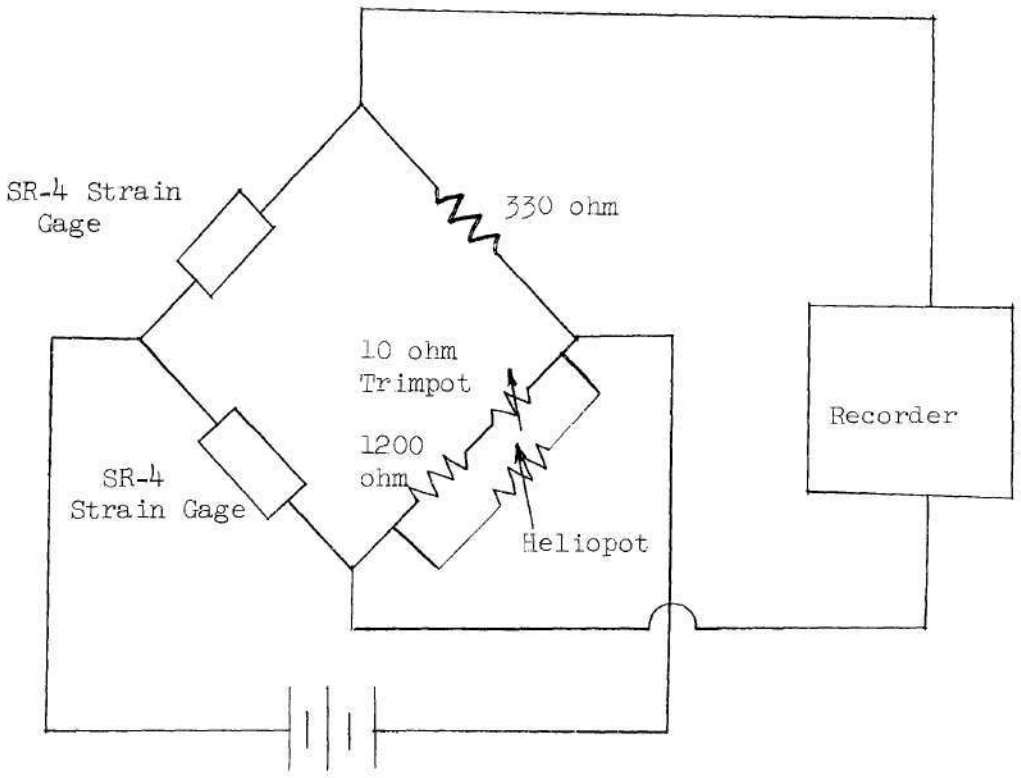

Figure 22. Wheatstone Bridge Circuit.

calculations indicated that a beam 1/2-inch wide and 0.020 inches thick would give the maximum bending deflection without transmitting an excessive pressure to the coating. A thicker tracer arm would cause the tracer foot to exert a greater pressure for the same deflection and would result in the foot scratching the coating. The tracer foot was mounted to a shortened phonograph needle attached to one end of the tracer arm. The tracer arm was cantilevered from a nut which rode through the test pipe on a one-inch diameter screw.

The screw was made from a standard one-inch lathe lead screw. The lead screw, with eight threads per inch, was modified at each end so that it could be used with the existing bearing supports and transmission unit. The threaded length was approximately 86 inches long.

The nut was fabricated from a two-inch length of two-inch diameter brass bar stock. The outside diameter was turned to 1.50 inches. With a portion of the lead screw as a pattern, threads were machined through the center of the nut. Three 1/8-inch guide wire holes were drilled at 90 degree intervals on a 1.125 inch radius. At 180 degrees from the middle guide wire hole, the outside of the nut was beveled at a 3°35' angle for 1-1/4 inches. The tracer arm was cantilevered from this beveled portion.

The guide wires which maintained the nut in an upright position during its travel along the screw were made from 1/8-inch airplane cable. After the guide wires had been inserted through the nut, straight-pull, 1/8-inch bolts were fastened to the ends with silver solder. Tension was applied to the wires by inserting them through holes in the bearing plates and tightening up on the bolts.

The screw was supported and turned by the motor, transmission, bearing plates,and supports used for the coating procedure. The test pipe was held in position by two pipe supports which could be aligned both laterally and vertically by an adjusting bolt and locked in position with Allen-head screws.

A vertical pipe stand centered the test pipe under a pulley system which was used to lower the screw into the pipe. So that the screw and test pipe assembly could be carried without damaging the coating or the tracer arm, centering clamps were used to center the screw relative to the axis of the pipe.

The amount of deflection caused to the tracer arm during a surface trace was measured by two SR-4 strain gages mounted on each side of the tracer arm. The gages were mounted as close as possible to the cantilever support so as to record maximum bending. The gages were series C-11, iso-elastic wire grids with a nominal resistance of 300 ohms. The strain gages comprised two adjacent legs of a Wheatstone bridge circuit. This arrangement doubled the millivolt output from the bridge and eliminated the need for a dummy gage for temperature compensation. The leads from the gages to a Wheatstone bridge circuit were four-strand, twisted stereo wires.

The Wheatstone bridge circuit consisted of the two strain gages, a fixed resistance leg, and a variable resistance leg. A 330 ohm precision resistor was used in the fixed resistance leg. The variable resistance leg, which was used to null the bridge circuit, was made up of a 500 ohm, 10 turn Heliopot in parallel with a 1200 ohm precision resistor and a 10 ohm trimpot. This parallel arrangement made it possible to reduce

the effective resistance of the heliopot from 50 ohms per turn to less than 1 ohm per turn. The trimpot was used in series with the 1200 ohm resistor in order to balance the resistance legs when the heliopot was at half its setting.

The voltage input to the bridge circuit was from a 12-volt wet cell battery. The millivolt output of the bridge, caused by a bending of the tracer arm, was measured and recorded by a Leeds and Northrup Speedomax H, Model S strip-chart recorder. The recorder had a range of zero to five millivolts and a chart drive speed of six inches per minute.

CHAPTER V

PROCEDURES

In the following procedure sections, details are given for the methods of conducting the experimental tests and analyzing the experimental data for a typical run.

A. Experimental Procedures

1. Coating Procedure.--Approximately 600 grams of purified naphthalene crystals were placed in the test pipe and the flanged axles bolted to the pipe flanges. With the bearing plates slipped on the axles, the test pipe was placed into the bearing plate supports and the "drive" axle aligned with the drive shaft of the transmission. Using a Dumpy engineering level, the test pipe was placed in a true horizontal attitude by vertical adjustment of the free axle bearing plate. Once this alignment had been affected the bearing plates were locked in position. The water pan and tubular gas burner were placed beneath the test pipe. With the motor and transmission rotating the test pipe at approximately 120 rpm, the pipe was heated with the tubular burner with additional heat directed on the flanges from a Bunsen burner. Preliminary tests indicated that a 20 minute heating period was sufficient to melt the naphthalene and allow it to be distributed along the length of the test pipe. Following the 20 minute heating period, the burners were turned off and the molten naphthalene solidified by pouring ice water over the

pipe. The test pipe and bearing plates were then removed from the bearing plate supports, dried, and disassembled.

2. Surface Trace Procedure.--The screw and nut assembly were prepared for insertion into the test pipe by first wrapping the guide wire bolts to the screw with masking tape so that the naphthalene surface would not be damaged as the screw was dropped through the pipe. The screw was raised up with the pulley system such that the test pipe could be mounted into the pipe stand and centered under the screw. The screw was then lowered very slowly into the test pipe. The pipe stand was designed such that the bottom end of the test pipe was held eight inches above the floor. This allowed proper positioning of the screw in the pipe when the screw was lowered to the floor. After the centering clamps were attached to the screw and pipe at each pipe flange, the assembly was transferred to a table and the bearing plates slipped onto the screw. The entire assembly was then carefully placed in the bearing supports and the centering clamps removed. The test pipe then rested in the pipe supports. The guide wires were inserted through the bearing plates and tension applied to the wires with nuts on the back faces of both bearing plates. The strain gage leads were connected to the Wheatstone bridge circuit by means of terminal lugs mounted on the panel board and the test pipe was vertically adjusted such that the bridge circuit would record approximately 3.0 millivolts when the tracer foot was 1/2-inch inside either end of the test pipe. This allowed a positive millivolt reading at the ends of the pipe and also assured that the bridge circuit range would not be exceeded during a trace.

The nut and tracer arm were run to the right end of the screw (see Figure 16 for direction orientation) and the test pipe positioned for the

first trace. Four traces were made before and after each run. The test pipe was marked in such a way that a trace could be made along a line that corresponded to the top of the pipe during the transfer run. Similarly, three other marks were placed at 90-degree intervals around the pipe such that a bottom and two side traces could also be obtained. By means of a spacer, the test pipe was positioned a fixed distance from the right-hand bearing plate. With the tracer foot placed just outside the mouth of the pipe, and the foot and end of the pipe covered with a plastic sheet to eliminate air currents, a "zero point start" was obtained on the recorder by an adjustment of the heliopot. The motor was started and the rotational speed of the screw was quickly adjusted to give the nut an approximate traverse speed of about nine inches per minute. As the nut traveled through the pipe, the leads from the strain gages were withdrawn by hand. The leads had previously been marked at irregularly spaced, but known distances from the nut, with masking tape. As the marks emerged from the pipe they were noted on the chart paper so as to approximately locate the position of the tracer foot in the pipe.

As the nut approached closer to the surface of the pipe due to the sag in the screw, the recorder range was changed by rotating the heliopot one revolution at a time. A typical trace usually required five or six revolutions in the first half of the pipe. After midpoint was passed this procedure was reversed until the pot had been returned to its original setting. After completion of a trace, the foot was allowed to hang free and a "zero point finish" was obtained.

On completion of the surface traces the guide wires were released and the centering clamps replaced. The pipe and screw were removed from

the bearing supports, placed on the pipe stand, and the screw removed. Again, extreme care was exercised so as not to cause damage to the naphthalene coating.

The above procedure was repeated following the mass-transfer run.

3. Mass-Transfer Procedure.--The test pipe was weighed on a triple beam balance and then bolted between the inlet plenum chamber and the exit section. Teflon gaskets were used to insure against leakage. Four thermocouples were taped on the outer surface of the pipe at regularly spaced intervals and the bath chamber lid set in place and bolted tight.

The bath air system was turned on and the controller regulated to the desired temperature. During the warm up period, the exit section was capped and the hand valve (valve L in Figure 6) in the test air line was closed to prevent any premature loss of naphthalene from the test pipe. Since the test pipe and bath air required considerably more time to reach thermal equilibrium than the test air, the test air was not turned on until the pipe was up to temperature.

The test air system was brought up to temperature by venting the air to the atmosphere through the by-pass solenoid valve. It was found that the heat generated in the solenoid valves was conducted through the valve bodies to the test air thus causing a delay in attaining the run temperature when the air was placed "on-stream" through a cold valve. Therefore, the over-ride switch was thrown so that the on-stream solenoid valve would be at operating temperature at the start of the mass-transfer run.

After both air systems had attained operating temperature, the over-ride switch was cut-off, the hand valve opened, and the exit section

uncapped. To start a run the solenoid switch was thrown to the on-stream position, thereby, changing the air flow to the test pipe and starting the electric timer. Temperature readings of the inlet and outlet test air and the test pipe wall were taken every five minutes for the first fifteen minutes and then every fifteen minutes thereafter. Air line pressures, chamber pressures, volumetric flow rate and elapsed time were also recorded. Following the transfer run the test pipe was reweighed, and an after trace made.

For the experimental runs in this study, the concentration of naphthalene in the entering test air, C_{Ao}, was zero.

4. Calibration Procedure.--The copper-constantan thermocouples used in these experiments were calibrated, after installation, with a mercury-glass thermometer which had been certified by the National Bureau of Standards. Since all thermocouples were made from the same roll of wire, only one couple was calibrated. The thermocouple was wrapped in close contact with the thermometer bulb and immersed in a constant temperature oil bath to a depth of 76 mm. The emf output from the thermocouple was measured with a L & N potentiometer at temperature intervals of 10° C from 30° C to 160° C. The calibration curve is shown in Figure 23.

The tracer arm was calibrated to determine the millivolt output from the Wheatstone bridge as a function of tracer arm deflection. This was accomplished by placing a micrometer beneath the tracer foot such that the foot could be raised a known amount. The millivolt output from the Wheatstone bridge corresponding to 5 mil increments was read from the strip chart recorder. In order to eliminate air currents, which the tracer arm picked up and recorded, it was necessary to enclose the arm and

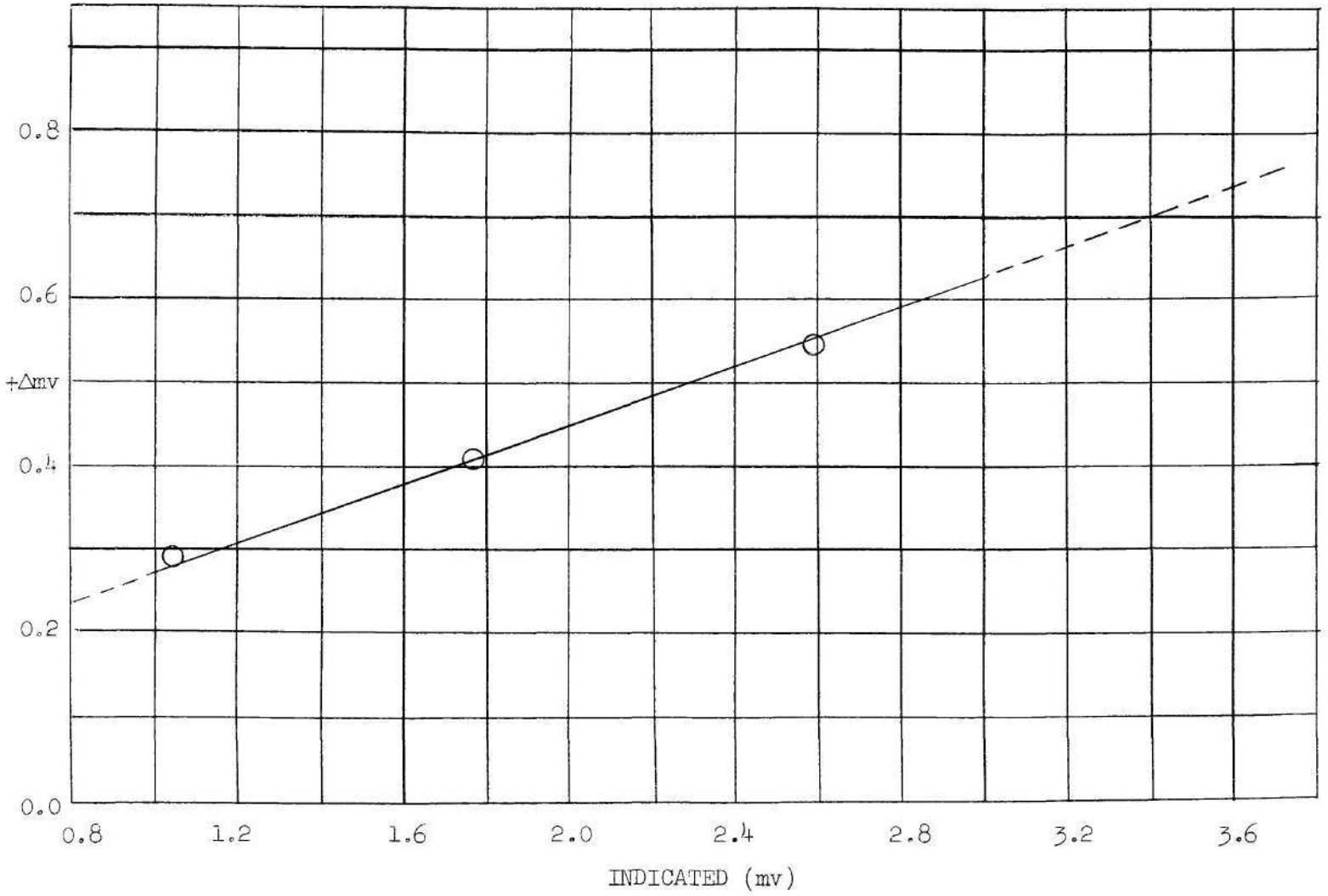

Figure 23. Thermocouple Calibration Curve.

micrometer during the calibration procedure. The results of the calibration test are shown in Table 2. The millivolt per mils ratio was determined to be 0.445 ± 0.0067 mv/5 mils. The foregoing figure represents the average of 39 measurements, with the ± value at 95 per cent confidence level.

Table 2. Strain Gage Calibration Tests

mils.	mv.	Δmv.	mils.	mv.	Δmv.
0	0.5		0	0.5	
5	0.94	0.44	5	0.96	0.46
10	1.39	0.45	10	1.40	0.44
15	1.84	0.45	15	1.87	0.47
20	2.29	0.45	20	2.30	0.43
25	2.73	0.44	25	1.76	0.46
30	3.16	0.43	30	3.18	0.42
35	3.61	0.45	35	3.60	0.42
40	4.02	0.41	40	4.02	0.42
45	4.42	0.40	45	4.50	0.48
50	4.89	0.47	50	4.96	0.46
45	4.38	-	45	4.48	0.48
40	3.90	0.48	40	4.00	0.48
35	3.46	0.44	35	3.53	0.47
30	3.02	0.44	30	3.10	0.43
25	2.57	0.45	25	2.66	0.44
20	2.12	0.45	20	2.23	0.43
15	1.66	0.46	15	1.79	0.44
10	1.23	0.43	10	1.34	0.45
5	0.78	0.45	5	0.90	0.44
0	0.32	0.46	0	0.50	0.40

It was found that a turn of the heliopot gave varying range changes depending on the amount of initial deflection of the tracer arm. The heliopot was calibrated using a micrometer mounted under the tracer foot. The recorder range change was noted with the tracer foot set so as to give an increase of five millivolts above zero and the millivolt per turn ratio determined. The foot was then raised and the procedure repeated until the heliopot had been rotated six full turns which covered the range encountered during a surface trace. These calibration results are shown in Table 3.

Table 3. Heliopot Calibration Tests

No. of Turns	mv/turn
0	2.50
1	2.55
2	2.62
3	2.67
4	2.73
5	2.79
6	2.84

B. Calculation Procedures

1. Mass-Transfer Data Reduction Procedure.--The physical properties used to calculate the Reynolds number were evaluated from average temperature, pressure, and pipe geometry measurements. An average diameter of 1.90 ±

0.01 inches was obtained by measuring the inside diameter of the coated pipe with a micrometer immediately before and after a mass-transfer run. The viscosity and density values of air (23) are given in Table 4. The air velocity was calculated from the volumetric flow rate measured by the dry-gas test meter and the total run time.

The overall average experimental molar flux was calculated from the weight loss of the test pipe by the relationship

$$(N_{Aw})_m = \frac{W_t}{A_{ST}\,\theta_T} \qquad (57)$$

The total surface area A_{ST} was calculated using the average diameter.

2. Surface Trace Reduction Procedure.--The before and after surface traces were reduced to give local molar fluxes. Portions of typical traces are shown in Figure 24. Corresponding points on the before and after traces were located by matching the peak millivolt values caused by an eccentricity of the nut on the screw. These oscillations, shown in Figure 24, while not planned, were beneficial in the data analysis. Calibration tests showed that they had no adverse effect on the results, and, in fact, there were exactly 432 peaks in a six foot trace regardless of the traverse speed. The peak to peak distance was 0.166 inches. The matching was done on the traces for the exit end of the pipe where the after surface profile was not greatly different from the before surface profile. Once the peaks were matched and numbered the millivolt values of each trace were reduced to absolute zero by first subtracting the

Table 4. Physical Property Data Used in Theoretical and Experimental Calculations

T °C	C_{Aw} (Eqn. 48) gm-moles/cm^3	μ (23) gm/cm-sec	ρ (23) gm/cc	$\mathcal{D}_{AB}$ (7) cm^2/sec	Sc (7)
40	17.009×10^{-9}	1.9065×10^{-4}	1.1282×10^{-3}	6.9893×10^{-2}	2.41[illegible]
45	25.879	1.9305	1.1103	7.2122	2.411
50	38.8586	1.9528	1.0931	7.432	2.404
55	57.614	1.9768	1.0765	7.6615	2.397
56	62.2457	1.9803	1.0731	7.7032	2.395
56.1	62.727	1.9803	1.0731	7.7036	2.395
60	84.4011	1.9991	1.06029	7.88808	2.390
65	122.2248	2.0214	1.0445	8.1189	2.384
70	175.0604	2.0438	1.0293	8.3528	2.377

Vapor Pressure (7)

$$\log_{10} P^{o} = \frac{-3765}{T} + 11.55 \qquad [P^{o}] = \text{mmHg} \qquad [T] = {}^{\circ}\text{K}$$

Schmidt Number (7)

$$Sc = \frac{\mu}{\rho \mathcal{D}_{AB}} = 7 \times (T)^{-0.185}; \quad T = {}^{\circ}\text{K} \ (100 \text{ to } 500{}^{\circ}\text{K})$$

Density of cast Naphthalene (7)

$$\rho_N = 1.078 \pm 0.012 \text{ gm/cm}^3 \text{ @ } 20{}^{\circ}\text{C}$$

Diffusivity (7)

$$\mathcal{D}_{AB} = 0.0611 \text{ cm}^2\text{/sec @ } 25{}^{\circ}\text{C \& 1 atm}$$

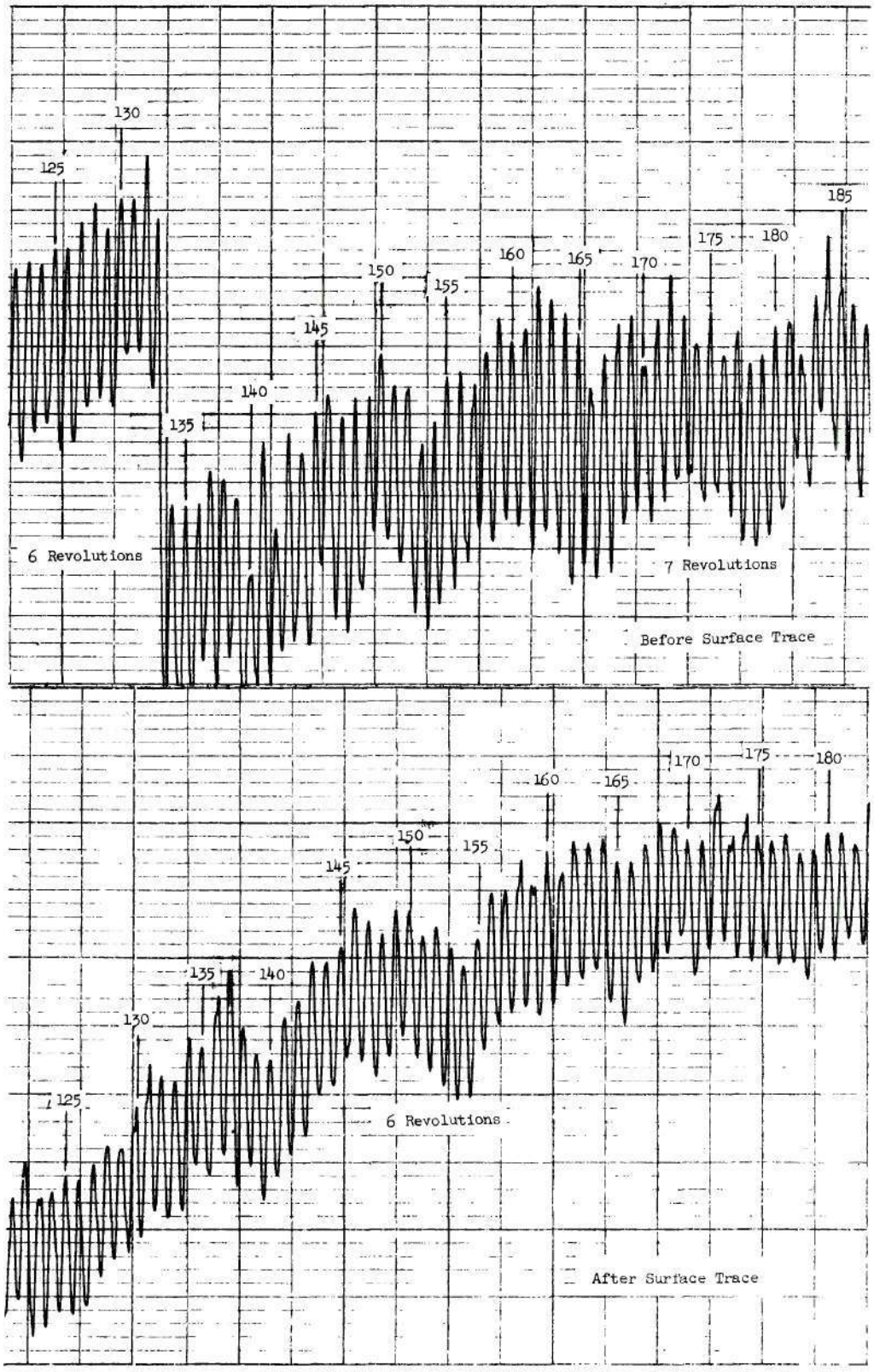

Figure 24. Typical Before and After Surface Traces.

respective zero point values and then adding the appropriate heliopot corrections. The raw data were "smoothed out" at this point by plotting the differences in millivolts versus peak numbers and drawing a curve through the resulting points. At regularly spaced intervals along the trace the millivolt differences were converted to give the local thickness decrease in thousandths of an inch by the relation

$$t_i = \frac{\Delta mv}{0.089} \tag{58}$$

where the constant 0.089 is the millivolt output from the Wheatstone bridge caused by a one mil deflection of the tracer beam. At each location the thickness decrease t_i represents the average thickness decrease for an incremental length of 0.166 inches. A local volume decrease V_i was then calculated for the incremental segment using the average pipe diameter. The local molar flux was determined at various positions along the pipe by the relation

$$N_{Aw} = \frac{V_i \rho_N}{A_{Si} (MW) \theta_T} \quad \frac{\text{gm-moles}}{\text{cm}^2\text{-sec}} \tag{59}$$

A local average flux was obtained for each mass transfer run by averaging the top and bottom traces. Average molar fluxes were determined for both the theoretical and experimental results by integrating the local average values over a given length of pipe. The concentration gradient at the wall, which is the product of the local Nusselt number and the dimensionless bulk concentration term $(1-C_b^*)$ was determined from equation (20) using the experimental local molar flux values.

$$(1-C_b^*)(Nu_{AB})_{loc} = \frac{(N_{Aw})_{loc} r_w}{\mathcal{D}_{AB}(C_{Aw} - C_{Ao})} = - \left.\frac{\partial C^*}{\partial R}\right|_{R=1} \qquad (20)$$

The diffusivity and vapor pressure data (7) used in both computer and experimental calculations are given in Table 4. The average values of $(\partial C^*/\partial R)$ were determined by numerical integration of the local values. An experimental determination of the mass transfer Nusselt number was not possible as no concentration data were collected for the runs.

CHAPTER VI

DISCUSSION OF RESULTS

A. General.--The object of this study was to determine, for an isothermal system, theoretical and experimental mass-transfer rates for a solid material subliming from the wall of a pipe, at low mass transfer rates, into an air stream flowing laminarly through the pipe with simultaneously developing velocity and concentration profiles. Mass-transfer rates for naphthalene subliming into air at a total pressure of one atmosphere were experimentally measured at 50°C, 55°C, 56°C, and 60°C, with air flow rates corresponding to Reynolds numbers of approximately 500 to 2000. The Schmidt number was practically constant for the temperature range at a value of 2.40. The theoretical results and experimental data are summarized in Tables 7 through 41, Appendix A, and in Figures 25 through 45. The complete theoretical results and experimental data are on file in the School of Chemical Engineering of the Georgia Institute of Technology, Atlanta, Georgia.

B. Theoretical Results.--Equations (13) and (14) were solved numerically using the Langhaar velocity profiles to obtain the theoretical results from $ReScD/z$ values of 4000 to 40. The Graetz equations (equations (54) and (55)) were used to extend the results to lower $ReScD/z$ values.

For the numerical scheme, two march steps were required before a concentration value for the second mesh point from the wall was obtained.

Therefore, the concentration gradients at the wall, the local molar flux, and the local mass-transfer Nusselt numbers (henceforth referred to as $(\partial C^*/\partial R)$, $(N_{Aw})_{loc}$, and $(Nu_{AB})_{loc}$) were in error for ReScD/z > 1000. The theoretical results were extrapolated for ReScD/z > 1000 as indicated by dashed lines. The theoretical and average values of N_{Aw} are shown in Figures 25 and 26 as functions of ReScD/z for a temperature range of 40°C to 70°C and 50°C to 60°C respectively. The local and average values of $\partial C^*/\partial R$ and Nu_{AB} are shown as functions of ReScD/z in Figures 27 and 28 respectively. Since the dependency of the Schmidt number on temperature was negligible for the temperature range used in this study, the dependency of $\partial C^*/\partial R$ and Nu_{AB} on Temperature was also negligible.

Since there was no a priori method to obtain an estimate of error magnitude for a numerical scheme, a check on the adequacy of the numerical method was made by calculating $(Nu_{AB})_{loc}$ from equations (13) and (14) using a fully established parabolic velocity profile in the numerical scheme and comparing the results with $(Nu_{AB})_{loc}$ calculated from the Graetz equation modified for mass transfer. The results are shown in Figure 29. The maximum deviation between the two methods occurred at high ReScD/z values but rapidly diminished so that the error was less than two per cent for ReScD/z of about 200. Since only ten eigenvalues, as mentioned previously, have been determined for equation (55), the differences between the numerical scheme and the Graetz equation, at high ReScD/z values, are due to inadequacies of the Graetz equation caused by truncation errors in the series solution. As pointed out by Lepkins in a discussion of Kays' work (15), the effect of truncating the series solution in the Graetz equation is to give too low a magnitude to the Nusselt number. The fact that the two agree for ReScD/z < 200 provides

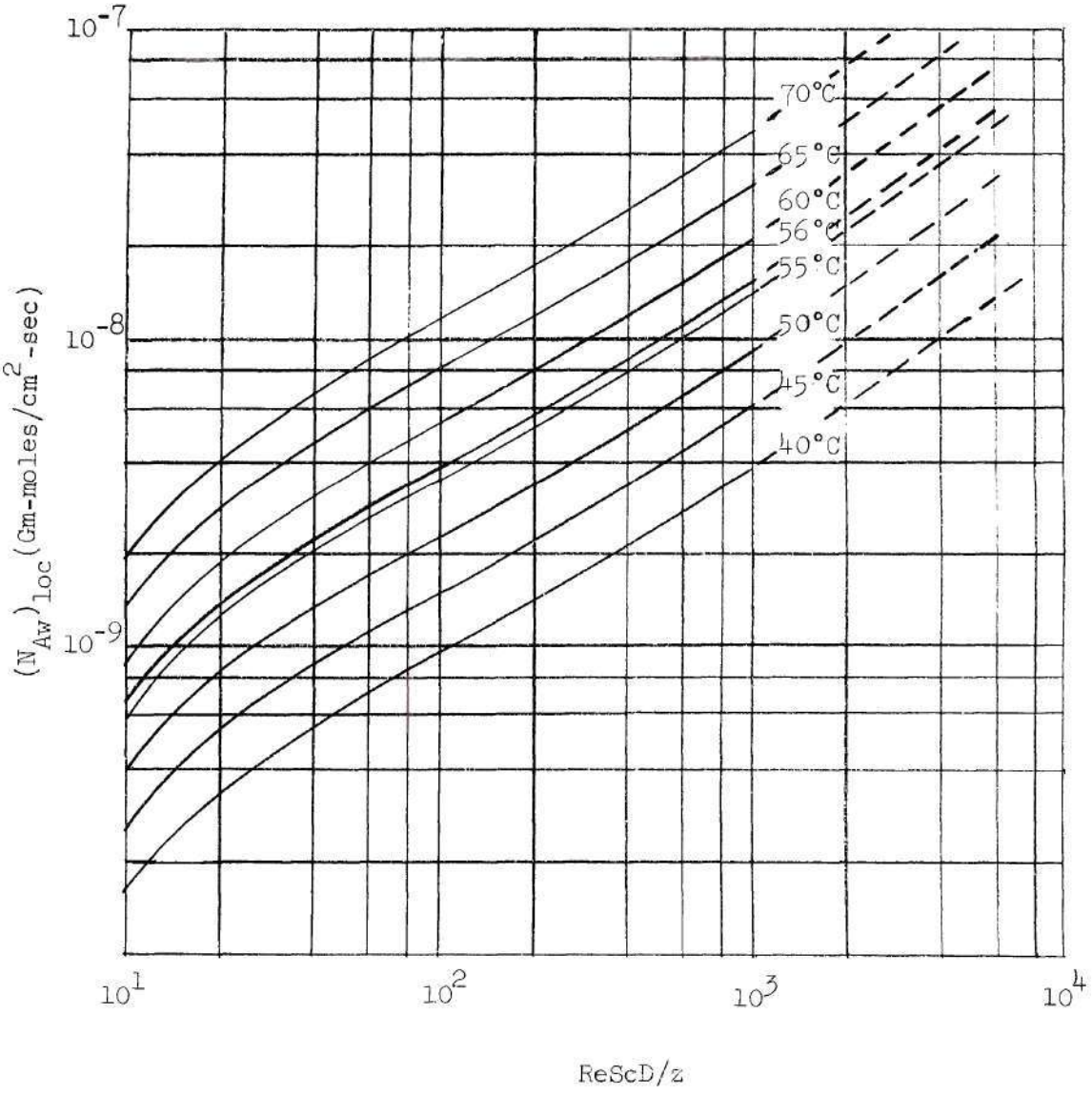

Figure 25. Theoretical Local Molar Fluxes for Laminar-Flow Mass Transfer in the Entrace Region of a Cylindrical Pipe (Sc = 2.4).

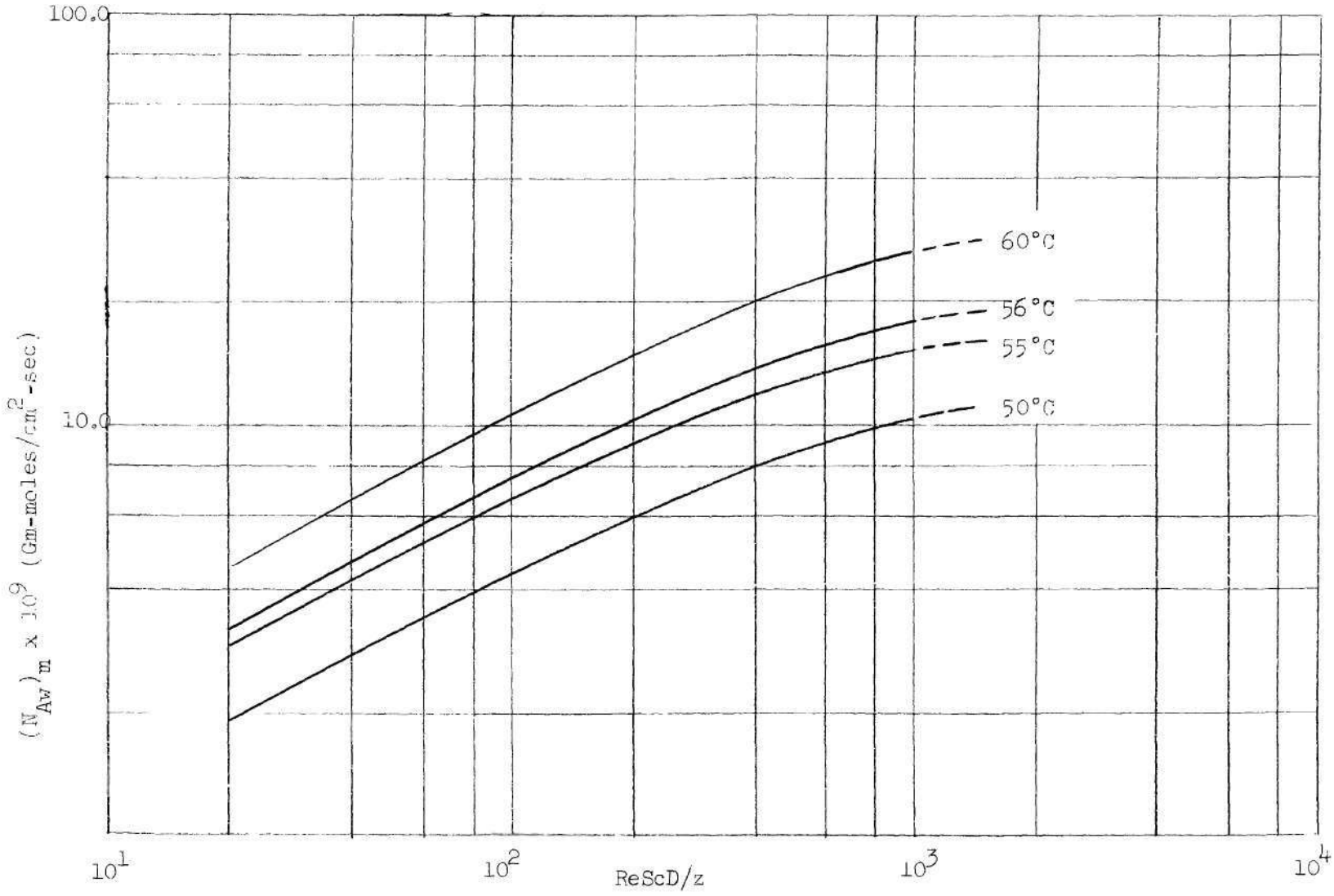

Figure 26. Theoretical Average Molar Fluxes for Laminar-Flow Mass Transfer in the Entrance Region of a Cylindrical Pipe (Sc = 2.4).

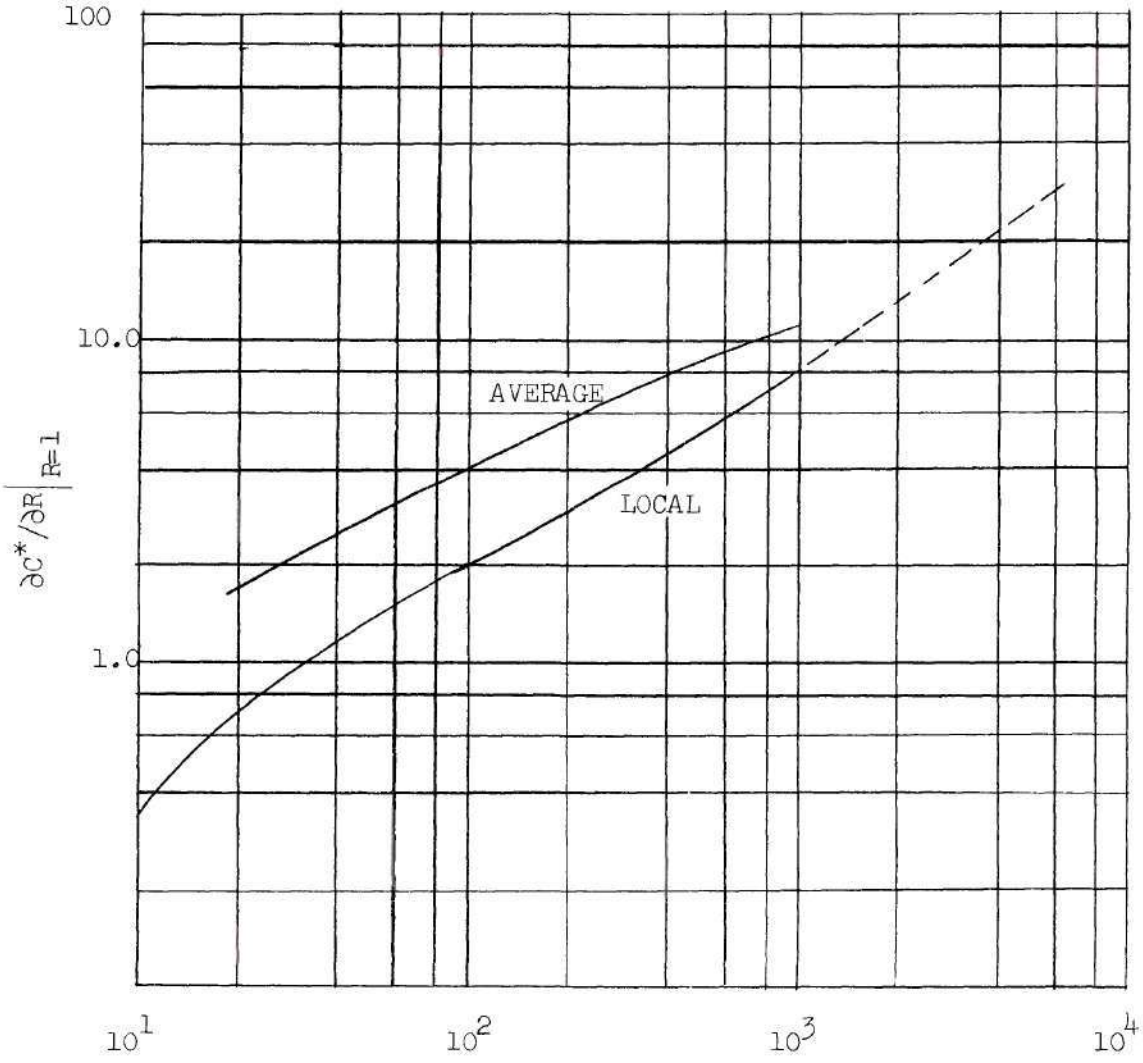

Figure 27. Theoretical Local and Average Concentration Gradients at the Wall for Laminar-Flow Mass Transfer in the Entrance Region of a Cylindrical Pipe (Sc = 2.4).

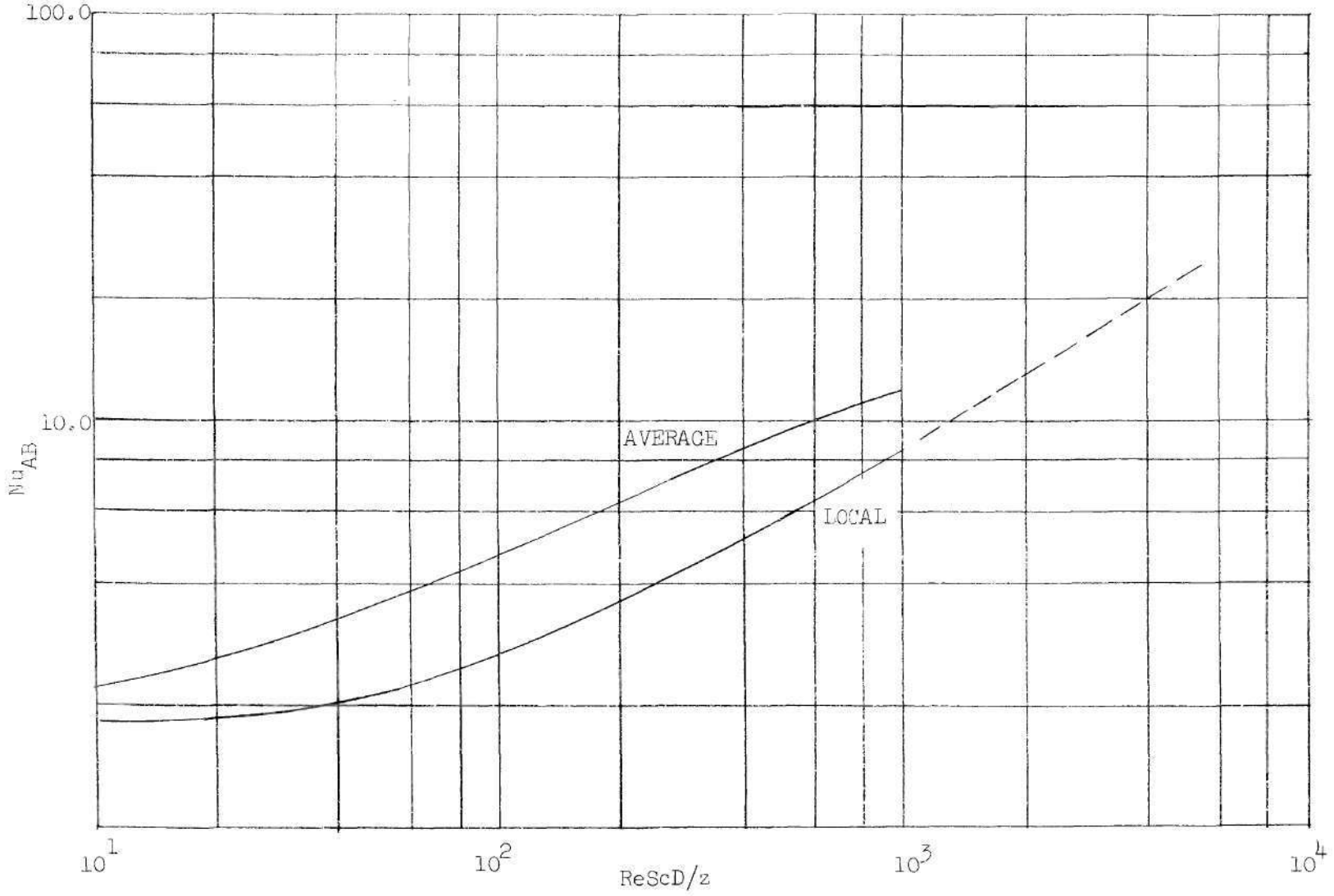

Figure 28. Theoretical Local and Average Mass-Transfer Nusselt Numbers for Laminar-Flow Mass Transfer in the Entrance Region of a Cylindrical Pipe (Sc = 2.4).

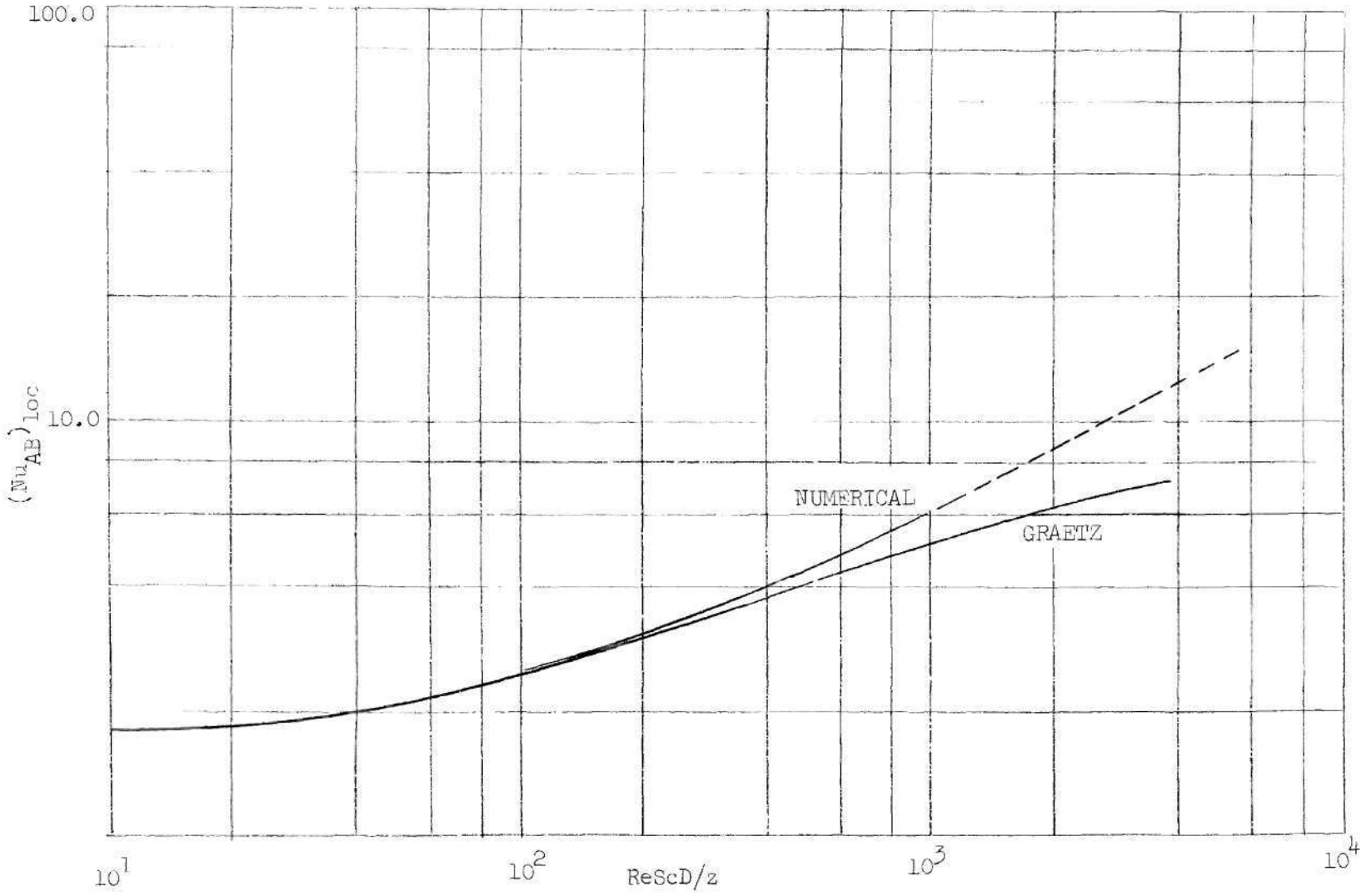

Figure 29. Comparison of Numerical Solution for Fully Established Parabolic Velocity Profile and Constant Wall Composition with Graetz Solution for Same Case (Sc = 2.4).

a measure of confidence in the technique employed in the numerical scheme.

A comparison of the local and average mass-transfer Nusselt numbers calculated by solving equations (13) and (14) numerically for developing and fully established velocity profiles are shown in Figure 30. The results show that the assumption of a fully established velocity profile can result in considerable error when the entrance length represents a considerable portion of the total flow length.

The values of $(Nu_{AB})_m$ numerically calculated from equations (13) and (14) using Langhaar's velocity profiles can be expressed by an empirical equation similar to that used for the analogous case of heat transfer (15). The equation is

$$(Nu_{AB})_m = 1.63 + \frac{0.0449 \left[\frac{ReSc}{z/D}\right]}{1 + 0.0139 \left[\frac{ReSc}{z/D}\right]^{0.5}} \qquad (60)$$

Equation (60) gives the average mass-transfer Nusselt number with an accuracy of about ± 2 per cent for ReScD/z values up to 1000.

As a matter of further interest, selected velocity and concentration profiles for the entrance region are shown in Figure 31. The velocity profiles are those of Langhaar and are direct plots of equation (15). The concentration profiles were taken from the numerical solution of equations (13) and (14) in which Langhaar's velocity profiles were used.

C. Experimental Results.--Mass-transfer runs were made at test air temperatures of 50°C, 55°C, 56°C, and 60°C. At each test air temperature, several runs were made at various flow rates. The experimental data for the mass-transfer runs are given in Table 5.

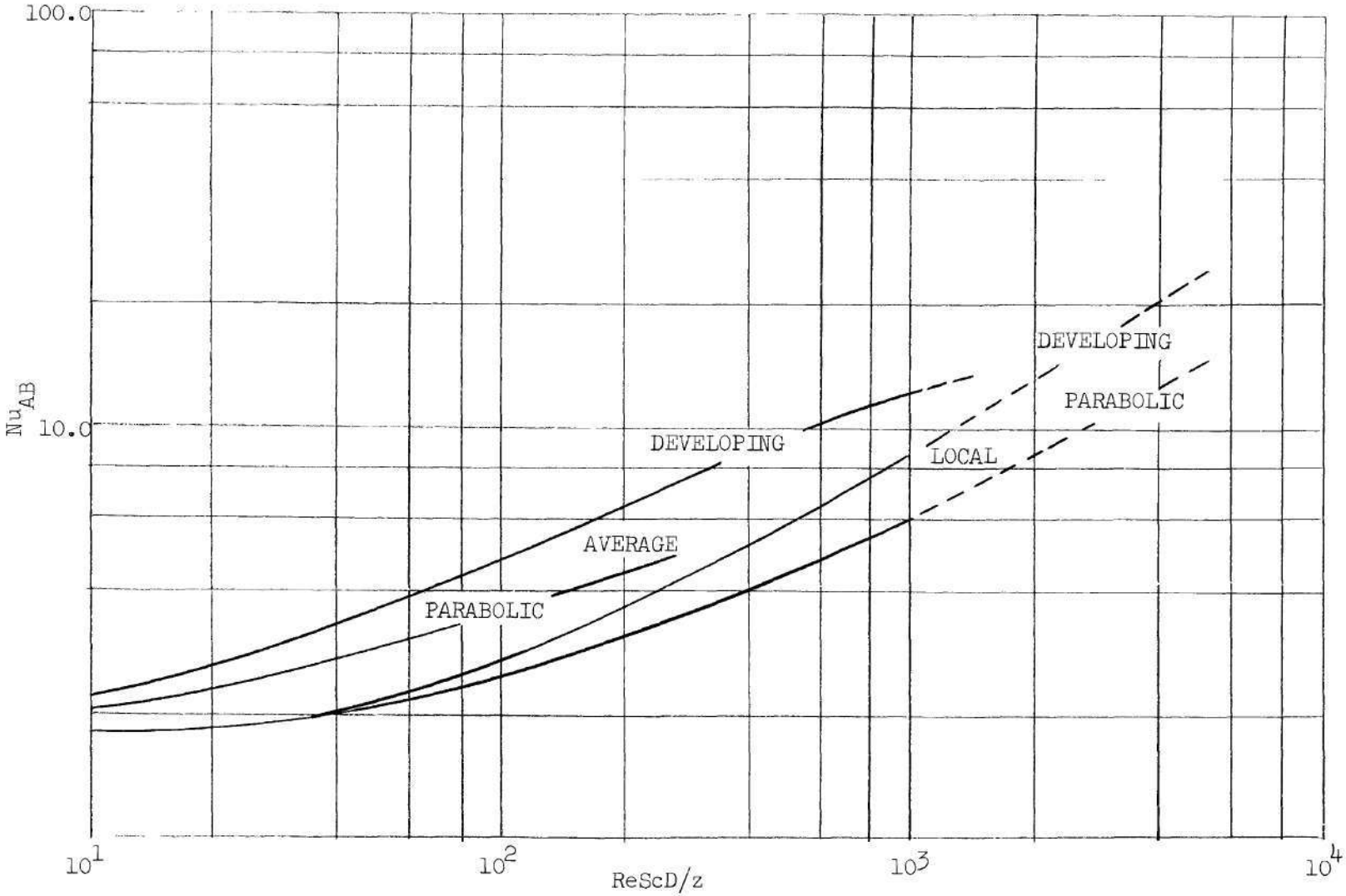

Figure 30. Comparison of Numerical Solutions for the Local and Average Mass-Transfer Nusselt Numbers using Developing and Fully Established Parabolic Velocity Profiles (Sc = 2.4).

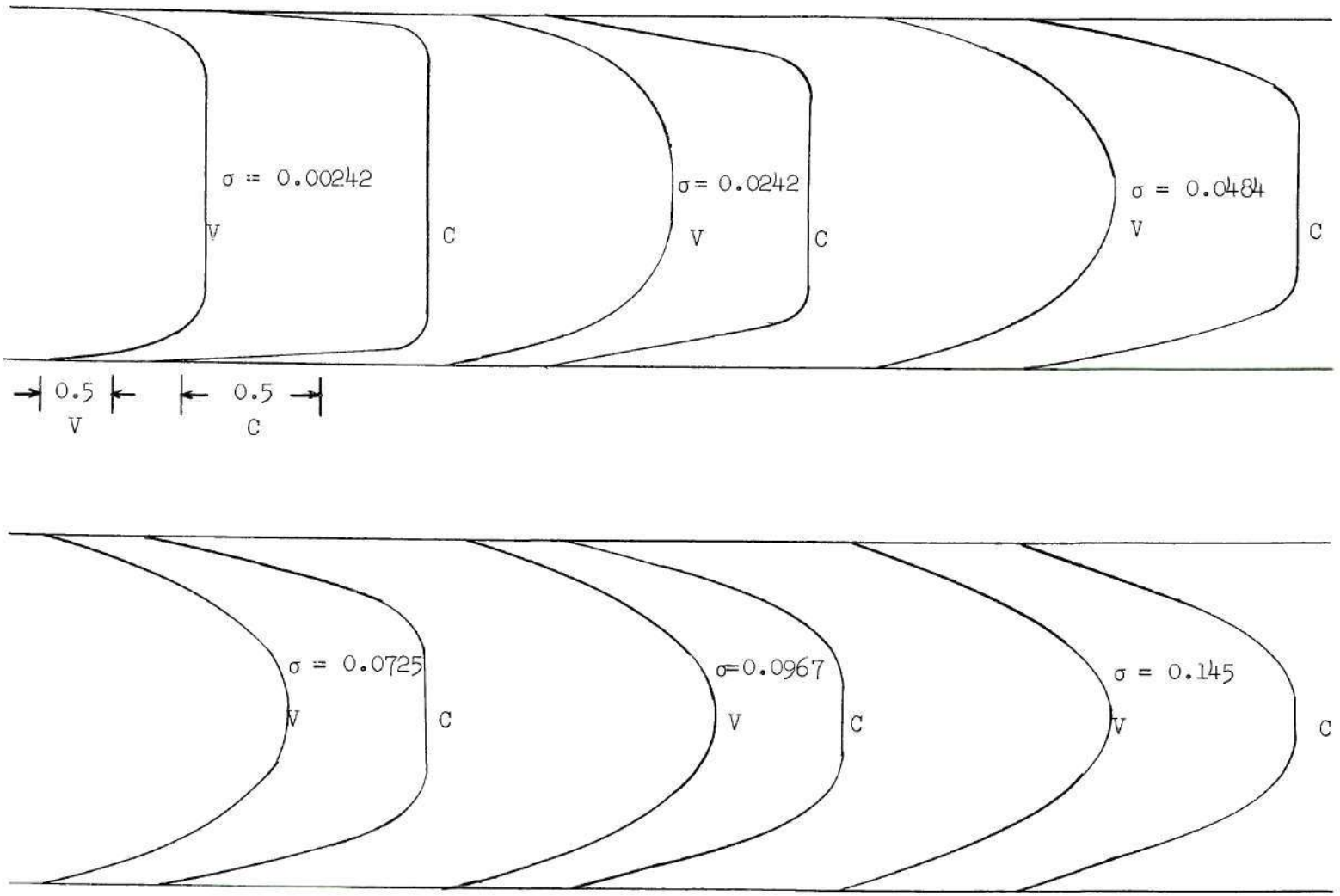

Figure 31. Dimensionless Velocity and Concentration Profiles for Constant Wall Composition and Uniform Velocity and Concentration at Pipe Entrance (Sc = 2.4).

Table 5. Experimental Data for Mass Transfer Runs

Run No.	Run Time (Hrs-Mins)	Total Air Flow (Cu. Ft.)	Test Air Temperature (°C)	Weight Loss (gms)	Inlet Plenum Pressure (in. H_2O)	ΔP Across Test Pipe (in. H_2O)	Type of Exit Section	No. of Traces
19	24-19.9	1295.0	50	122	< 0.03	negligible	Pipe	4
28	15-58.0	1507.0	50	114	< 0.03	negligible	Pipe	4
27	9-58.1	1698.0	50	113	< 0.03	negligible	Pipe	4
23	10-12.3	490.0	55	83	< 0.03	negligible	Pipe	4
1[illegible]	8-31.5	969.0	55	95	< 0.03	negligible	Pipe	4
24	6- 5.0	833.5	55	101	< 0.03	negligible	Pipe	4
21	8-52.3	440.1	60	88	< 0.03	negligible	Pipe	4
22	8- 4.0	964.0	60	*	< 0.03	negligible	Pipe	4
26	6- 3.9	866.0	60	128	< 0.03	negligible	Pipe	4
13	8-14.3	1038.3	56	115	< 0.03	negligible	Pipe	1
14	8- 1.1	1224.0	56	116	< 0.03	negligible	Pipe	1
5	7-16.2	348.0	56	*	< 0.2	negligible	Plenum	1
8	8-29.8	581.9	56	*	< 0.2	negligible	Plenum	1
9	8-47.6	676.6	56	*	< 0.2	negligible	Plenum	1
10	8-20.1	991.3	56	*	< 0.2	negligible	Plenum	1

*Weight loss data were not obtained

Theoretical and experimental values of $(N_{Aw})_{loc}$ are compared in Figures 32 through 36. The local flux values for the top and bottom surface traces are given for 50°C, 55°C, and 60°C. The runs made at 56°C were preliminary in nature and only one trace was made. It was found that the values of $(N_{Aw})_{loc}$ for the two side traces were approximate averages of $(N_{Aw})_{loc}$ for the top and bottom traces and, therefore, the results of the side traces are not reported in detail. However, to illustrate typical results, values of $(N_{Aw})_{loc}$ for side traces are shown in Figure 36 for two runs made at 60°C.

The experimental local molar fluxes agreed favorable with the theoretical values near the pipe entrance, but deviated by as much as 60 per cent for ReScD/z values around 200. For ReScD/z < 200, a sharp fall-off of mass-transfer rate occurred. In addition, as reported in Tables 15 through 29, Appendix A, the local flux values actually became negative at the exit end of the pipe for some of the runs. It was observed that the axial location in the pipe where the fall-off began, and the extent of the fall-off, were functions of temperature, flow rate, and angular location. Larger negative fluxes occurred at the lower temperatures and flow rates. The top traces, for all runs, showed the fall-off effect at a greater ReScD/z value than the bottom traces, with the side traces affected at intermediate ReScD/z values. At Re = 500, the velocity profile is nearly developed at the exit end of the test pipe. By increasing the flow rate, the entrance length is increased. Therefore, at high Reynolds numbers, the test pipe contained less of the entrance length development than at the low Reynolds numbers. The fact that the fall-off occurred at all for the higher flow rates indicated

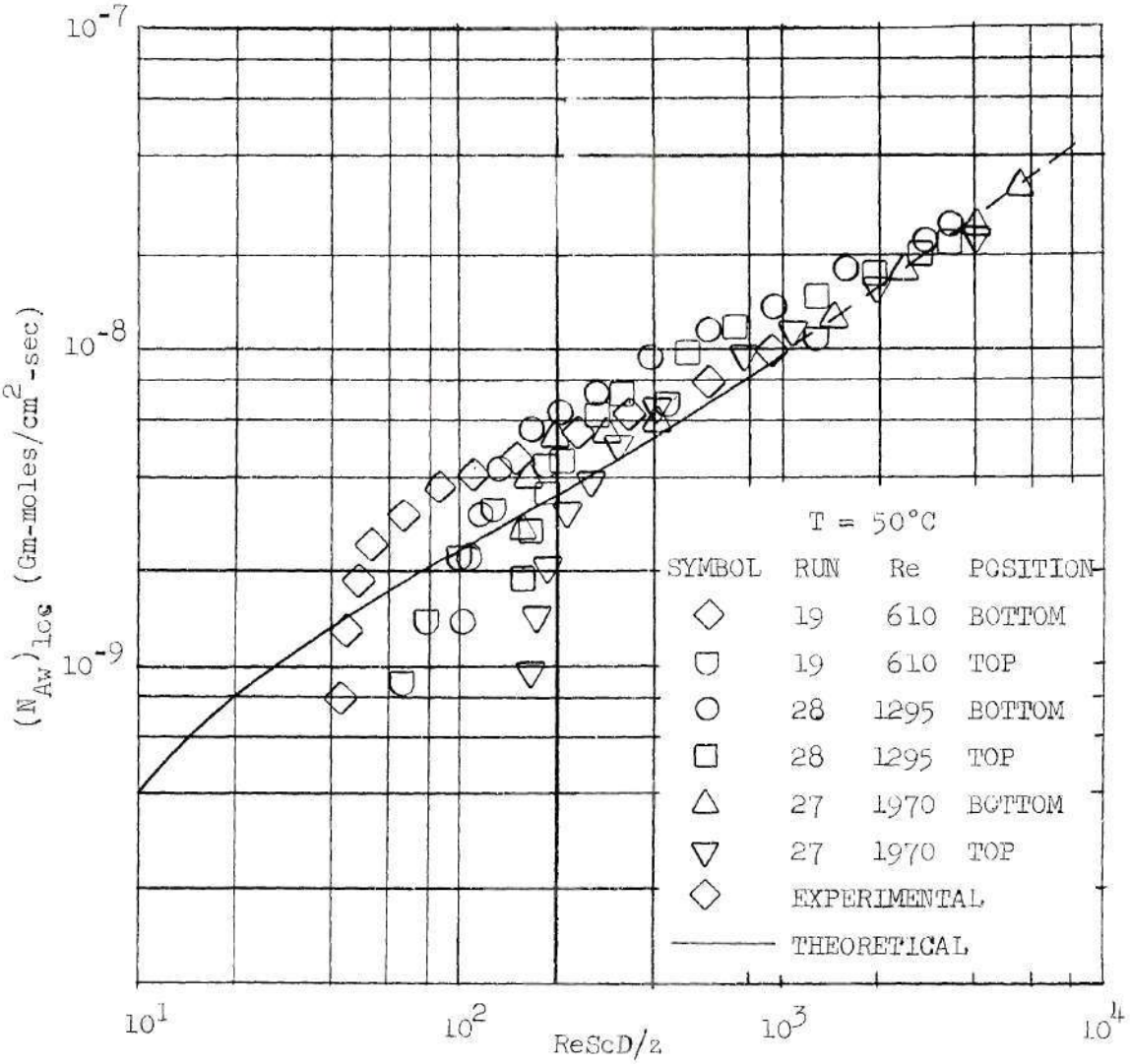

Figure 32. Comparison of Experimental and Theoretical Local Molar Fluxes for 50°C (Sc = 2.4).

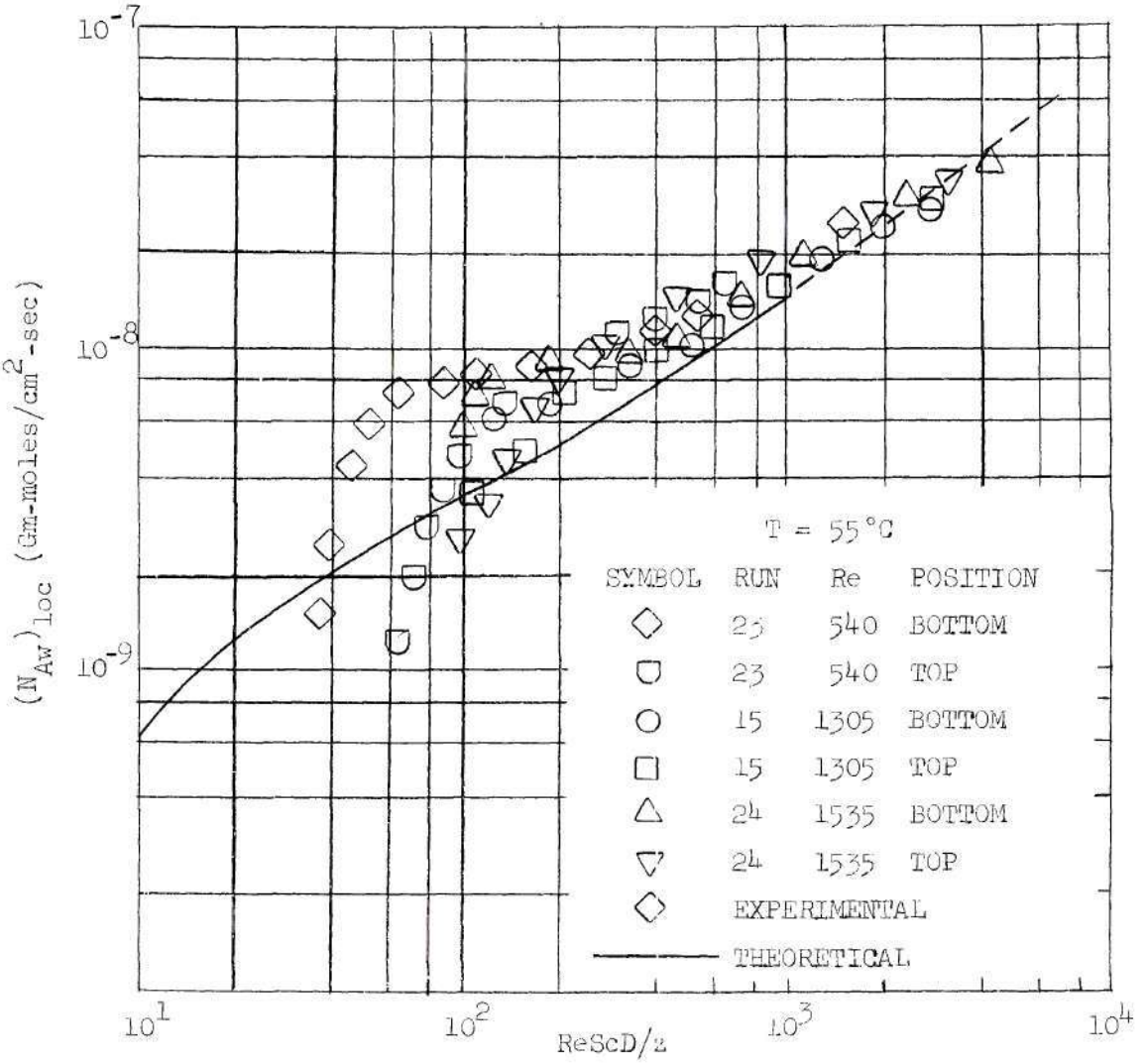

Figure 33. Comparison of Experimental and Theoretical Local Molar Fluxes for 55°C (Sc = 2.4).

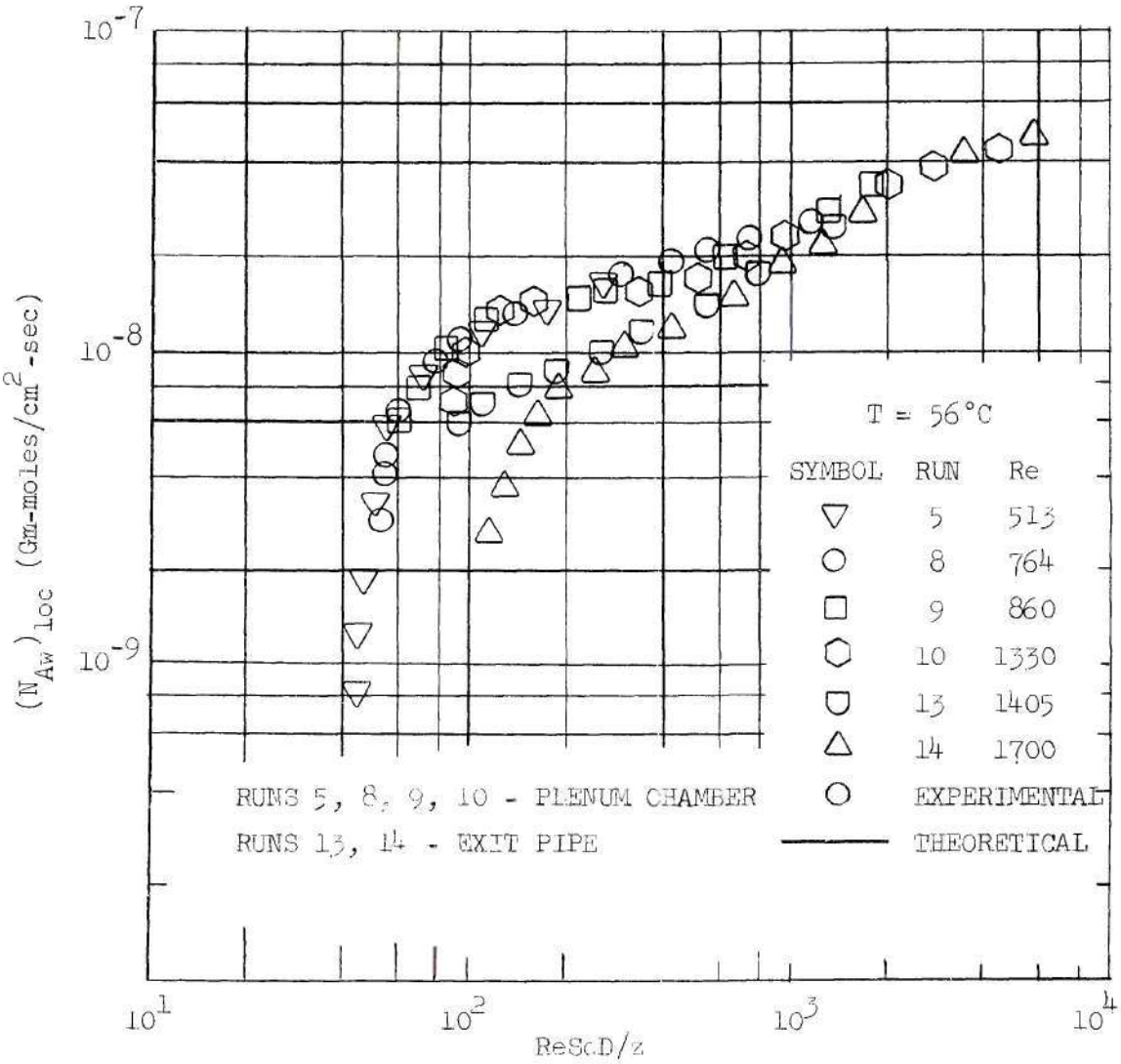

Figure 34. Comparison of Experimental and Theoretical Local Molar Fluxes for 56°C (Sc = 2.4).

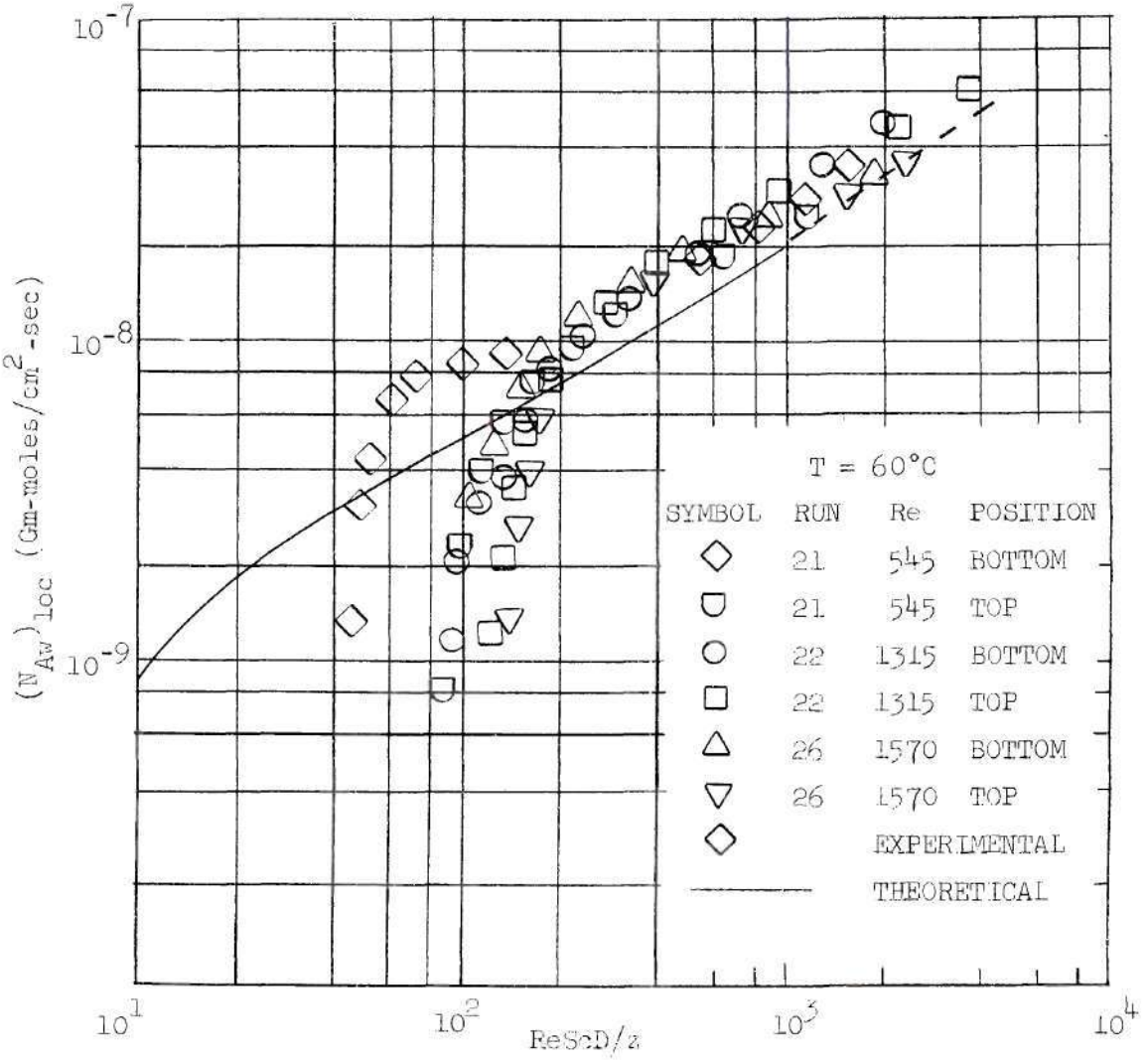

Figure 35. Comparison of Experimental and Theoretical Local Molar Fluxes for 60°C (Sc = 2.4).

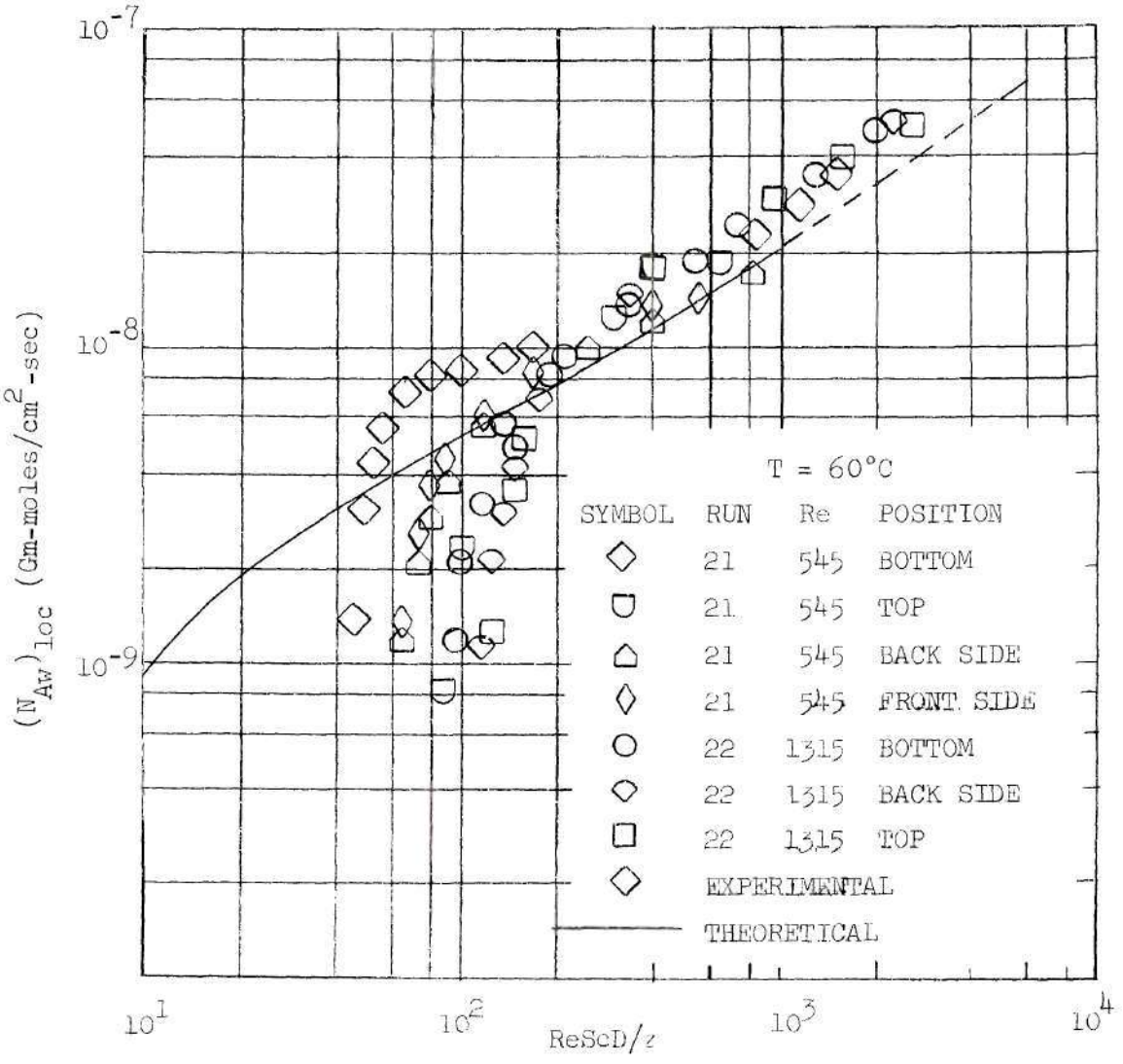

Figure 36. Comparison of Experimental and Theoretical Local Molar Fluxes from 60°C. Includes Experimental Molar Fluxes for Sides of Pipe (Sc = 2.4).

that there was some factor, unaccounted for, controlling the mass-transfer rate at the pipe exit. The general shape of the experimental curves indicated that free-convection mass-transfer due to density differences was not negligible. This point was emphasized by the dependency of the mass-transfer rates on angular position. It is suggested that the angular velocity, set up by gravity settling of the heavy naphthalene vapor from the top half of the pipe, increased the mass-transfer rate along the bottom of the pipe and thereby delayed the fall-off effect for the bottom half of the pipe.

Valid theoretical considerations are not presently available to quantitatively explain this rapid reduction of mass-transfer rate. However, some plausible explanations are indicated from crystallography considerations (24) (25) (26) (27). By virtue of their more ordered structure, the sublimation of solids is more complex than the evaporation of liquids. Molecules can join and leave the crystals only at certain definite points on the surface and diffusion of molecules over the surface occurs when crystals form or sublime. Sublimation studies with perfect crystals, carried out by Sears (28), indicated that, the fact that a molecule must diffuse over the surface before it can pass into the vapor, can materially reduce the rate of sublimation. While the above discussion indicates that the surface orientation of a crystalline material can effect the transfer of material, further studies are required before even a qualitative interpretation of the results found in this study can be attempted. Referring back to the experimental work of Plewes, Butler, and Marshall (11) discussed in the introduction, it is possible that what they call slip at the wall could actually have been a surface orientation of

the crystalline structures of the various materials used in their study.

The preliminary runs made at 56 °C used a plenum chamber as an exit section. It was found that naphthalene built up on the plenum chamber walls. When it was replaced with a pipe having the same diameter as the test pipe, no build up of naphthalene was found in the exit pipe. The exit-pipe section was used in all subsequent runs. The effect of the exit sections on the local molar fluxes is shown in Figure 36.

The local average molar fluxes, obtained by averaging the top and bottom molar fluxes, were used to calculate $(N_{Aw})_m$ and $(\partial C^*/\partial R)_{loc}$. As shown in Figures 37 through 39, averaging the two local fluxes damps out the free-convection effects for $ReScD/z < 200$ which were observed in Figures 32 through 36.

As a check on the surface trace technique for obtaining molar flux values, an overall molar flux was obtained for each run by weighing the test pipe on a triple beam balance immediately before and after the mass-transfer run. The overall molar fluxes, based on weight loss, and the overall molar fluxes, based on surface trace procedures, are compared in Table 6 and Figures 40 through 43 along with complete average molar fluxes calculated from the local average values. While individual agreement between the two experimental values was not good in some runs, the average deviation was only 20 per cent. It was found that it was impossible to accurately weigh the test pipe on the triple beam balance closer than ± 5 grams. Considering the fact that the test pipe weighed approximately 11,000 grams, and that weight losses of approximately 100 grams occurred, this deviation is quite small. The discrepancies between the theoretical and experimental results shown in Figures 40 through 43 are probably due

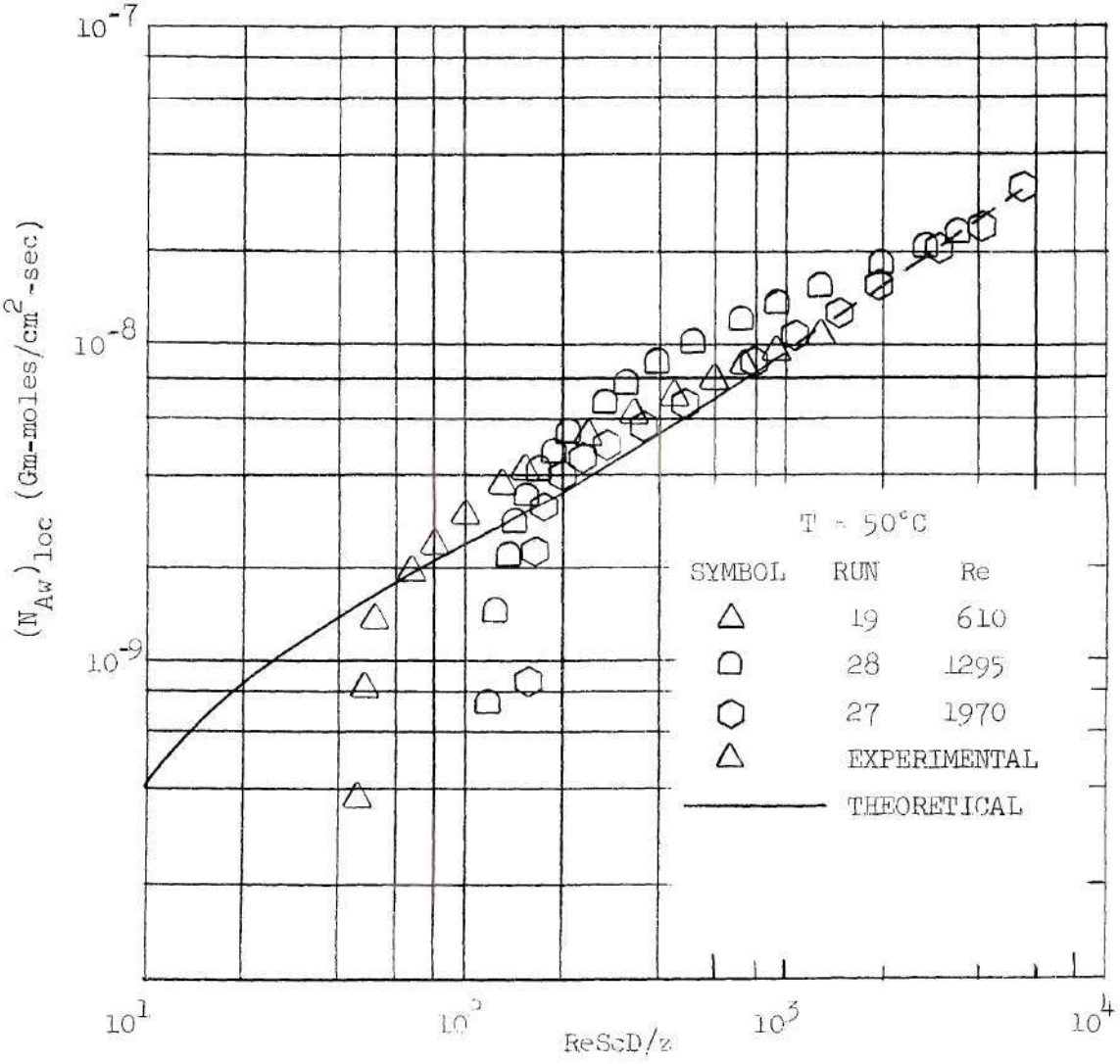

Figure 37. Local Average Molar Fluxes at 50°C Obtained by Averaging Local Molar Fluxes for Top and Bottom of Pipe (Sc = 2.4).

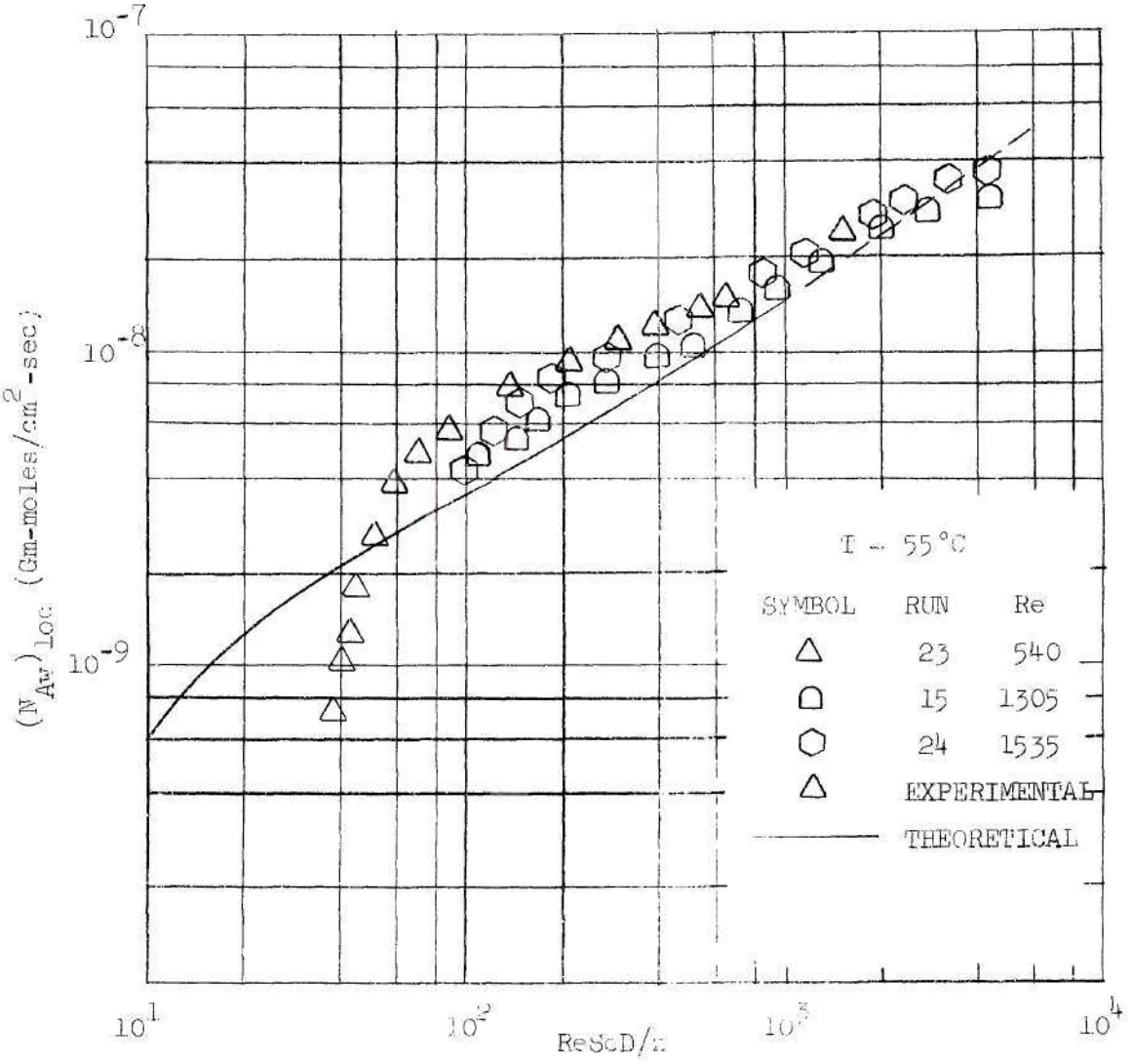

Figure 38. Local Average Molar Fluxes at 55°C Obtained by Averaging Local Molar Fluxes for Top and Bottom of Pipe (Sc = 2.4).

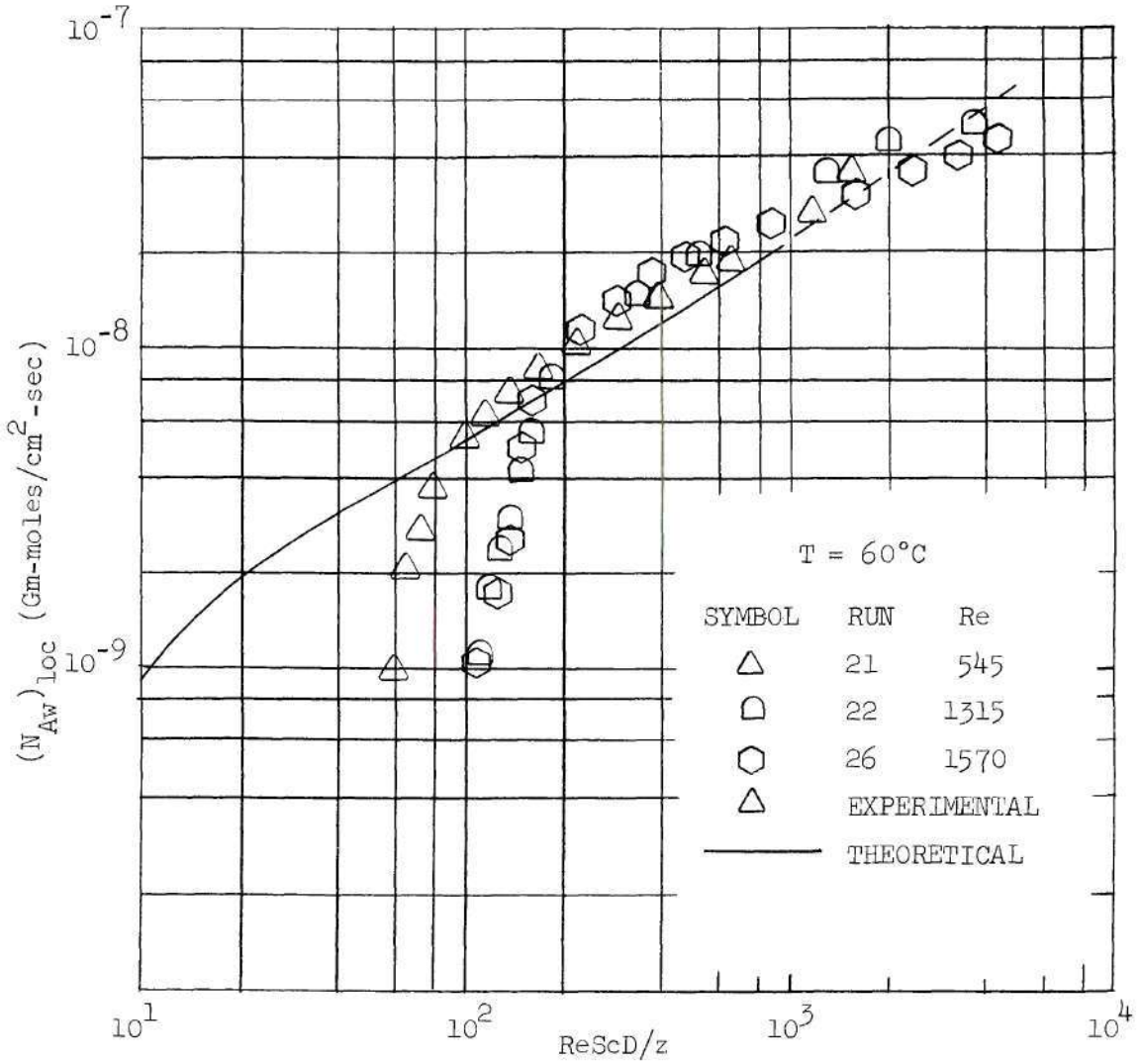

Figure 39. Local Average Molar Fluxes at 60°C Obtained by Averaging Local Molar Fluxes for Top and Bottom of Pipe (Sc = 2.4).

Table 6. Overall Molar Flux Based on Weight Loss Measurements

Run	T(°C)	Re	Experimental Weight Loss (Gms)	$\frac{ReSc}{z/D} \times 10^{-2}$	$(N_{Aw})_m \times 10^9$ (gm-moles/cm^2-sec)		Per cent Error	$(\partial C^*/\partial R)_m$
					Weight Loss Method	Surface Trace Method		
19	50	610	128	0.39	3.93	2.71	31.0	3.28
28	50	1295	114	0.88	5.59	5.39	3.6	4.67
27	50	1970	113	1.25	8.88	5.50	38.1	7.42
23	55	540	83	0.34	6.37	5.53	13.2	3.48
15	55	1305	95	0.83	8.72	8.50	2.5	4.76
24	55	1535	101	0.97	13.0	10.5	19.2	7.10
21	60	545	88	0.34	7.77	3.43	55.6	2.82
22	60	1315	*	-	-	-	-	-
26	60	1570	128	0.99	16.5	11.7	29.0	6.00
13	56	1405	115	0.89	10.9	10.5	3.7	5.50
14	56	1700	116	1.08	11.3	10.3	8.8	5.70
							ave 20.5	

*Weight loss data were not obtained.

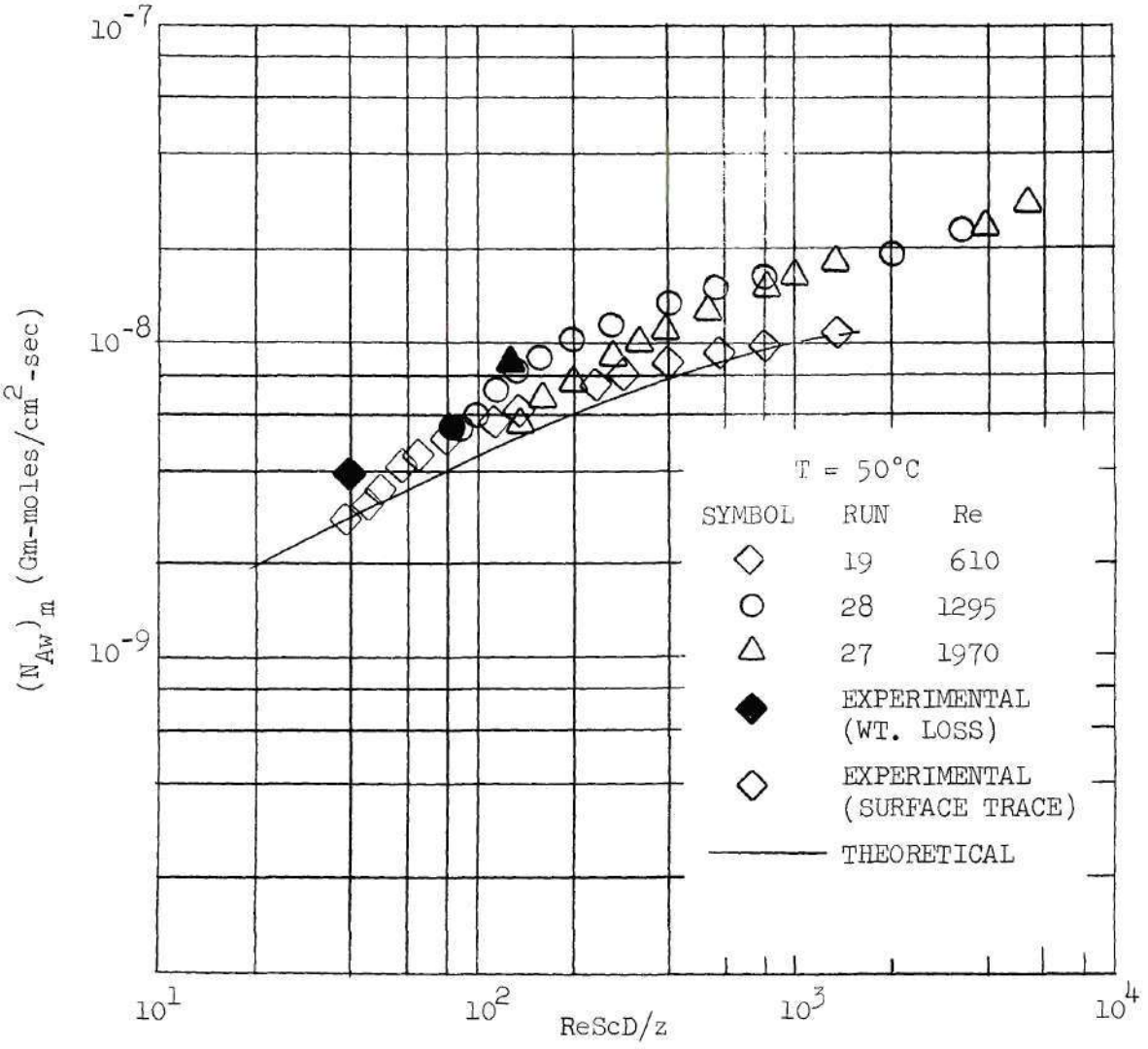

Figure 40. Comparison of Experimental and Theoretical Average Molar Fluxes for 50°C (Sc = 2.4).

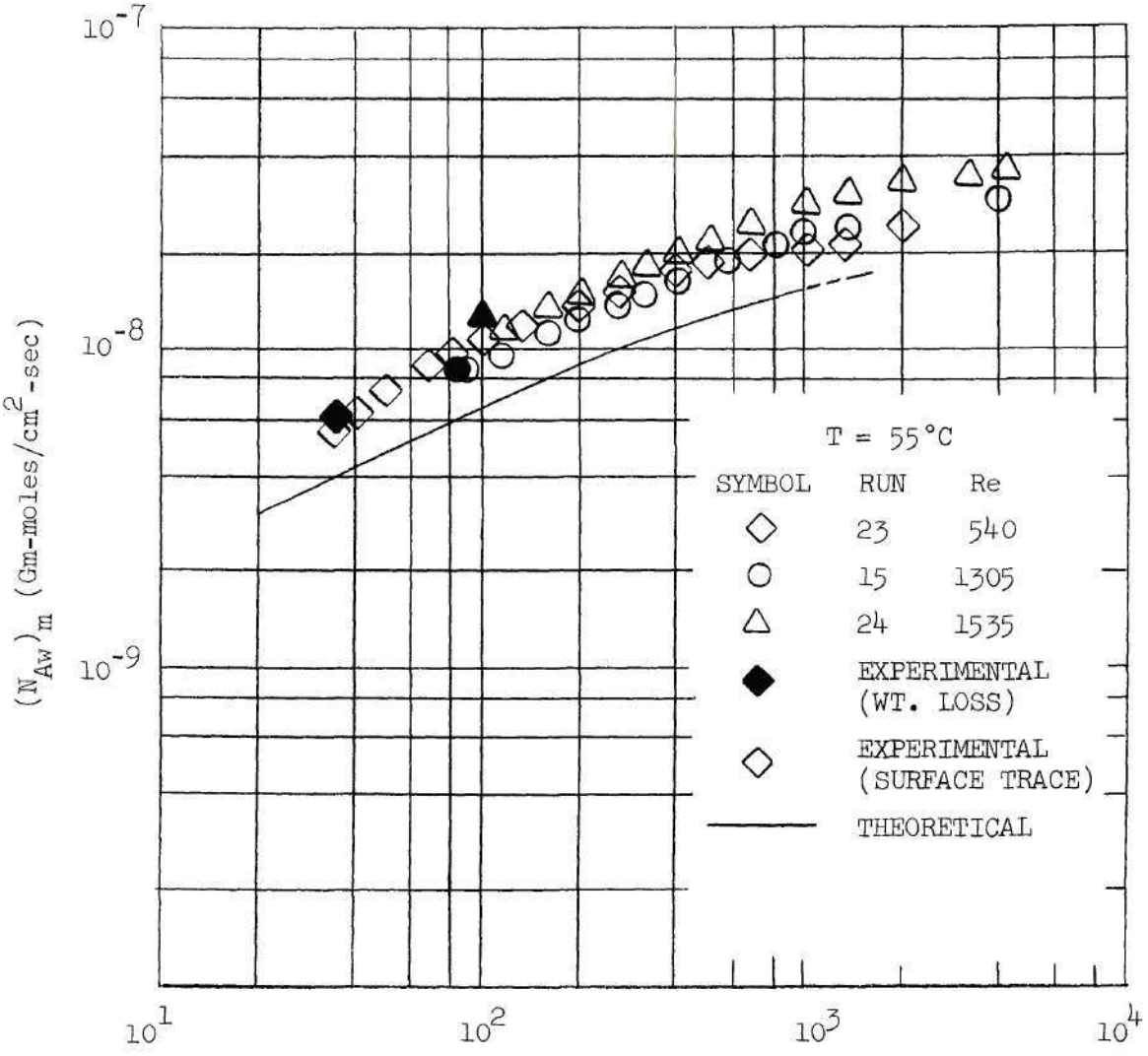

Figure 41. Comparison of Experimental and Theoretical Average Molar Fluxes for 55°C (Sc = 2.4).

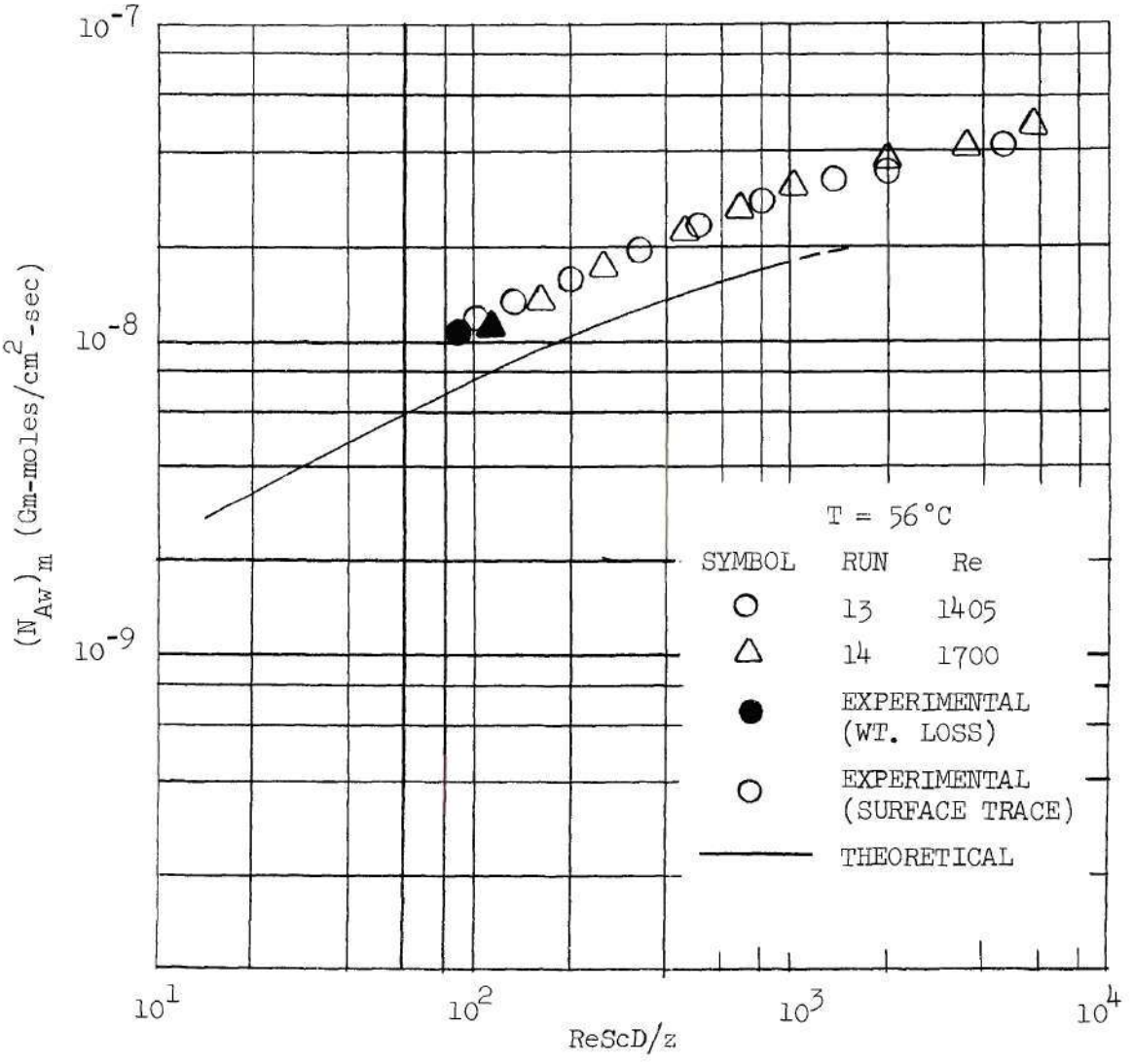

Figure 42. Comparison of Experimental and Theoretical Average Molar Fluxes for 56°C (Sc = 2.4).

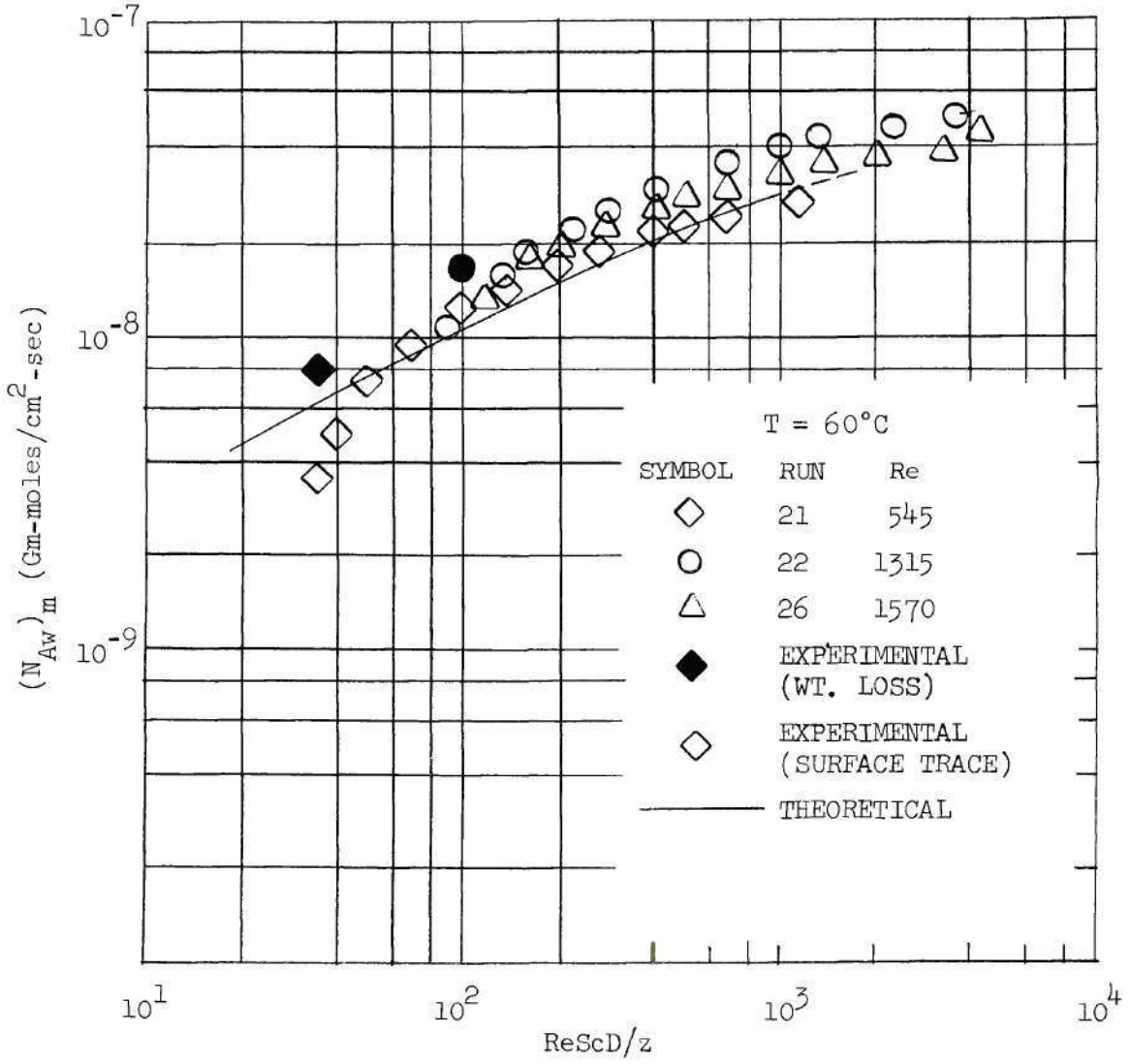

Figure 43. Comparison of Experimental and Theoretical Average Molar Fluxes for 60°C (Sc = 2.4).

to free-convection effects. And, while the experimental results based on surface trace measurements are consistently higher than the theoretical results, the fact that the weight loss method agrees closely with the surface trace technique lends support to the validity of the experimental results.

Experimental and theoretical values of $(\partial C^*/\partial R)_{loc}$ and $(\partial C^*/\partial R)_m$ are compared in Figures 44 and 45 respectively. The experimental values of $(\partial C^*/\partial R)_m$ determined from weight loss measurements are also shown in Figure 45. For the average values shown in Figure 45, the agreement of the experimental results with the theoretical results is ± 25 per cent for ReScD/z above 1000 and below 100. The high experimental results for ReScD/z between these limits is probably due to free-convection effects mentioned previously. A comparison of the results of Figures 44 and 45 again emphasizes the fact that the rapid fall-off of the mass-transfer rate observed for local results is obscured when average results are determined.

The fact that the theoretical results agree favorably with the experimental results lends valid support to the mathematical model developed in Chapter II for predicting mass-transfer rates. If it is assumed that the concentrations calculated theoretically are correct, then, the mathematical model can be used to calculate the mass-transfer Nusselt number expressed by equation (60). Due to free-convection effects, the results will be approximately 20 per cent conservative.

D. Experimental Errors.--During a mass-transfer run, experimental errors could be introduced from temperature and flow rate measurements. The accuracy of the L & N potentiometer to obtain temperatures was set at

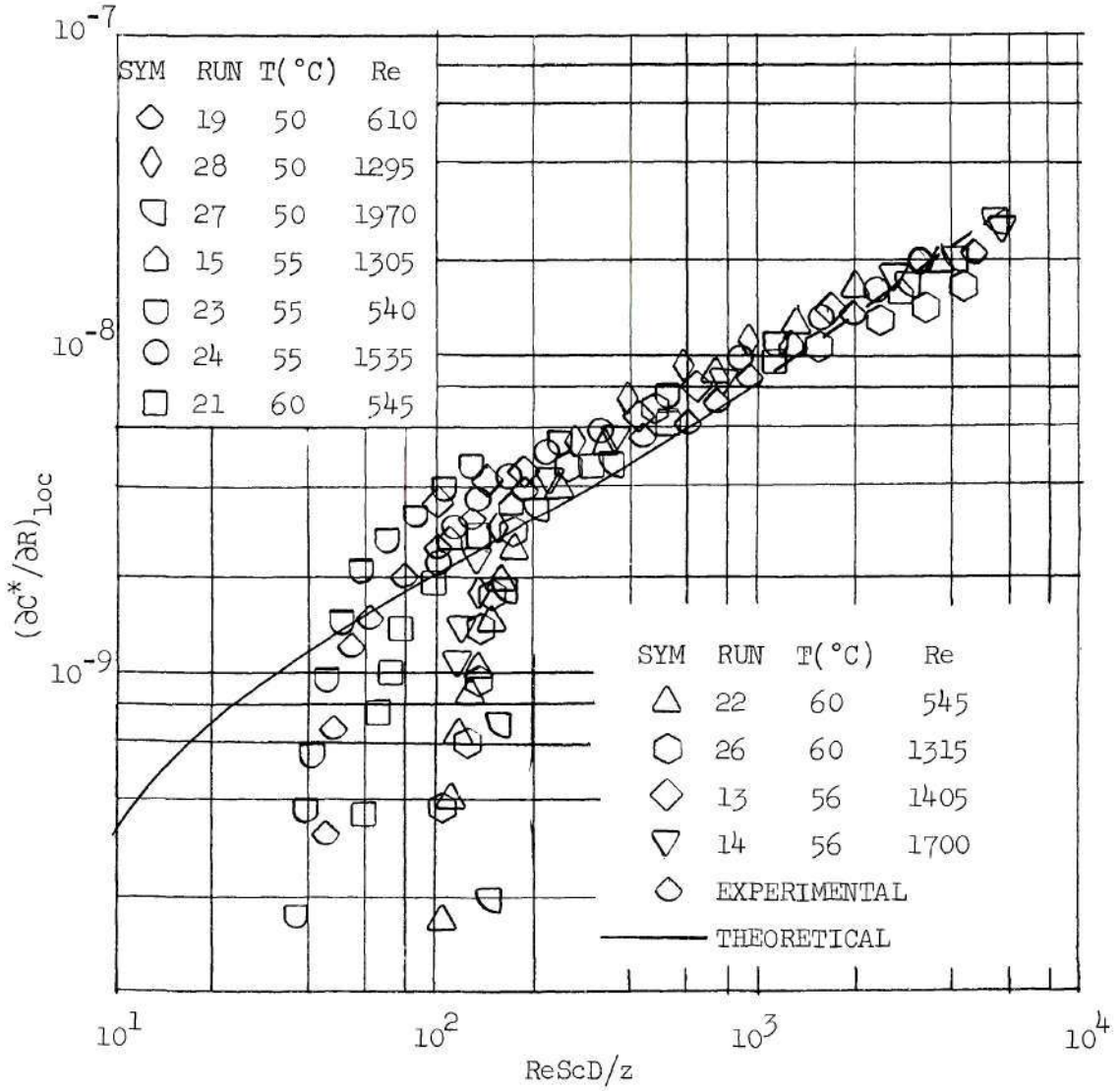

Figure 44. Comparison of Experimental and Theoretical Local Concentration Gradients at the Wall (Sc = 2.4).

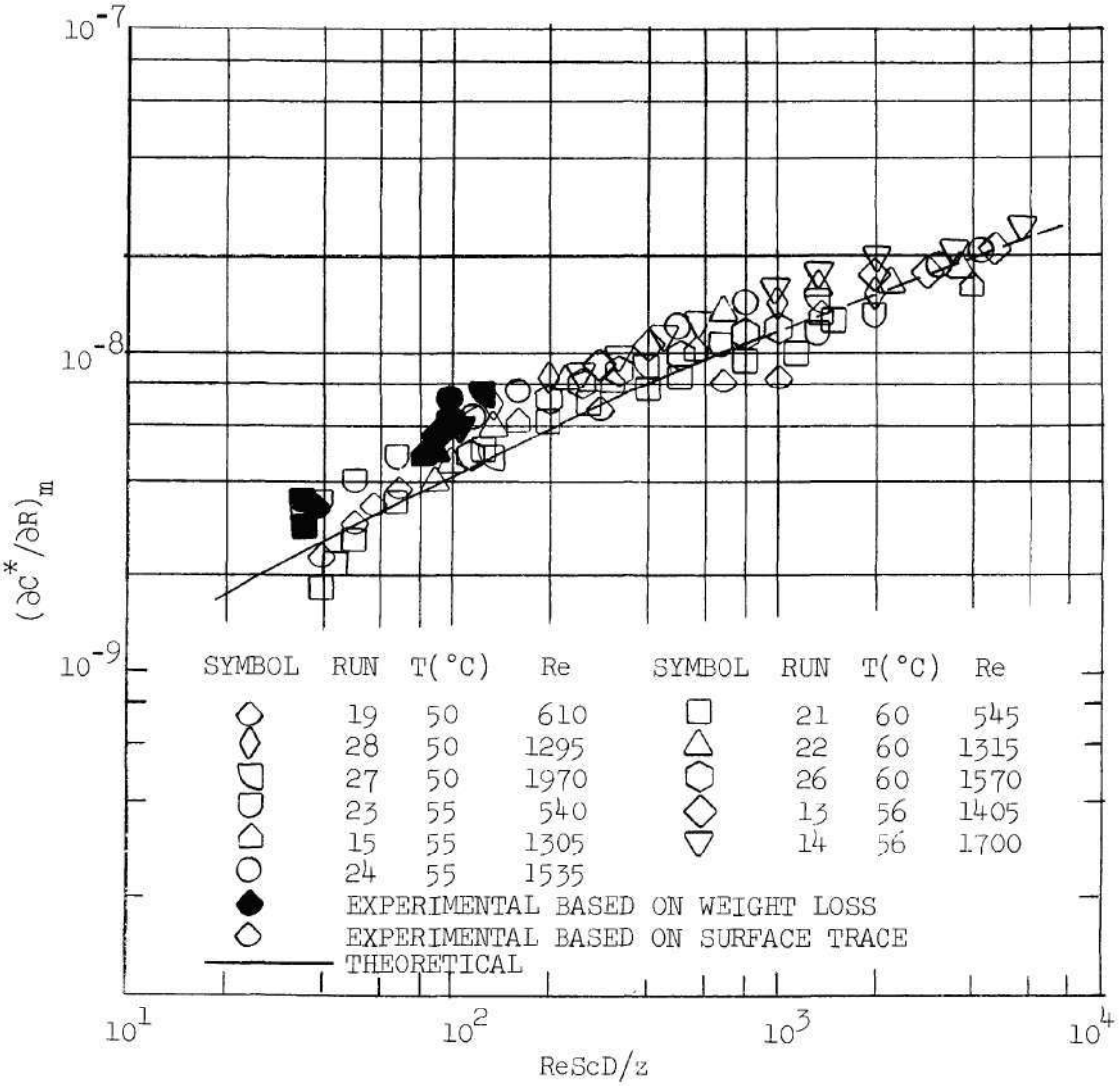

Figure 45. Comparison of Experimental and Theoretical Average Concentration Gradients at the Wall (Sc = 2.4).

± 0.1°C by the manufacturer. The average test air and outside pipe wall temperatures were controlled to within ± 0.25°C, and in most cases this number is pessimistic.

It was assumed in the theoretical development, that the wet-bulb depression of the naphthalene surface was negligible. An estimate of the wet-bulb depression can be obtained if it is assumed that the effect of air flowing past a cylinder of naphthalene is, in some sense, similar to air flowing through a cylinder of naphthalene. Bedingfield and Drew (29) developed an equation which satisfactorily predicts the wet-bulb temperature for an organic, solid cylinder with air flowing parallel to its axis. Using their equation, air, flowing over a naphthalene cylinder, at a velocity corresponding to the upper limit of laminar flow (Re = 2000) and at a temperature of 50°C would produce a wet-bulb depression of less than 0.5°C. While this value can only be used as an approximation, it does show that the error involved in C_{Aw} would be less than 3 per cent.

The dry-gas meter was factory calibrated. The calibration curve supplied with the meter showed that the maximum deviation occurred at low flow rates and gave readings that were 0.15 per cent low. The percentage error decreased as the flow rate increased with the result that, for flow rates in the range of 2.5 cfm, the meter readings were correct to within -0.05 per cent. Hence, any error introduced because of meter indication was negligible.

It was assumed in the theoretical development that the velocity was uniform across the pipe at the entrance. A bell-shaped entrance section was designed for the experimental investigation in order to match this assumption as close as possible. Conclusive proof that a

bell-shaped entrance actually does produce a uniform velocity profile across the entire diameter at the entrance is not available. However, Griffith (30), in his work on mass transfer from single spheres, measured the entrance velocities produced by a bell-shaped entrance. He used both an ultramicroscope technique and a colloidal tellurium photographic technique. While Griffith's measurements did not extend to the wall, the results of his work showed excellent agreement with Langhaar's equation and the experimental work of Nikuradse (31). A visual study of entrance velocity profiles was made by Spurlock (32) using smoke techniques in a two inch diameter glass pipe. The findings indicated that at the entrance there was a slight amount of burbling at the wall. However, this effect was quickly damped out and disappeared completely within a few inches down the pipe. Observations were made for various entrance configurations, but the burbling effect was a minimum for the bell-shaped entrance section.

In the development leading to equation (7) the diffusion of material down the pipe was assumed negligible compared to the material carried down the pipe by convection. Schneider (33) and Singh (34) independently calculated the importance of the conduction term $\partial^2 T/\partial z^2$ for heat transfer. They found that the conduction contribution is negligible for RePr greater than 100. Since the Schmidt number, analogous to the Prandtl number, is large (Sc = 2.4 for air-naphthalene system), the axial diffusion contribution can be safely neglected for Reynolds numbers greater than 50.

The density used in the experimental study was that reported by Sherwood and Träss (7). The density value experimentally measured in

their work was for naphthalene cast on a flat plate and was determined to be 1.078 ± 0.012 grams/cc at 20°C. This is five per cent below the true density of naphthalene. While the bulk density of the cast naphthalene used in this work was not accurately measured, it was determined to be greater than 1.00 grams/cc. Therefore, the density values obtained by Sherwood represented the actual fact to within ± five per cent at least. However, this percentage error is probably high since other investigations (9) using cast naphthalene cylinders and spheres have been satisfactorily correlated using Sherwood's density value. The diffusivity has been estimated to be correct to within ±1.5 per cent (7).

Another matter of concern in any transport phenomena where irregularly shaped surfaces are involved is the transfer area. This is of particular concern for solids which exhibit large crystalline structures as is the case for naphthalene. A microscopic examination of the cast naphthalene used in this work showed that the surface area was quite irregular due to the thin plate structure of the crystals. This would increase the surface area available for mass transfer over what would be calculated from the average pipe diameter. Since the actual surface area was not obtained, the transfer area used was based on the average pipe diameter. In order to estimate an overall experimental error it was estimated, based on microscopic observations, that the transfer area could be in error by 10 per cent.

The technique used to measure the thickness decrease was reproducible to within ± 0.0007 inches providing the guide wires were tightened the same amount for the before and after traces. Since the

taughtness of the guide wires affected the amount of sag of the screw, which in turn affected the initial deflection of the tracer arm, a technique was developed to produce the same amount of sag in the screw for each trace. This was done by placing the tracer foot on a particular position in the pipe and observing the tracer beam deflection on the recorder as the guide wires were tightened. A secondary check used was to count the turns applied to each guide wire nut and to always tighten to approximately the same number of turns. It was observed that after a certain amount of turns, a turn, one way or the other, produced little effect on the amount of sag. It was to this point that each run was set up.

In order to estimate the experimental error involved in this study, equation (20) was rewritten as

$$\left(\frac{\partial C^*}{\partial R}\right)_{R=1,L} = \frac{(N_{Aw})_{loc}\, r_w}{\mathcal{D}_{AB}(C_{Aw})} = \frac{\Delta mv\, \rho_N\, r_w}{0.039\, A_{Si}(MW)\theta_T \mathcal{D}_{AB} C_{Aw}}$$

or

$$\left(\frac{\partial C^*}{\partial R}\right)_{R=1,L} = f\left(\frac{\Delta mv\, \rho_N\, r_w}{A_{Si}\theta_T \mathcal{D}_{AB} C_{Aw}}\right) \qquad (61)$$

Equation (61) was put in typical error analysis form as

$$\frac{\Delta\left(\frac{\partial C^*}{\partial R}\right)}{\frac{\partial C^*}{\partial R}} = \frac{\Delta(mv)}{MV} + \frac{\Delta\rho_N}{\rho_N} - \frac{\Delta r_w}{r_w} - \frac{\Delta A_{Si}}{A_{Si}} - \frac{\Delta\theta_T}{\theta_T} - \frac{\Delta\mathcal{D}_{AB}}{\mathcal{D}_{AB}} - \frac{\Delta C_{Aw}}{C_{Aw}} \qquad (62)$$

If the assumption is made that all errors occur in the same direction at their maximum values, then the maximum experimental error is 23.9 per cent. The experimental results agree within this limit.

CHAPTER VII

CONCLUSIONS AND RECOMMENDATIONS

Theoretical and experimental results have been obtained for the mass-transfer rates of naphthalene subliming from an isothermal, horizontal pipe wall to an air stream flowing laminarly through the pipe with simultaneously developing velocity and concentration profiles. From the results of this study, it is concluded that:

1. The theoretical average results calculated from the mathematical model give agreement within ± 25 per cent of those obtained from the experimental investigation.

2. The average Nusselt numbers for mass-transfer, determined by

$$(Nu_{AB})_m = \frac{k_{x,m} r_w}{C\mathcal{D}_{AB}} = 1.83 + \frac{0.0449 \left[\frac{ReSc}{z/D}\right]}{1 + 0.0139 \left[\frac{ReSc}{z/D}\right]^{0.8}}$$

can be used to calculate the average mass-transfer coefficient $k_{x,m}$. The average mass-transfer rate determined by using $k_{x,m}$ in the equation

$$w_A = \frac{k_{x,m} (\pi D L_p) (X_{AbL_p} - X_{Abo})}{\ln\left(\frac{X_{Aw} - X_{Abo}}{X_{Aw} - X_{AbL_p}}\right)}$$

is approximately 20 per cent conservative.

3. The experimental local mass-transfer rates show a dependency on angular position in the tube.

4. The experimental local mass-transfer rates are drastically suppressed at the exit end of the pipe by some unknown factor.

It is recommended that further theoretical and experimental studies be conducted in connection with sublimation from crystalline materials. The following studies are suggested:

1. Additional investigations should be undertaken to explain the effect of angular velocities, set up by free-convection effects, on the local mass-transfer rates.

2. Additional experimental studies should be conducted to determine the cause for the rapid fall-off of the mass-transfer rate at the exit end of the pipe. The effect of pressure, temperature, flow rate, and concentration should be studied as well as the crystalline structures of the subliming materials.

A P P E N D I C E S

APPENDIX A

SUMMARY OF THEORETICAL AND EXPERIMENTAL RESULTS

Table 7. Theoretical Local Molar Flux* $N_{Aw} \times 10^{9}$

(Gm-moles/cm^2-sec) For T = (°C)

L	$\frac{ReSc}{z/D} \times 10^{-2}$	40	45	50	55	56	56.1	60	65	70
.001	40.0	6.53	10.3	15.9	24.2	26.3	26.5	36.6	54.5	80.3
.002	20.0	5.46	8.57	13.3	20.3	22.0	22.2	30.6	45.6	67.2
.003	13.3	4.58	7.19	11.1	17.0	18.5	18.6	25.7	38.2	56.4
.004	10.0	3.89	6.11	9.45	14.5	15.7	15.8	21.8	32.5	47.9
.005	8.0	3.37	5.29	8.19	12.5	13.6	13.7	18.9	28.2	41.5
.006	6.67	2.98	4.67	7.23	11.1	12.0	12.1	16.7	24.9	36.7
.007	5.71	2.67	4.20	6.50	9.94	10.8	10.9	15.0	22.4	33.0
.008	5.00	2.44	3.84	5.94	9.08	9.86	9.94	13.7	20.4	30.1
.009	4.44	2.26	3.55	5.49	8.40	9.13	9.20	12.7	18.9	27.9
.010	4.00	2.11	3.32	5.14	7.85	8.53	8.60	11.9	17.7	26.1
.013	3.08	1.80	2.83	4.38	6.69	7.27	7.32	10.1	15.1	22.2
.016	2.50	1.59	2.50	3.87	5.92	6.43	6.48	8.93	13.3	19.6
.020	2.00	1.40	2.20	3.40	5.20	5.65	5.70	7.85	11.7	17.3
.025	1.60	1.23	1.94	3.00	4.58	4.98	5.02	6.91	10.3	15.2
.032	1.25	1.07	1.69	2.61	3.99	4.33	4.37	6.02	8.97	13.2
.040	1.00	0.95	1.49	2.30	3.52	3.82	3.85	5.31	7.92	11.7
.050	0.80	0.84	1.31	2.03	3.11	3.37	3.40	4.69	6.98	10.3
.064	0.63	0.73	1.14	1.77	2.70	2.93	2.96	4.08	6.07	8.95
.080	0.50	0.64	1.00	1.55	2.38	2.58	2.60	3.58	5.34	7.87
.100	0.40	0.56	0.88	1.36	2.08	2.26	2.28	3.14	4.68	6.89

(Continued)

Table 7. Theoretical Molar Flux (Continued)

L	$\frac{ReSc}{z/D} \times 10^{-2}$	40	45	50	55	56	56.1	60	65	70
.110	0.36	0.51	0.81	1.25	1.91	2.07	2.09	2.88	4.29	6.31
.120	0.33	0.49	0.77	1.18	1.81	1.97	1.98	2.73	4.07	6.00
.130	0.31	0.46	0.73	1.13	1.72	1.87	1.89	2.60	3.87	5.71
.150	0.27	0.42	0.66	1.03	1.57	1.71	1.72	2.37	3.53	5.20
.170	0.24	0.39	0.61	0.94	1.44	1.56	1.58	2.17	3.24	4.77
.200	0.20	0.34	0.54	0.83	1.27	1.38	1.40	1.92	2.86	4.22
.220	0.18	0.32	0.50	0.77	1.18	1.28	1.29	1.78	2.65	3.90
.250	0.16	0.28	0.44	0.69	1.05	1.14	1.15	1.58	2.36	3.48
.280	0.14	0.25	0.40	0.61	0.94	1.02	1.03	1.42	2.11	3.11
.350	0.11	0.20	0.31	0.48	0.72	0.79	0.79	1.09	1.63	2.40
.400	0.10	0.16	0.26	0.40	0.60	0.66	0.66	0.91	1.36	2.00

*The data from L = 0.001 to L = 0.100 are taken from the numerical solution of equations (13) and (14). The remainder are from the solution of equation (55).

Table 8. Theoretical Average Molar Flux

(Gm-moles/cm^2-sec x 10^9)

$\frac{ReSc}{z/D}$ x 10^{-2}	50°C	55°C	56°C	60°C
40.0	-	-	-	36.6
20.0	-	-	22.2	30.6
13.3	11.1	17.0	18.5	29.8
10.0	9.45	14.5	18.2	28.3
8.00	9.32	14.3	17.4	26.7
6.67	9.05	13.9	16.6	25.3
5.71	8.73	13.4	15.8	23.9
5.00	8.42	12.9	15.2	22.7
4.44	8.12	12.4	-	-
4.00	7.84	12.0	14.0	20.8
3.33	7.34	11.2	-	19.2
2.86	6.91	10.6	-	17.9
2.66	-	-	11.8	-
2.50	-	10.0	-	-
2.35	6.39	-	-	-
2.22	-	9.56	-	-
2.00	5.79	9.14	10.4	15.1
1.60	5.42	8.29	9.40	13.6
1.33	4.99	7.62	8.57	12.4
1.14	4.65	7.12	-	-
1.00	4.36	6.69	7.46	10.7
0.89	4.13	6.33	-	-
0.80	3.92	6.02	6.68	9.59
0.73	3.75	5.75	-	-
0.67	3.59	5.51	-	8.73
0.62	-	5.29	-	-
0.57	3.33	5.16	5.63	8.06
0.50	3.12	4.78	-	7.32
0.44	2.94	4.50	4.94	-
0.40	2.78	4.27	4.68	6.70
0.33	2.53	3.88	4.25	6.07
0.29	2.33	3.57	3.91	5.57
0.25	2.17	3.32	3.64	5.17
0.22	2.03	3.11	3.41	4.84
0.20	1.91	2.93	3.21	4.55

Table 9. Theoretical Local $\partial C^*/\partial R$

$\frac{ReSc}{z/D} \times 10^{-2}$	$\partial C^*/\partial R$	$\frac{ReSc}{z/D} \times 10^{-2}$	$\partial C^*/\partial R$
40.0	13.9	1.00	2.03
20.0	11.7	0.80	1.79
13.3	9.79	0.63	1.53
10.0	8.31	0.50	1.37
8.00	7.21	0.40	1.20
6.67	6.37	0.36	1.04
5.71	5.72	0.33	0.99
5.00	5.22	0.31	0.94
4.44	4.84	0.27	0.86
4.00	4.52	0.24	0.79
3.08	3.85	0.20	0.70
2.50	3.41	0.18	0.64
2.00	2.99	0.16	0.57
1.60	2.64	0.14	0.51
1.25	2.29	0.11	0.40
		0.10	0.33

Table 10. Theoretical Average $\partial C^*/\partial R$

$\frac{ReSc}{z/D} \times 10^{-2}$	$\partial C^*/\partial R$	$\frac{ReSc}{z/D} \times 10^{-2}$	$\partial C^*/\partial R$
40.0	13.9	1.33	4.72
20.0	11.7	1.00	4.08
13.3	11.4	0.80	3.64
10.0	10.8	0.67	3.32
8.00	10.2	0.57	3.06
6.67	9.63	0.50	2.85
5.71	9.13	0.40	2.54
5.00	8.67	0.33	2.29
4.00	7.92	0.29	2.10
2.83	6.61	0.25	1.94
2.00	5.77	0.22	1.82
1.60	5.17	0.20	1.70

Table 11. Theoretical Local Nusselt Numbers

$\frac{ReSc}{z/D} \times 10^{-2}$	$(Nu_{AB})_{loc}$	$\frac{ReSc}{z/D} \times 10^{-2}$	$(Nu_{AB})_{loc}$
40.0	14.1	3.08	4.41
20.0	12.0	2.50	3.97
13.3	10.3	2.00	3.57
10.0	8.84	1.60	3.23
8.0	7.75	1.25	2.91
6.67	6.91	1.00	2.67
5.71	6.26	0.80	2.47
5.00	5.77	0.63	2.28
4.44	5.38	0.50	2.14
4.00	5.07	0.40	2.03

Table 12. Theoretical Average Nusselt Number

(Langhaar Velocity)

$\frac{ReSc}{z/D} \times 10^{-2}$	$(Nu_{AB})_m$	$\frac{ReSc}{z/D} \times 10^{-2}$	$(Nu_{AB})_m$
40.0	18.2	1.33	5.35
20.0	12.8	1.00	4.71
13.3	12.4	0.80	4.28
10.0	11.7	0.571	3.74
8.0	11.0	0.471	3.48
6.67	10.4	0.400	3.31
5.00	9.37	0.33	3.09
4.00	8.60	0.286	2.93
2.5	7.05	0.20	2.61
1.6	5.78	0.10	2.23

Table 13. Theoretical Nusselt Numbers

(Graetz Solution)

$\frac{ReSc}{z/D} \times 10^{-2}$	$(Nu_{AB})_{loc}$	$(Nu_{AB})_m$
40.0	7.30	12.9
20.0	6.23	9.82
13.3	5.54	8.50
10.0	5.05	7.70
8.0	4.69	7.12
6.67	4.42	6.70
5.71	4.20	6.35
5.00	4.02	6.07
4.44	3.87	5.85
4.00	3.74	5.62
2.00	3.00	4.47
1.33	2.66	3.92
1.00	2.46	3.57
0.80	2.32	3.35
0.67	2.22	3.15
0.57	2.14	3.02
0.50	2.09	2.90
0.44	2.04	2.82
0.40	2.00	2.72
0.33	1.95	2.60
0.31	1.93	2.55
0.27	1.90	2.47
0.24	1.87	2.40
0.20	1.85	2.32
0.18	1.85	2.28
0.16	1.84	2.22
0.14	1.83	2.18
0.11	1.83	2.11
0.10	1.83	2.08

Table 14. Transfer Numbers for Fully Developed Flow

(Numerical Scheme)

$\frac{ReSc}{z/D} \times 10^{-2}$	$N_{Aw} \times 10^{9}$ (gm-moles/cm^2-sec)	$\partial C^*/\partial R$	$(Nu_{AB})_{loc}$
40.0	35.3	13.9	14.0
20.0	22.7	8.98	9.24
13.3	17.2	6.79	7.09
10.0	14.4	5.68	6.00
8.0	12.7	5.03	4.94
6.67	11.6	4.59	4.62
5.71	10.8	4.26	4.38
5.00	10.1	4.00	4.17
4.44	9.57	3.78	4.00
4.00	9.11	3.60	3.62
3.08	8.06	3.18	3.35
2.50	7.32	2.89	3.10
2.00	6.60	2.61	2.88
1.60	5.95	2.35	2.66
1.25	5.29	2.09	2.49
1.00	4.76	1.88	2.34
0.80	4.26	1.68	2.20
0.63	3.76	1.48	2.09
0.50	3.34	1.32	2.00
0.40	2.95	1.16	2.00

Table 15. Experimental Local Molar Flux (Gm-moles/cm^2-sec)

Run 19

T = 50°C Re = 610

z	$\frac{ReSc}{z/D} \times 10^{-2}$	$N_{Aw} \times 10^9$ Top Trace	$N_{Aw} \times 10^9$ Bottom Trace	Local Average Molar Flux $(N_{Aw})_{loc.\ av.} \times 10^9$
71.40	0.390	-0.91	-0.03	-0.47
68.08	0.41	-0.85	0.192	-0.329
64.89	0.43	-0.74	0.795	0.027
61.41	0.455	-0.55	1.29	0.37
58.2	0.48	-0.25	1.86	0.805
54.9	0.51	0.439	2.24	1.34
52.8	0.54	0.494	2.40	1.45
48.5	0.58	0.617	2.55	1.58
45.1	0.62	0.742	2.77	1.76
41.8	0.67	0.879	2.99	1.94
38.5	0.73	1.07	3.21	2.14
35.2	0.79	1.33	3.40	2.37
32.2	0.87	1.73	3.62	2.68
28.6	0.98	2.14	3.78	2.96
25.2	1.10	2.58	4.00	3.29
21.9	1.27	3.09	4.25	3.67
18.5	1.50	3.68	4.47	4.07
15.2	1.83	4.29	4.80	4.55
11.7	2.39	4.97	5.35	5.16
10.0	2.79	5.43	5.73	5.58
8.3	3.35	6.02	6.22	6.14
6.3	4.40	6.75	6.85	6.80
4.7	5.95	7.85	7.81	7.83
3.9	7.24	8.65	8.55	8.60
3.0	9.24	9.64	9.75	9.69
2.19	12.70	10.70	-	10.70

Table 16. Experimental Local Molar Flux (Gm-moles/cm^2-sec)

Run 28

T = 50°C Re = 1295

z	$\frac{ReSc}{z/D} \times 10^{-2}$	$N_{Aw} \times 10^9$ Top Trace	$N_{Aw} \times 10^9$ Bottom Trace	Local Average Molar Flux $(N_{Aw})_{loc.\ av.} \times 10^9$
71.40	0.828	-1.67	1.30	-0.185
68.08	0.868	-3.14	0.627	-1.256
64.89	0.913	-3.30	0.46	-1.42
61.41	0.965	-3.22	0.712	-1.254
58.2	1.011	-2.76	1.34	-0.71
54.9	1.08	-2.17	2.18	0.0
52.8	1.14	-1.46	2.93	0.739
48.5	1.22	-0.669	3.56	1.446
45.1	1.31	0.167	4.14	2.15
41.8	1.41	0.964	4.56	2.762
38.5	1.53	1.84	4.94	3.39
35.2	1.68	2.68	5.40	4.04
32.2	1.83	3.45	5.82	4.63
28.6	2.07	4.23	6.28	5.26
25.2	2.34	5.12	6.78	5.95
21.9	2.69	5.98	7.70	6.59
18.5	3.18	7.00	8.20	7.60
15.2	3.87	8.21	9.25	8.73
11.7	5.06	9.60	10.62	10.11
10.0	5.91	10.45	11.4	10.93
8.3	7.09	11.50	12.4	11.95
6.3	9.33	12.80	13.77	13.29
4.7	12.6	14.4	15.71	15.06
3.9	15.3	15.5	17.35	16.43
3.0	19.5	16.79	19.2	17.99
2.19	27.9	19.24	21.35	20.29
1.66	33.6	20.95	24.25	22.60

Table 17. Experimental Local Molar Flux (Gm-moles/cm^2-sec)

Run 27

T = 50°C Re = 1970

z	$\frac{ReSc}{z/D} \times 10^{-2}$	$N_{Aw} \times 10^9$ Top Trace	$N_{Aw} \times 10^9$ Bottom Trace	Local Average Molar Flux $(N_{Aw})_{loc.\ av.} \times 10^9$
71.40	1.26	4.07	5.81	+.94
68.08	1.32	1.20	3.81	2.50
64.89	1.39	-0.267	2.34	1.04
61.41	1.47	-1.20	1.67	0.235
58.2	1.55	-1.00	2.68	0.84
54.9	1.64	0.467	3.94	2.20
52.8	1.73	1.41	4.75	3.08
48.5	1.86	2.01	5.08	3.55
45.1	2.00	2.48	5.28	3.88
41.8	2.15	3.01	5.25	4.13
38.5	2.34	3.48	5.35	4.42
35.2	2.56	3.81	5.35	4.59
32.2	2.80	4.35	5.35	4.85
28.6	3.15	4.95	5.42	5.19
25.2	3.56	5.62	5.48	5.55
21.9	4.11	6.29	5.85	6.07
18.5	4.86	6.90	6.52	6.71
15.2	5.92	7.76	7.42	7.59
11.7	7.73	9.04	8.64	8.84
10.0	9.01	9.77	9.44	9.60
8.3	10.8	10.9	10.4	10.7
6.3	14.2	12.5	12.4	12.5
4.7	19.2	15.3	15.2	15.3
3.9	23.4	17.3	17.3	17.3
3.0	29.8	19.91	20.35	20.1
2.19	41.2	23.40	24.10	23.8
1.66	54.3		31.35	31.4

Table 18. Experimental Local Molar Flux (Gm-moles/cm^2-sec)

Run 23

T = 55°C Re = 540

z	$\frac{ReSc}{z/D} \times 10^{-2}$	$N_{Aw} \times 10^9$ Top Trace	$N_{Aw} \times 10^9$ Bottom Trace	Local Average Molar Flux $(N_{Aw})_{loc.\ av.} \times 10^9$
71.40	0.345	-0.915	-0.718	-0.817
68.08	0.361	-0.980	1.50	0.26
64.89	0.380	-1.045	2.48	0.719
61.41	0.401	-1.045	3.07	1.01
58.2	0.423	-0.980	3.52	1.27
54.9	0.448	-0.915	4.37	1.73
52.8	0.475	-0.915	5.10	2.09
48.5	0.509	-0.588	5.81	2.61
45.1	0.545	-0.131	6.40	3.14
41.8	0.489	0.522	6.93	3.73
38.5	0.639	1.24	7.25	4.25
35.2	0.700	1.96	7.45	4.71
32.2	0.765	2.81	7.59	5.20
29.6	0.861	3.66	7.78	5.72
25.2	0.975	4.65	8.05	6.35
21.9	1.07	5.69	8.24	6.97
18.5	1.33	6.86	8.50	7.68
15.2	1.61	8.11	8.63	8.37
11.7	2.11	9.48	9.15	9.32
10.0	2.46	10.02	9.65	9.84
8.3	2.95	11.25	10.31	10.8
6.3	3.89	12.41	11.30	11.9
4.7	5.26	14.38	12.72	13.6
3.9	6.40	16.01	13.71	14.9
3.0	8.15	17.98	16.32	17.2
2.19	11.20	20.00	20.35	20.2
1.66	14.80	22.50	24.50	23.5

Table 19. Experimental Local Molar Flux (Gm-moles/cm^2-sec)

Run 19

T = 55 °C Re = 1305

z	$\frac{ReSc}{z/D} \times 10^{-2}$	$N_{Aw} \times 10^9$ Top Trace	$N_{Aw} \times 10^9$ Bottom Trace	Local Average Molar Flux $(N_{Aw})_{loc.\ av.} \times 10^9$
71.40	-	-	-	-
68.08	0.873	3.21	6.26	4.73
64.89	0.917	3.29	7.91	5.60
61.41	0.968	3.44	8.22	5.83
58.2	1.02	3.52	7.59	5.56
54.9	1.08	3.60	5.87	4.74
52.8	1.15	3.72	5.94	4.83
48.5	1.23	3.84	6.03	4.94
45.1	1.32	3.99	6.10	5.05
41.8	1.42	4.30	6.26	5.28
38.5	1.55	4.89	6.34	5.62
35.2	1.69	5.71	6.57	6.14
32.2	1.85	6.42	6.74	6.58
28.6	2.08	7.12	6.97	7.05
25.2	2.35	7.63	7.44	7.54
21.9	2.71	8.22	7.99	8.10
18.5	3.21	8.93	8.76	8.85
15.2	3.90	9.71	9.32	9.51
11.7	5.11	10.64	10.25	10.45
10.0	5.95	11.70	11.72	11.71
8.3	7.14	13.15	13.15	13.15
6.3	9.40	15.6	15.65	15.6
4.7	12.70	19.3	18.8	19.05
3.9	15.45	22.0	21.1	21.6
3.0	19.70	25.1	23.6	24.35
2.19	27.10	28.9	26.45	27.68
1.66	43.7	-	30.0	30.0

Table 20. Experimental Local Molar Flux (Gm-moles/cm^2-sec)

Run 24

T = 55°C Re = 1535

z	$\frac{ReSc}{z/D} \times 10^{-2}$	$N_{Aw} \times 10^9$ Top Trace	$N_{Aw} \times 10^9$ Bottom Trace	Local Average Molar Flux $(N_{Aw})_{loc.\ av.} \times 10^9$
71.40	0.982	2.52	5.75	4.14
68.08	1.03	2.63	6.69	4.66
64.89	1.08	2.74	7.24	4.99
61.41	1.14	2.96	7.68	5.32
58.2	1.21	3.29	8.11	5.70
54.9	1.28	3.94	8.22	6.08
52.8	1.35	4.60	8.44	6.52
48.5	1.45	5.25	8.66	6.96
45.1	1.55	5.75	8.76	7.26
41.8	1.68	6.46	8.87	7.67
38.5	1.82	7.12	9.05	8.09
35.2	1.99	8.00	9.20	8.60
32.2	2.18	8.65	9.32	8.99
28.6	2.46	9.53	9.37	9.45
25.2	2.77	10.4	9.54	9.97
21.9	3.20	11.67	9.65	10.66
18.5	3.78	13.05	9.97	11.51
15.2	4.60	14.50	10.95	12.72
11.7	6.02	16.30	12.8	14.55
10.0	7.00	17.52	14.4	15.96
8.3	8.41	18.95	16.7	17.83
6.3	11.05	20.8	19.5	20.15
4.7	14.95	24.0	23.7	23.85
3.9	18.2	26.3	26.5	26.4
3.0	23.2	29.2	30.1	29.65
2.19	32.0	32.9	35.4	34.15
1.66	42.3	37.2	36.7	36.95

Table 21. Experimental Local Molar Flux (Gm-moles/cm^2-sec)

Run 21

T = 60°C Re = 545

z	$\frac{ReSc}{z/D} \times 10^{-2}$	$N_{Aw} \times 10^9$ Top Trace	$N_{Aw} \times 10^9$ Bottom Trace	Local Average Molar Flux $(N_{Aw})_{loc.\ av.} \times 10^9$
71.40	0.349	-8.65	-6.91	-7.78
68.08	0.365	-8.65	-5.45	-7.05
64.89	0.383	-8.65	-3.91	-6.28
61.41	0.405	-8.42	-2.33	-5.38
58.2	0.428	-8.12	0.0	-4.06
54.9	0.454	-7.81	1.35	-3.23
52.8	0.480	-7.29	3.01	-2.14
48.5	0.514	-6.46	4.36	-1.05
45.1	0.552	-5.56	5.56	0.0
41.8	0.594	-4.58	6.54	0.980
38.5	0.647	-3.06	7.14	2.04
32.2	0.774	-0.601	8.15	3.78
28.6	0.872	-0.0826	8.33	4.12
25.2	0.987	2.33	8.37	5.35
21.9	1.14	3.98	8.64	6.31
18.5	1.34	5.71	9.16	7.44
15.2	1.64	7.52	10.0	8.76
11.7	2.14	9.70	10.7	10.20
10.0	2.49	10.72	11.7	11.21
8.3	2.99	12.2	12.7	12.45
6.3	3.93	14.0	14.4	14.2
4.7	5.32	16.6	17.3	16.95
3.9	6.47	18.5	19.3	18.90
3.0	8.24	21.0	22.2	21.6
2.19	11.35	24.4	27.7	26.05
1.66	15.0	-	34.6	34.6

Table 21 (Continued)

Run 21

T = 60°C Re = 545

z	$\frac{ReSc}{z/D} \times 10^{-2}$	$N_{Aw} \times 10^{9}$ Back Side Trace	$N_{Aw} \times 10^{9}$ Front Side Trace
71.40	0.349	-5.66	-7.29
68.08	0.365	-5.48	-6.98
64.89	0.383	-5.26	-6.54
61.41	0.405	-4.88	-5.93
58.2	0.428	-4.21	-5.18
54.9	0.454	-3.46	-4.43
52.8	0.480	-2.63	-3.16
48.5	0.514	-1.73	-1.95
45.1	0.552	-0.827	-0.902
41.8	0.594	0.15	- ---
38.5	0.647	1.13	1.35
35.2	0.709	2.03	2.55
32.2	0.774	2.86	3.61
28.6	0.872	3.68	4.51
25.2	0.987	4.36	5.26
21.9	1.138	5.42	6.08
18.5	1.34	6.57	6.98
15.2	1.64	7.90	8.19
11.7	2.14	9.02	9.61
10.0	2.49	9.77	10.68
8.3	2.99	10.60	11.90
6.3	3.93	11.80	13.09
4.7	5.32	13.60	14.29
3.9	6.47	14.90	15.05
3.0	8.24	16.81	15.79
2.19	11.35	19.81	16.55
1.66	15.0	23.80	17.65

Table 22. Experimental Local Molar Flux (Gm-moles/cm^2-sec)

Run 22

T = 60°C Re = 1315

z	$\frac{ReSc}{z/D} \times 10^{-2}$	$N_{Aw} \times 10^9$ Top Trace	$N_{Aw} \times 10^9$ Bottom Trace	Local Average Molar Flux $(N_{Aw})_{loc.\ av.} \times 10^9$
71.40	0.841	-2.90	-4.14	-3.52
68.03	0.88	-2.73	-0.497	-1.61
64.89	0.925	-2.48	1.16	-0.66
61.41	0.975	-2.15	2.07	-0.04
58.2	1.03	-1.57	2.48	0.46
54.9	1.09	-0.580	2.81	1.12
52.8	1.15	0.414	3.14	1.78
48.5	1.23	1.24	3.52	2.38
45.1	1.33	2.15	3.80	2.98
41.8	1.43	3.48	4.72	4.10
38.5	1.56	5.13	5.71	5.42
35.2	1.70	6.70	6.79	6.74
32.2	1.86	8.03	8.11	8.07
28.6	2.10	9.35	9.11	9.23
25.2	2.37	11.0	10.5	10.75
21.9	2.73	13.0	12.0	12.5
18.5	3.23	15.2	13.6	14.40
15.2	3.93	17.4	15.4	16.4
11.7	5.14	19.6	18.4	19.0
10.0	5.99	21.8	20.6	21.2
8.3	7.20	24.9	24.0	24.45
6.3	9.46	29.6	28.6	29.1
4.7	12.8	35.6	34.6	35.1
3.9	15.6	39.0	39.3	39.15
3.0	19.8	42.6	46.2	44.4
3.19	22.7	46.0	-	46.0
1.66	36.0	50.0	0	50.0

Table 22 (Continued)

Run 22

T = 60°C Re = 1315

z	$\frac{ReSc}{z/D} \times 10^{-2}$	$N_{Aw} \times 10^{9}$ Back Side Trace
71.40	0.841	-1.99
68.08	0.88	-1.41
64.89	0.925	-1.24
61.41	0.975	-0.99
58.2	1.03	-0.79
54.9	1.09	0.20
52.8	1.15	1.16
48.5	1.23	2.07
45.1	1.33	2.98
41.8	1.43	4.14
38.5	1.56	5.30
35.2	1.70	6.55
32.2	1.86	7.86
28.6	2.10	9.31
25.2	2.37	10.78
21.9	2.73	12.41
18.5	3.23	14.32
15.2	3.93	16.59
11.7	5.14	19.56
10.0	5.99	22.00
8.3	7.20	25.1
6.3	9.46	29.8
4.7	12.80	35.6
3.9	15.6	39.1
3.0	19.8	44.3
2.19	22.7	51.3
1.66	36.0	-

Table 23. Experimental Local Molar Flux (Gm-moles/cm^2-sec)

Run 26

T = 60°C Re = 1370

z	$\frac{ReSc}{z/D} \times 10^{-2}$	$N_{Aw} \times 10^9$ Top Trace	$N_{Aw} \times 10^9$ Bottom Trace	Local Average Molar Flux $(N_{Aw})_{loc.\ av.} \times 10^9$
71.40	1.00	-0.549	3.18	1.32
68.08	1.05	-1.21	3.29	1.04
64.89	1.11	-1.64	3.73	1.05
61.41	1.17	-1.86	4.28	1.21
58.2	1.23	-1.53	4.94	1.70
54.9	1.31	-0.438	5.59	2.58
52.8	1.38	1.32	6.31	3.82
48.5	1.48	2.64	7.24	4.94
45.1	1.59	3.95	8.23	6.09
41.8	1.71	5.71	9.43	7.57
38.5	1.86	7.58	10.3	8.94
35.2	2.03	9.34	11.2	10.27
32.2	2.23	10.4	12.1	11.25
28.6	2.51	11.7	13.2	12.45
25.2	2.84	13.2	14.5	13.85
21.9	3.27	14.8	15.8	15.30
18.5	3.86	16.6	17.4	16.95
15.2	4.70	18.7	19.2	18.95
11.7	6.14	21.0	21.4	21.2
10.0	7.16	22.2	22.7	22.45
8.3	8.60	23.7	24.2	23.95
6.3	11.3	25.8	26.8	26.3
4.7	15.3	28.6	30.1	29.35
3.9	18.6	31.8	32.4	32.10
3.0	23.7	34.6	34.9	34.75
2.19	32.7	-	38.4	38.4
1.66	43.2	-	44.4	44.4

Table 24. Experimental Local Molar Flux (Gm-moles/cm^2-sec)

Run 13

T = 56°C Re = 1405

z	$\frac{ReSc}{z/D} \times 10^{-2}$	$N_{A_s} \times 10^9$
71.40	-	-
68.08	0.939	5.97
64.89	0.988	6.29
61.41	1.04	6.62
58.2	1.10	6.85
54.9	1.17	7.18
52.8	1.24	7.43
48.5	1.32	7.66
45.1	1.42	7.99
41.8	1.53	8.72
38.5	1.66	8.47
35.2	1.82	8.71
32.2	1.99	9.07
28.6	2.24	9.47
25.2	2.54	10.0
21.9	2.92	10.7
18.5	3.45	11.5
15.2	4.19	12.6
11.7	5.48	14.3
10.0	6.40	15.7
8.3	7.68	17.6
6.3	10.1	20.5
4.7	13.7	24.9
3.9	16.6	27.8
3.0	21.2	31.2
2.19	29.2	35.6
1.66	47.1	41.7

Table 25. Experimental Local Molar Flux (Gm-moles/cm^2-sec)

Run 14

T = 56°C Re = 1700

z	$\frac{ReSc}{z/D} \times 10^{-2}$	$N_{Aw} \times 10^9$
71.40	-	-
68.08	1.14	2.16
64.89	1.20	2.82
61.41	1.26	3.73
58.2	1.33	4.47
54.9	1.42	5.14
52.8	1.50	5.72
48.5	1.60	6.38
45.1	1.72	6.96
41.8	1.85	7.46
38.5	2.01	7.80
35.2	2.21	8.13
32.2	2.41	8.62
28.6	2.72	9.28
25.2	3.07	10.02
21.9	3.54	10.9
18.5	4.18	12.0
15.2	5.08	13.2
11.7	6.65	14.7
10.0	7.76	16.4
8.3	9.31	18.8
6.3	12.2	21.9
4.7	16.6	27.8
3.9	20.1	31.2
3.0	25.7	35.5
2.19	35.4	41.4
1.66	57.0	48.1

Table 26. Experimental Local Molar Flux (Gm-moles/cm^2-sec)

Run 5

T = 56°C Re = 513

z	$\frac{ReSc}{z/D} \times 10^{-2}$	$N_{Aw} \times 10^9$
71.40	0.34	-2.66
68.08	0.358	-2.02
64.89	0.376	-3.49
61.41	0.397	-3.12
58.2	0.419	-1.47
54.9	0.44	-0.826
52.8	0.47	1.84
48.5	0.50	3.31
45.1	0.54	5.15
41.8	0.58	6.52
38.5	0.63	7.58
35.2	0.68	8.26
32.2	0.75	8.81
28.6	0.84	9.64
25.2	0.95	10.7
21.9	1.08	11.7
18.5	1.29	12.3
15.2	1.57	13.2
11.7	1.99	14.4
10.0	2.22	15.2
8.3	2.61	16.5
6.3	3.18	18.2
4.7	3.94	21.2
3.9	4.56	24.2
3.0	-	-
2.19	-	-
1.66	-	-

Table 27. Experimental Local Molar Flux (Gm-moles/cm^2-sec)

Run 8

T = 56°C Re = 764

z	$\frac{ReSc}{z/D} \times 10^{-2}$	$N_{Aw} \times 10^9$
71.40	0.488	-
68.08	0.512	2.82
64.89	0.528	4.07
61.41	0.568	5.41
58.2	0.60	6.59
54.9	0.635	7.45
52.8	0.673	8.15
48.5	0.720	8.78
45.1	0.773	9.25
41.8	0.834	10.2
38.5	0.904	10.9
35.2	0.992	11.6
32.2	1.08	12.2
28.6	1.22	12.7
25.2	1.38	13.2
21.9	1.59	13.9
18.5	1.88	14.7
15.2	2.29	15.7
11.7	2.99	17.1
10.0	3.48	18.1
8.3	4.18	19.2
6.3	5.50	20.7
4.7	7.44	22.4
3.9	9.05	23.6
3.0	11.6	25.1
2.19	15.9	27.4
1.66	-	-

Table 28. Experimental Local Molar Flux (Gm-moles/cm^2-sec)

Run 9

T = 56°C Re = 860

z	$\frac{ReSc}{z/D} \times 10^{-2}$	$N_{Aw} \times 10^{9}$
71.40	-	-
68.08	0.576	5.69
64.89	0.604	6.37
61.41	0.638	6.90
58.2	0.674	7.58
54.9	0.713	8.26
52.8	0.756	9.03
48.5	0.81	10.0
45.1	0.869	16.8
41.8	0.936	11.7
38.5	1.02	12.3
35.2	1.11	12.5
32.2	1.22	12.6
28.6	1.37	12.9
25.2	1.55	13.3
21.9	1.79	13.8
18.5	2.11	14.4
15.2	2.57	15.0
11.7	3.36	15.9
10.0	3.92	16.5
8.3	4.70	17.5
6.3	6.19	19.3
4.7	8.38	22.3
3.9	10.2	24.5
3.0	13.0	27.5
2.19	17.9	32.2
1.66	28.8	42.4

Table 29. Experimental Local Molar Flux (Gm-moles/cm^2-sec)

Run 10

T = 56°C Re = 1330

z	$\frac{ReSc}{z/D} \times 10^{-2}$	$N_{Aw} \times 10^9$
71.40	-	-
68.08	0.89	6.86
64.89	0.935	8.39
61.41	0.986	9.75
58.2	1.04	11.1
54.9	1.10	12.2
52.8	1.17	13.1
48.5	1.25	13.7
45.1	1.34	14.0
41.8	1.44	14.1
38.5	1.57	14.1
35.2	1.72	14.1
32.2	1.88	14.2
28.6	2.12	14.4
25.2	2.39	14.5
21.9	2.76	14.9
18.5	3.26	15.3
15.2	3.97	15.8
11.7	5.19	16.7
10.0	6.05	17.9
8.3	7.26	19.7
6.3	9.55	22.3
4.7	12.9	26.2
3.9	15.7	29.1
3.0	20.0	32.8
2.19	27.6	37.2
1.66	44.5	42.5

Table 30. Experimental Average Molar Flux (Gm-moles/cm^2-sec)

T = 50°C

Run 19		Run 28		Run 27	
$\frac{ReSc}{z/D}$ x 10^{-2}	$(N_{Aw})_m$ x 10^9	$\frac{ReSc}{z/D}$ x 10^{-2}	$(N_{Aw})_m$ x 10^9	$\frac{ReSc}{z/D}$ x 10^{-2}	$(N_{Aw})_m$ x 10^9
13.3	10.8	33.6	22.6	53.3	27.8
10.0	9.90	20.0	18.1	40.0	23.6
8.0	9.82	13.3	17.7	20.0	19.7
6.67	9.60	10.0	17.0	13.3	17.8
5.71	9.36	8.0	16.2	10.0	16.1
5.0	9.13	6.67	15.5	8.0	14.8
4.44	8.89	5.71	14.9	5.33	12.5
4.0	8.67	5.00	14.4	4.00	11.0
3.33	8.26	4.00	13.4	3.20	9.93
2.86	7.90	2.67	11.5	2.66	9.10
2.35	7.45	2.00	10.1	2.00	7.63
2.00	7.08	1.60	9.00	1.78	7.21
1.60	6.56	1.33	8.01	1.60	6.65
1.33	6.13	1.14	7.08	1.45	6.23
1.14	5.76	1.00	6.19	1.33	5.71
1.00	5.44	0.89	5.39	-	-
0.89	5.15	-	-	-	-
0.80	4.89	-	-	-	-
0.67	4.44	-	-	-	-
0.57	4.05	-	-	-	-
0.53	3.88	-	-	-	-
0.50	3.47	-	-	-	-
0.44	3.09	-	-	-	-
0.39	2.71	-	-	-	-

Table 31. Experimental Average Molar Flux (Gm-moles/cm^2-sec)

T = 55°C

Run 23		Run 15		Run 24	
$\frac{ReSc}{z/D} \times 10^{-2}$	$(N_{Aw})_m \times 10^9$	$\frac{ReSc}{z/D} \times 10^{-2}$	$(N_{Aw})_m \times 10^9$	$\frac{ReSc}{z/D} \times 10^{-2}$	$(N_{Aw})_m \times 10^9$
20.0	24.1	40.0	29.7	42.3	37.0
13.3	21.1	20.0	24.6	32.0	34.2
10.0	20.8	13.3	23.8	20.0	33.0
8.00	20.7	10.0	23.0	13.3	30.3
6.67	19.6	8.00	21.1	10.0	28.0
5.00	18.3	5.71	18.7	8.00	26.1
4.00	17.2	4.00	16.3	6.67	24.4
2.67	15.2	3.20	14.9	5.71	23.1
2.00	13.8	2.67	13.8	5.00	21.9
1.33	12.0	2.00	12.3	4.00	20.0
1.00	10.8	1.60	11.1	3.20	18.3
0.80	9.63	1.33	10.2	2.67	16.9
0.67	8.83	1.14	9.43	2.00	15.0
0.51	8.14	1.00	8.88	1.60	13.6
0.50	7.49	0.89	8.52	1.33	12.4
0.44	6.89	-	-	1.14	11.5
0.40	6.33	-	-	1.00	10.7
0.36	5.82	-	-	-	-
0.35	5.53	-	-	-	-

Table 32. Experimental Average Molar Flux (Gm-moles/cm^2-sec)

T = 56°C

Run 13		Run 14	
$\frac{ReSc}{z/D} \times 10^{-2}$	$(N_{Aw})_m \times 10^9$	$\frac{ReSc}{z/D} \times 10^{-2}$	$(N_{Aw})_m \times 10^9$
47.1	41.7	57.0	48.1
29.2	35.6	35.4	41.4
20.0	34.8	20.0	39.2
13.3	32.4	13.3	35.2
10.0	29.9	10.0	31.7
8.00	27.8	8.00	29.0
6.67	25.9	6.67	26.8
5.71	24.4	5.71	25.0
5.00	23.1	5.00	23.6
4.00	21.1	4.44	22.4
3.33	19.5	4.00	21.3
2.86	18.3	3.33	19.7
2.00	15.8	2.86	18.3
1.60	14.4	2.50	17.2
1.33	13.3	2.00	15.4
1.14	12.5	1.60	13.7
1.00	11.8	1.33	12.3
		1.14	11.0

Table 33. Experimental Average Molar Flux (Gm-moles/cm^2-sec)

T = 56 °C

Run 21		Run 22		Run 26	
$\frac{ReSc}{z/D} \times 10^{-2}$	$(N_{Aw})_m \times 10^9$	$\frac{ReSc}{z/D} \times 10^{-2}$	$(N_{Aw})_m \times 10^9$	$\frac{ReSc}{z/D} \times 10^{-2}$	$(N_{Aw})_m \times 10^9$
15.0	34.6	36.0	50.0	43.2	44.4
11.4	26.0	22.7	46.0	32.7	38.4
8.00	25.2	20.0	45.9	20.0	37.3
6.67	24.3	13.3	43.5	13.3	34.9
5.00	22.7	10.0	41.3	10.0	32.8
4.00	21.2	8.00	38.6	8.00	31.1
2.67	18.5	6.67	36.3	6.67	29.7
2.00	16.6	5.71	34.2	5.71	28.5
1.33	13.9	5.00	32.4	5.00	27.5
1.00	12.1	4.00	29.4	4.00	25.7
0.80	10.6	3.33	27.1	3.33	24.2
0.67	9.36	2.86	25.2	2.86	22.8
0.57	8.23	2.50	23.6	2.50	21.6
0.50	7.13	2.22	22.1	2.00	19.5
0.44	6.03	2.00	20.9	1.60	17.3
0.40	4.95	1.60	18.1	1.33	15.1
0.35	3.43	1.33	15.9	1.14	13.2
-	-	1.14	13.9	1.00	11.7
-	-	1.00	12.3	-	-
-	-	0.89	10.9	-	-

Table 34. Experimental Local $\partial C^*/\partial R$

T = 50°C

Run 19		Run 28		Run 27	
$\frac{ReSc}{z/D} \times 10^{-2}$	$\partial C^*/\partial R$	$\frac{ReSc}{z/D} \times 10^{-2}$	$\partial C^*/\partial R$	$\frac{ReSc}{z/D} \times 10^{-2}$	$\partial C^*/\partial R$
0.390	-0.392	0.828	-0.154	1.26	4.13
0.41	-2.75	0.868	-1.06	1.32	2.09
0.43	0.022	0.913	-1.18	1.39	0.87
0.455	0.309	0.965	-1.04	1.47	1.96
0.48	0.675	1.01	-0.595	1.55	0.70
0.51	1.12	1.08	0	1.64	1.84
0.54	1.21	1.14	0.62	1.73	2.58
0.58	1.32	1.22	1.21	1.86	2.97
0.62	1.47	1.31	1.79	2.00	3.24
0.67	1.62	1.41	2.30	2.15	3.45
0.73	1.79	1.53	2.83	2.34	3.69
0.79	1.98	1.68	3.38	2.56	3.83
0.87	2.24	1.83	3.87	2.80	4.05
0.98	2.47	2.07	4.39	3.15	4.33
1.10	2.75	2.34	4.97	3.56	4.63
1.27	3.06	2.69	5.50	4.11	5.05
1.50	3.40	3.18	6.35	4.86	5.60
1.83	3.80	3.87	7.30	5.92	6.35
2.39	4.31	5.06	8.45	7.73	7.40
2.79	4.66	5.91	9.10	9.01	8.00
3.35	5.15	7.09	10.0	10.8	8.95
4.40	5.70	9.33	11.1	14.2	10.4
5.95	6.55	12.6	12.6	19.2	12.3
7.24	7.20	15.3	13.7	23.4	14.5
9.24	8.10	19.5	15.0	29.8	16.8
12.7	8.95	27.9	16.9	41.2	19.9
-	-	33.6	18.9	54.3	26.3

Table 35. Experimental Local $\partial C^*/\partial R$

T = 55°C

Run 23		Run 15		Run 24	
$\frac{ReSc}{z/D} \times 10^{-2}$	$\partial C^*/\partial R$	$\frac{ReSc}{z/D} \times 10^{-2}$	$\partial C^*/\partial R$	$\frac{ReSc}{z/D} \times 10^{-2}$	$\partial C^*/\partial R$
0.345	-0.446	0.873	2.58	0.982	2.27
0.361	0.142	0.917	3.10	1.03	2.54
0.380	0.392	0.968	3.18	1.08	2.73
0.401	0.55	1.02	3.04	1.14	2.91
0.423	0.695	1.08	2.59	1.21	3.11
0.448	0.945	1.15	2.64	1.28	3.33
0.475	1.14	1.23	2.70	1.35	3.57
0.509	1.43	1.32	2.76	1.45	3.80
0.545	1.71	1.42	2.89	1.55	3.98
0.589	2.04	1.55	3.07	1.68	4.19
0.639	2.33	1.69	3.36	1.82	4.42
0.700	2.58	1.85	3.59	1.99	4.70
0.765	2.85	2.08	3.85	2.18	4.91
0.861	3.12	2.35	4.12	2.46	5.15
0.975	3.47	2.71	4.43	2.77	5.45
1.07	3.81	3.21	4.89	3.20	5.85
1.33	4.20	3.90	5.20	3.78	6.30
1.61	4.57	5.11	5.75	4.60	6.95
2.11	5.10	5.95	6.40	6.02	8.00
2.46	5.40	7.14	7.20	7.00	8.75
2.95	5.90	9.40	8.55	8.41	9.75
3.89	6.50	12.7	10.4	11.05	11.0
5.26	7.45	15.5	11.8	15.0	13.0
6.40	8.15	19.7	13.3	18.2	14.5
8.15	9.40	27.1	15.2	23.2	16.3
11.2	11.0	43.7	16.4	32.0	18.7
14.8	12.8	-	-	42.3	20.2

Table 36. Experimental Local $\partial C^*/\partial R$

T = 56°C

Run 13		Run 14	
$\frac{ReSc}{z/D} \times 10^{-2}$	$\partial C^*/\partial R$	$\frac{ReSc}{z/D} \times 10^{-2}$	$\partial C^*/\partial R$
0.939	3.00	1.14	1.29
0.988	3.17	1.20	1.42
1.04	3.33	1.26	1.88
1.10	3.45	1.33	2.25
1.17	3.61	1.42	2.59
1.24	3.74	1.50	2.88
1.32	3.85	1.60	3.21
1.42	4.02	1.72	3.50
1.53	4.14	1.85	3.75
1.66	4.26	2.01	3.93
1.82	4.38	2.21	4.09
1.99	4.56	2.41	4.34
2.24	4.77	2.72	4.67
2.54	5.03	3.07	5.03
2.92	5.98	3.54	5.49
3.45	5.79	4.18	6.04
4.19	6.34	5.08	6.64
5.48	7.20	6.65	7.40
6.40	7.90	7.76	8.25
7.68	8.86	9.31	9.46
10.1	10.3	12.2	11.0
13.7	12.5	16.6	14.0
16.6	14.0	20.1	15.7
21.2	15.7	25.7	17.9
29.2	17.9	35.4	20.8
47.1	21.0	57.0	24.2

Table 37. Experimental Local $\partial C^*/\partial R$
T = 60°C

Run 21		Run 22		Run 26	
$\frac{ReSc}{z/D} \times 10^{-2}$	$\partial C^*/\partial R$	$\frac{ReSc}{z/D} \times 10^{-2}$	$\partial C^*/\partial R$	$\frac{ReSc}{z/D} \times 10^{-2}$	$\partial C^*/\partial R$
0.349	-2.82	0.841	-1.28	1.00	0.478
0.365	-2.56	0.88	-0.584	1.05	3.77
0.383	-2.28	0.925	-0.239	1.11	0.381
0.405	-1.95	0.975	-0.014	1.17	0.439
0.428	-1.47	1.03	0.167	1.23	0.616
0.454	-1.17	1.09	0.406	1.31	0.935
0.480	-0.776	1.15	0.645	1.38	1.38
0.514	-0.381	1.23	0.863	1.48	1.79
0.552	0.0	1.33	1.08	1.59	2.21
0.594	0.355	1.43	1.49	1.71	2.74
0.647	0.739	1.56	1.96	1.86	3.24
0.709	1.01	1.70	2.44	2.03	3.73
0.774	1.37	1.86	2.92	2.23	4.10
0.872	1.49	2.10	3.35	2.51	4.53
0.987	1.94	2.37	3.91	2.84	5.04
1.14	2.29	2.73	4.53	3.27	5.54
1.34	2.70	3.23	5.22	3.86	6.16
1.64	3.17	3.93	5.94	4.70	6.89
2.14	3.70	5.14	6.89	6.14	7.68
2.49	4.06	5.99	7.68	7.16	8.15
2.99	4.53	7.20	8.88	8.60	8.70
3.93	5.15	9.46	10.5	11.3	9.53
5.32	6.16	12.8	12.7	15.3	10.7
6.47	6.85	15.6	14.2	18.6	11.6
8.24	7.83	19.8	16.1	23.7	12.6
11.4	9.42	22.7	16.7	32.7	13.9
15.0	12.5	36.0	18.1	43.2	16.1

Table 38. Experimental Average $\partial C^*/\partial R$

T = 50°C

Run 19		Run 28		Run 27	
$\frac{ReSc}{z/D} \times 10^{-2}$	$\partial C^*/\partial R$	$\frac{ReSc}{z/D} \times 10^{-2}$	$\partial C^*/\partial R$	$\frac{ReSc}{z/D} \times 10^{-2}$	$\partial C^*/\partial R$
13.3	9.02	33.6	18.9	53.3	23.2
10.0	8.27	20.0	15.1	40.0	19.7
8.00	8.20	13.3	14.8	20.0	16.5
6.67	8.02	10.0	14.2	13.3	14.9
5.71	7.83	8.0	13.6	10.0	13.5
5.00	7.64	6.67	13.0	8.0	12.4
4.44	7.42	5.71	12.5	5.33	10.4
4.00	7.25	5.00	12.0	4.00	9.19
3.33	6.81	4.00	11.2	3.00	8.30
2.86	6.60	2.67	9.61	2.66	7.61
2.35	6.23	2.00	8.44	2.00	6.39
2.00	5.92	1.60	7.53	1.78	6.03
1.60	5.49	1.33	6.70	1.60	5.56
1.33	5.12	1.14	5.92	1.45	5.13
1.14	4.82	1.00	5.16	1.33	4.77
1.00	4.54	0.89	4.50	-	-
0.89	4.31	-	-	-	-
0.80	4.08	-	-	-	-
0.67	3.71	-	-	-	-
0.57	3.38	-	-	-	-
0.53	3.24	-	-	-	-
0.50	2.90	-	-	-	-
0.44	2.58	-	-	-	-
0.39	2.27	-	-	-	-

Table 39. Experimental Average $\partial C^*/\partial R$

T = 55°C

Run 23		Run 15		Run 24	
$\frac{ReSc}{z/D} \times 10^{-2}$	$\partial C^*/\partial R$	$\frac{ReSc}{z/D} \times 10^{-2}$	$\partial C^*/\partial R$	$\frac{ReSc}{z/D} \times 10^{-2}$	$\partial C^*/\partial R$
20.0	13.2	40.0	16.2	42.3	20.2
13.3	11.5	20.0	13.5	32.0	18.7
10.0	11.4	13.3	13.0	20.0	18.0
8.00	11.3	10.0	12.6	13.3	16.6
6.67	10.7	8.00	11.5	10.0	15.3
5.00	10.0	5.71	10.2	8.00	14.3
4.00	9.4	4.00	8.91	6.67	13.3
2.67	8.31	3.20	8.15	5.71	12.6
2.00	7.55	2.67	7.55	5.00	12.0
1.33	6.56	2.00	6.72	4.00	10.9
1.00	5.90	1.60	6.06	3.20	10.0
0.80	5.26	1.33	5.57	2.69	9.24
0.67	4.82	1.14	5.15	2.00	8.20
0.51	4.45	1.00	4.85	1.60	7.44
0.50	4.05	0.89	4.66	1.33	6.78
0.44	3.76	-	-	1.14	6.29
0.40	3.46	-	-	1.00	5.85
0.36	3.18	-	-	-	-
0.35	3.02	-	-	-	-

Table 40. Experimental Average $\partial C^*/\partial R$

T = 56°C

Run 13		Run 14	
$\frac{ReSc}{z/D} \times 10^{-2}$	$\partial C^*/\partial R$	$\frac{ReSc}{z/D} \times 10^{-2}$	$\partial C^*/\partial R$
47.1	21.0	57.0	24.2
29.2	17.9	35.4	20.8
20.0	17.5	20.0	19.7
13.3	16.3	13.3	17.7
10.0	15.1	10.0	16.0
8.00	14.0	8.0	14.6
6.67	13.0	6.67	13.5
5.71	12.3	5.71	12.6
5.00	11.6	5.00	11.9
4.00	10.6	4.44	11.3
3.33	9.57	4.00	10.7
2.86	9.21	3.33	9.92
2.00	7.95	2.86	9.21
1.60	7.25	2.50	8.65
1.33	6.70	2.00	7.75
1.14	6.30	1.60	6.90
1.00	5.95	1.33	6.19
-	-	1.14	5.53

Table 41. Experimental Average $\partial C^*/\partial R$

T = 60°C

$\frac{ReSc}{z/D} \times 10^{-2}$	$\partial C^*/\partial R$	$\frac{ReSc}{z/D} \times 10^{-2}$	$\partial C^*/\partial R$	$\frac{ReSc}{z/D} \times 10^{-2}$	$\partial C^*/\partial R$
15.0	12.5	36.0	18.1	43.2	16.1
11.4	9.43	22.7	16.7	32.7	13.9
8.00	9.14	20.0	16.6	20.0	13.5
6.67	8.80	13.3	15.9	13.3	12.7
5.00	8.23	10.0	15.0	10.0	11.9
4.00	7.68	8.0	14.0	8.00	11.3
2.67	6.71	6.67	13.2	6.67	10.8
2.00	6.01	5.71	12.4	5.71	10.3
1.33	5.04	5.00	11.7	5.00	9.96
1.00	4.38	4.00	10.7	4.00	9.31
0.80	3.84	3.33	9.81	3.33	8.77
0.67	3.39	2.86	9.13	2.86	8.26
0.57	2.98	2.50	8.55	2.50	7.83
0.50	2.58	2.22	8.01	2.00	7.07
0.44	2.18	2.00	7.58	1.60	6.27
0.40	1.80	1.60	6.55	1.33	5.47
0.35	1.24	1.33	5.76	1.14	4.78
-	-	1.14	5.04	1.00	4.24
-	-	1.00	4.46	-	-
-	-	0.89	3.95	-	-

APPENDIX B

COMPUTER PROGRAMS FOR NUMERICAL SCHEME AND GRAETZ EQUATION

```
COMMENT MASS TRANSFER LANGHAAR VELOCITY PROFILE; INTEGER I, J, N, M;
ARRAY CONC(21,2), VEL(21, 2), A1(21), A2(21), A3(21); SUBROUTINE VELOC;
BEGIN IF SIGMA GTR 0.0143; GO TO BIG; GAMMA=EXP(2.89592-0.415LOG(1000
(SIGMA))); GO TO JOE; BIG..IF SIGMA GTR 0.0947; GO TO LOU; GAMMA = (1)/
(0.11483 + 3.98(SIGMA)); GO TO JOE; LOU..GAMMA = EXP (1.444845-7.937642
(SIGMA)); JOE..ARG = GAMMA; ENTER IZERO; IO1 = IO; IF ARG GTR 5.0; BEGIN
WHY = 8.0(ARG); PART 1=(15.0)/ WHY; PART 2 = (3.5(Part 1))/WHY; PART 3
= (3.0(PART 2))/WHY; PART 4 = (8.25(PART 3))/WHY; PART 5 = (13.0(PART 4))/
WHY; I2 = ((EXP(ARG))(1.0-PART 1 + PART 2 + PART 3 + PART 4 + PART 5))/
SQRT(6.28318(ARG)); GO TO LYNN END; GAM= GAMMA/2; I2 = (GAM)(GAM)/2; F1 =
1.0; F2 = 2.0; I=0; BACK..I= I+1; S = 2 + 2I; F1=I.F1; F2 = (S-I).F2;
TEST = I2; I2 = I2 + (((GAM)*S)/F1.F2)); IF I2-TEST GTR 1.0**-5; GO TO
BACK; LYNN..FOR J= (1,1,M-1); BEGIN ARG = (GAMMA)(J-1)(H); ENTER IZERO;
VEL (J,2) = (IO1-IO)/I2 END; RETURN; SUBROUTINE IZERO; BEGIN IF ARG GTR
5.0; BEGIN EX = (8.0)(ARG); TERM1 = (1.0)/(EX); TERM2 = (4.5/EX)(TERM 1);
TERM 3 = ((3.333333)/EX)(TERM 2); TERM 4 = ((12.25)/EX)(TERM 3); TERM 5 =
((16.2)/EX)(TERM 4); IO = ((EXP(ARG)(1 + TERM 1 + TERM 2 + TERM 3 + TERM 4
+ TERM 5))/(SQRT (6.28318 ARG))); GO TO BOB END; I = 0; F1 = 1.0; IO =
1.0; ARG = ARG/2; BACK 1.. I = I + 1; S + 2I; F 1 = I.F1; F2 = F1.F1; TEST
= IO; IC = IO + ((ARG)* S1/F2; IF IC-TEST GTR 1.0**-5; GO TO BACK 1; BOB..
RETURN  END IZERO  END VELOC; TRANS.. READ (($$DATA); FOR I = (1,1,M-1);
BEGIN CONC(I,1)=0.0; VEL(I,1) = 1.0END; VEL (M,1) = CONC(M,1) = 0.5; SC =
7.0(T*-0.185); L = 0; LAMDA = K/(H.H); LOOP 1.. L = L + K; SIGMA = L.SC;
ENTER VELOC;  FOR I = (2,1,M-1); BEGIN A1(I) = (LAMDA/VEL(I,1)) (1 + (1.0/
(2.0(I-1)))); A2 (I) = 1 - (2LAMDA/VEL(I,1)); IF A2(E) LEQ 0.0; GO TO TRANS;
```

```
A3(I) = -A1(I) + (2LAMDA/VEL(I,1)) END; FOR I = (M-1,-1, 2); CONC(I,2) =
A1(I)CONC (I + 1) + A2(I)CONC (I,1) + A3(I)CONC(I-1, 1); CONC (M,2) = 1.0;
VEL (M,2) = 0.0; CONC (1,2) = (4CONC (2,2) - CONC (3,2))/3; SLOPE = -5(4
CONC(M-1,2)-CONC(M-2,2) -3); CAW = (EXP((-8670.795/T) + 26.59965))/(82.06T
(760.0)); DAB = (MEW)/((ROE)(SC)); NAW = (DAB)(CAW)(SLOPE)/RAD; C1 = C2 =
C3 = C4 = 0.0; FOR I + (2,2,M-1); BEGIN C1 = C1 + VEL(I,2)CONC(I,2)(I-1);
C2 = C2 + VEL(I + 1,2)CONC (I + 1,2)I; C3 = C3 + VEL (I,2)(I-1); C4 = C4 +
VEL (I + 1,2)I END; CAB = 2(CAW - CA0) (2C1 + C2)/(2C3 + C4); NUAB = ((CAW
- CA0)/(CAW - CAB))(SLOPE); WRITE ($$NO1, FMT1); WRITE ($$NO 3, FMT3);
WRITE ($$NO4, FMT4); WRITE ($$FMT2A); FOR I = (1, 1, M); BEGIN  R = (I-1)
H; WRITE ($$NO2, FMT 2B); CONC(I,1) = CONC (I,2); VEL (I,1) = VEL (I,2)
END; IF SIGMA LEQ 0.2418; GO TO LOOP 1; GO TO TRANS; INPUT DATA (M,H,K,T,
PRESS,MEW,ROE,RAD,CA0); OUTPUT NO 1(L,SIGMA, NAW, NUAB); OUTPUT NO 2 (R,
VEL (I,2),CONC (I,2)); OUTPUT NO 3 (GAMMA, CAB, SLOPE, CAW); OUTPUT NO 4
(T, MEW, DAB, ROE); FORMAT FMT1(*L = *, F14.8,B5,* SIGMA = *, F14.8, B5,
*NAW = *,F14.8,B5, *NUAB = *,F14.8,W0); FORMAT FMT2A(B6,*RADIUS*, B13,*
VELOCITY*,B10,*CONCENTRATION*,W0); FORMAT FMT2B(B3,F14.8,B6,F14.8,B6,F14.8,
W0); FORMAT FMT3(*GAMMA = *, F14.8,85,*CAB = *,F14.8,85,*SLOPE = *,F14.8,85,
*CAW = *,F14.8,W0); FORMAT FMT4 (*T = *,F14.8,B5, *MEW = *, F14.8,B5, *DAB
= *, F14.8,B5, *ROE = *, F14.8,W0);  FINISH
```

```
COMMENT MASS TRANSFER GRAETZ SOLUTION PARABOLIC VELOCITY PROFILE; INTEGER
I, J, M, N.; TRANS..READ($$DATA); L = 0.0; LOOP 1..IF L GEQ 0.01; L = L
+ K + 0.008; L = L + K; E 1 + EXP(-(2.7043644)(2.7043644)L/2); E 2 = EXP
(-(6.6790314)(6.6790314)L/2); E3 = EXP(-(10.673379)(10.673379)L/2); E4 =
EXP (-(14.671078)(14.671078)L/2); E5 = EXP(1(18.669872)(18.669872)L/2); E6
= EXP(-(22.669143)(22.669143)L/2); E7 = EXP(-(26.668662)(26.668662)L/2);
E8 = EXP(-(30.668323)(30.668323)L/2); E9 = EXP(-(34.668074)(34.668074)L/2);
E 10 = EXP(-(38.667883)(38.667883)L/2); E11 = EXP(-(42.667734)(42.667734)
L/2); T1 = (-1.0143(05)/((-0.5008992)(2.7043644)) T2 = (1.3492416)/
((0.3714623)(6.6790314)); T3 = (-1.5723193)/((-0.3182645)(10.673379));
T4 = (1.746 43)/((0.2864821)(14.671078)); T5 = (-1.89 8571)/((-0.2644906)
(18.669872)); T6 = (2.0164667)/((0.2479945)(22.669143)); T7 = (-2.1281648)
/((-0.2349676)(26.668662); T8 = (2.2292554)/((0.2243063)(30.668323)); T9 =
(-2.3219433)/((-0.2153485)(34.668074)); T10 = (2.4077812)/((0.2076688)
(38.66783)); T11 = (-2.4879083)/((-0.2009787)(42.667734)); B1 = T1/((2.7043644)
(2.7043644)); B2 = T2/((6.6790314)(6.6790314)); B3 = T3/((10.673379)
(10.673379)); B4 = T4/((14.671078)(14.671078)); B5=T5/((18.669872)(18.669872));
B6 = T6/((22.669143)(22.669143)); B7 = T7/((26.668662)(26.668662)); B8 = T8/
((30.668323)(30.668323)); B9 = T9/((34.668074)(34.668074)); B10 = T10/
((38.667883)(38.667883)); B11 = T11/(42.667734)(42.667734)); TOP = 2(E1.T1
+ E2.T2 + E3.T3 + E4. T4 + E5. T5 + E6. T6 + E7. T7 + E8.T8 + E9.T9 + E10.
T10 + E11. T11); BOT = 8(B1.E1 + B2.E2 + B3.E3 + B4 . E4 + B5. E5 + B6. E6
+ B7. E7 + B8. E8 + B9. E9 + B 10. E 10 + B 11. E11); NAWZ = (DAB)(TETA0)
(TOP)/RAD); NUABZ = (TOP)/(BOT); NUABL = (1.0/4L) LOG(BOT); WRITE ($$NO1,
FMT1); IF L LEQ 0.40; GO TO LOOP 1; GO TO TRANS; INPUT DATA (K,DAB,TETA0,
RAD); OUTPUT NO1 (L,NAWZ,NUABZ,NUABL); FORMAT FMT1(*L = *,F14.8, B5,*NAWZ =
*,F14.8,B5,*NUABZ = *,F14.8,B5, *NUABL = *, F14.8,WO);  FINISH
```

APPENDIX C

AVERAGE CONCENTRATION DIFFERENCE IN MASS-TRANSFER RATE EQUATION

Average Concentration Difference in Mass-Transfer Rate Equation

The average Nusselt number for mass transfer is defined by equation (28) as

$$(Nu_{AB})_m = \frac{1}{\ell_e} \int_o^{\ell_e} (Nu_{AB})_{loc} dL = \frac{1}{\ell_e} \int_o^{\ell_e} \frac{k_{x,loc} r_w dL}{C \mathcal{D}_{AB}} \quad (28)$$

For a system with constant physical properties, equation (28) becomes

$$k_{x,m} = \frac{1}{L_p} \int_o^{L_p} k_{x,loc}\, dz \quad (63)$$

Consider a differential length in a cylindrical pipe. The mass-transfer rate is

$$d\mathcal{w}_A = \mathcal{w} dX_{Ab} = k_{x,loc} (\pi D)(X_{Aw} - X_{Ab})\, dz \quad (64)$$

Rearranging gives

$$\frac{dX_{Ab}}{X_{Aw} - X_{Ab}} = \frac{\pi D}{\mathcal{w}} k_{x,loc}\, dz \quad (65)$$

Integrating gives

$$-\int_{(X_{Aw} - X_{Abo})}^{(X_{Aw} - X_{AbL_p})} \frac{d(X_{Aw} - X_{Ab})}{X_{Aw} - X_{Ab}} = \frac{\pi D}{\mathcal{w}} \int_o^{L_p} k_{x,loc}\, dz \quad (66)$$

Substituting equation (62) and performing the integration gives

$$\ln \frac{(X_{Aw} - X_{Abo})}{(X_{Aw} - X_{AbL_p})} = \frac{\pi D(k_{x,m} L_p)}{w} \tag{67}$$

But by equation (63)

$$w_A = w(X_{AbL_p} - X_{Abo}) \tag{68}$$

Substituting equation (68) into equation (67) gives

$$\ln \frac{(X_{Aw} - X_{Abo})}{(X_{Aw} - X_{AbL_p})} = \frac{(\pi D L_p)\, k_{x,m}\, (X_{AbL_p} - X_{Abo})}{w_A} \tag{69}$$

which reduces to equation (29)

$$w_A = \frac{k_{x,m}\, (\pi D L_p)(X_{AbL_p} - X_{Abo})}{\ln \left(\frac{X_{Aw} - X_{Abo}}{X_{Aw} - X_{AbL_p}} \right)} = k_{x,m} A_{ST} (\Delta X_{Ab})_{\ell m} \tag{29}$$

where

$$(\Delta X_{Ab})_{\ell m} = \frac{(X_{AbL_p} - X_{Abo})}{\ln \left(\frac{X_{Aw} - X_{Abo}}{X_{Aw} - X_{AbL_p}} \right)} \tag{70}$$

BIBLIOGRAPHY

1. Wilke, C. R., J. M. Prausnitz, and A. Acrivos, "Mass Transfer Review," Industrial and Engineering Chemistry, 52, 441 (1960).

2. Steele, L. R., and C. J. Geankoplis, "Mass Transfer from a Solid Sphere to Water in Highly Turbulent Flow," A.I.Ch.E., Journal (American Institute of Chemical Engineers) 5, 178 (1959).

3. Garner, F. H., and R. B. Keey, "Mass Transfer from Single Solid Spheres-I," Chemical Engineering Science 9, 119 (1958).

4. Ibid, p. 218.

5. Kreith, F., J. H. Taylor and J. P. Chong, "Heat and Mass Transfer from a Rotating Disk," Journal of Heat Transfer, 81, 95 (1959).

6. Bird, R. B., W. E. Stewart, and E. N. Lightfoot, Transport Phenomena, John Wiley and Sons, Inc., New York, N. Y. (1960).

7. Sherwood, T. K., and O. Träss, "Sublimation Mass Transfer through Compressible Boundary Layers on a Flat Plate," Paper No. 59 - A137, Presented at the Annual Meeting, Atlantic City, N. J., Nov. 29 - Dec. 4, 1959, of the American Society of Mechanical Engineers.

8. Deissler, R. G., and A. L. Loeffler, Jr., "Analysis of Turbulent Flow and Heat Transfer on a Flat Plate at High Mach Numbers with Variable Fluid Properties," National Advisory Committee for Aeronautics, Technical Note 4262 (1958)

9. Christian, W. J., and S. P. Kezios, "Sublimation from Sharp-edged Cylinders in Axisymmetric Flow, Including Influence of Surface Curvature," A. I. Ch.E. Journal, 5,61 (1959).

10. Butler, R. M., and A. C. Plewes, "Evaporation of Solids into Laminar Air Streams," Chemical Engineering Progress Symposium Series, 50, 121 (1954).

11. Plewes, A. C., R. M. Butler, and H. E. Marshall, "The Evaporation of Solids into Laminar Air Streams," Chemical Engineering Progress, 50, 77 (1954).

12. Southwell, R. V., Relaxation Methods in Thecretical Physics, 1st Ed., Clarendon Press, Oxford, England (1946).

13. Linton, W. H., and T. K. Sherwood, "Mass Transfer from Solid Shapes to Water in Streamline and Turbulent Flow," Chemical Engineering Progres, 46, 258 (1950).

14. Langhaar, H. L., "Steady Flow in the Transition Length of a Straight Tube," Journal of Applied Mechanics, 9, 55 (1942).

15. Kay, W. M., "Numerical Solutions for Laminar-Flow Heat Transfer in Circular Tubes," Transactions of the American Society of Mechanical Engineers, 77, 1265 (1955).

16. Keller, H. B., "The Numerical Solution of Parabolic Partial Differential Equations," Mathematical Methods for Digital Computers, John Wiley and Sons, New York, N. Y. (1960).

17. Douglas, Jr., J., and H. H. Rachford, J. R., "On the Numerical Solution of Heat Conduction Problems in Two and Three Space Variables," Transactions of the American Mathematical Society, 82, 421 (1956).

18. Crank, J., and P. Nicolson, "A Practical Method for Numerical Evaluation of Solutions of Partial Differential Equations of Heat Condition Type," Proceedings of the Cambridge Philosophical Society, 43, 50 (1947).

19. John, F., "On Integration of Parabolic Equations by Difference Methods," Committee of Pure and Applied Mathematics, 5, 155 (1952).

20. Blanch, G., "On the Numerical Solution of Parabolic Partial Differential Equations," Journal of Research of the National Bureau of Standards, 50, 343 (1953).

21. Jakob, M., Heat Transfer, Sixth Printing, John Wiley and Sons, New York, N. Y. (1949).

22. Brown, G. M., "Heat or Mass Transfer in a Fluid in Laminar Flow in a Circular or Flat Corduit," A. I. Ch.E. Journal, 6, 179 (1960).

23. Tables of Thermal Properties of Gases, United States Bureau of Standards Circular 564, 33, 69 (1955)

24. Verma, A. R., Crystal Growth and Dislocations, Butterworth Scientific Publications, London, England (1953).

25. Read, W. T., Jr., Dislocations in Crystals, McGraw-Hill Book Company, Incorporated, New York, N. Y. (1953).

26. Robertson, J. M., Organic Crystals and Molecules, Cornell University Press, Ithaca, N. Y. (1953).

27. Sherwood, T. K., and N. E. Cooke, "Mass Transfer at Low Pressures," A.I.Ch.E. Journal, 3, 37 (1957).

28. Sears, G. W., "Evaporation of Perfect Crystals," Journal of Chemistry and Physics, 24, 868 (1956).

29. Bedingfield, C. H., Jr., and T. B. Drew, "Analogy between Heat Transfer and Mass Transfer," Industrial and Engineering Chemistry, 42, 1164 (1950).

30. Griffith, R. M., "Mass Transfer from Drops and Bubbles," Chemical Engineering Science, 12, 198 (1960).

31. Prandtl, L. and O. G. Tietjens, Applied Hydro-Aeromechanics, McGraw-Hill Book Company, Incorporated, 1st Ed. New York, N. Y. (1934).

32. Spurlock, J. M. (Assistant Professor, School of Chemical Engineering, Georgia Institute of Technology, Atlanta, Georgia), Personal Communication.

33. Schneider, P. J., "Effects of Axial Fluid Conduction on Heat Transfer in the Entrance Regions of Parallel Plates and Tubes," Transactions of the American Society of Mechanical Engineers, 79, 765 (1957).

34. Singh, S. N., "Heat Transfer by Laminar Flow in a Cylindrical Tube," Applied Scientific Research, 7A, 325 (1957-8).

VITA

Robert Thomas Bosworth was born in St. Petersburg, Florida on August 8, 1934. He attended elementary schools in Miami, Florida, and was graduated from Miami Edison High School. In 1952 he entered the University of Florida, from which he was graduated in 1956, receiving the degree of Bachelor of Chemical Engineering with honors. After graduation he was employed by ACF Industries, Inc., Albuquerque, New Mexico, as a Design Engineer.

In 1958 he was enrolled in the Graduate Division of the Georgia Institute of Technology, Atlanta, Georgia where he began his work towards a Ph. D. degree in the School of Chemical Engineering. During this time, he was employed as a Research Assistant by the Radioisotopes Laboratory and taught undergraduate courses in the School of Chemical Engineering.

At the National Convention of the American Chemical Society in 1959 he presented the paper, "Application of Computers to Solvent Extraction Problems," by R. W. Pike, R. T. Bosworth, and T. H. Goodgame. He is a member of Sigma Xi.

In 1957 he was married to the former Julia Lawana Averitt of Jacksonville, Florida. They have a daughter, Julie Lynn, and a son, Robert Raymond.